University of Liège

Aerospace and Mechanical Engineering Department

Topology optimization under static and fatigue failure constraints

Thesis submitted in partial fulfillment of the requirements for the degree of Doctor of Philosophy in Engineering Sciences

by

Maxime Collet
M.Sc. Mechanical Engineer

September 2018

Author's Contact details

Maxime Collet

Automotive Engineering Research Group
Aerospace and Mechanical Engineering Department
University of Liège

Quartier Polytech 1,
Allée de la découverte 9,
4000 Liège, Belgium

Email : maxime.collet@uliege.be
Phone : +3243669512

Funding : This PhD research was supported by the Belgian National Fund for Scientific Research through a F.R.I.A (*Fond pour la Recherche en Industrie et en Agriculture*) scholarship.

Members of the Examination Committee

Pr. Jean-Philippe Ponthot (President)
University of Liège

Pr. Pierre Duysinx (Advisor)
University of Liège

Pr. Davide Ruffoni (Co-Advisor)
University of Liège

Pr. Michaël Bruyneel
University of Liège & Scientific director - GDTech SA

Assoc. Pr. Matteo Bruggi
Politecnico di Milano

Pr. Piotr Breitkopf - Deputy Director
Université de Technologie de Compiègne
Laboratoire Roberval

Assoc. Pr. Mattias Schevenels
KU Leuven

Abstract

The rationalization of energy consumption, to meet today's environmental concerns, can be improved by reducing, in particular, the mechanical components mass in vehicles. To achieve this goal, structural optimization offers a flexible and rigorous tool to continuously improve the design chain. The resistance to static but also time varying efforts is essential for part certification. In addition, the emergence of additive manufacturing techniques enables to consider and fabricate components comprising porous material regions defined by architectured mesostructures. The objective of this thesis is to contribute to the extension of the structural optimization tool to the design of fatigue resistant layouts and to propose an approach allowing the design of mesostructures with high load resistance.

This thesis exploits density–based topology optimization and in particular revisits the introduction of stress constraints within the design problem. Linear elastic behavior is assumed and static load cases are applied to the structures. In order to take into account the time varying behavior of the loading, essential for fatigue design, specific procedures are tailored.

Stress-constrained topology optimization has been the subject of numerous publications over the last twenty years. Nowadays, it is difficult to have a clear idea of the effectiveness of these methods compared to each other due to the lack of a fair comparison investigation. Hence, a series of standardized test cases are proposed and confronted against the most commonly encountered approaches in the literature thus providing a fair comparison of their performance. Some specific characteristics to the stress–based design problem are also revisited.

Classically, using topology optimization for the design of architectured materials provides solutions that reveal stress concentrations that can lead to failure. Hence, the mitigation of stress concentrations is developed and introduced into the design problem to achieve optimized solutions that also enclose resistance within the microstructural geometry.

The design of fatigue resistant components is introduced in two stages. A first approach is based on the classical hypothesis of proportional loads with constant amplitude. The fatigue phenomenon is accounted for by means of a static reference load case enabling to evaluate the quantities of interest involved in the various resistance criteria. In a second step, in order to consider more complex loads, the Dang Van criterion, which is of common use in the french automotive industry, is considered. The latter accounts for the stress state at the grain level to built the fatigue criterion. The two stages procedure of the criterion is adapted and an original approach is tailored to consider the fatigue resistance constraint in a topology design cycle.

Résumé

La rationalisation de la consommation énergétique, permettant de répondre aux enjeux environnementaux, peut être améliorée en réduisant, notamment, la masse des composants mécaniques utilisés dans les véhicules. Pour ce faire l'optimisation structurale offre un outil flexible et rigoureux aidant à l'amélioration de la chaine de conception. La résistance aux sollicitations statiques mais également variables dans le temps est primordiale pour certifier un composant. De plus, l'émergence des techniques d'impression additive permet de considérer et de fabriquer des composants légers comprenant des régions à gradient de matière définies par des mésostructures architecturées. L'objectif de cette thèse est d'étendre l'outil d'optimisation des structures au design de composants résistant au phénomène de fatigue ainsi que de proposer une démarche permettant de concevoir des mésostructures ne rompant pas aux sollicitations extérieures.

Cette thèse exploite l'optimisation topologique basée sur les densités et en particulier revisite l'introduction des contraintes de résistance au sein du problème de conception. Le comportement élastique des structures est supposé et des chargements statiques sont appliqués à celles-ci. Afin de prendre en compte la variation temporelle du chargement, aspect essentiel pour le dimensionnement à la fatigue, des procédures spécifiques sont à considérer.

L'optimisation topologique incluant les contraintes de résistance a fait l'objet de nombreuses publications au cours de ces vingt dernières années. Il est aujourd'hui difficile de se faire une idée claire de l'efficacité des méthodes les unes par rapport aux autres par manque de points de comparaison. Dès lors, une série de cas tests standardisés sont proposés et confrontés aux approches les plus couramment rencontrées dans la littérature apportant ainsi une comparaison équitable de leurs performances. Des caractéristiques propres au problème de conception avec contraintes sont également revisitées.

Classiquement, l'utilisation de l'optimisation topologique pour le design de matériaux architecturés fournit des solutions faisant apparaître des concentrations de contraintes susceptibles de mener celles-ci rapidement à la rupture. Dès lors, la réduction des concentrations de contraintes est développée et introduite dans le problème de conception pour réaliser des solutions optimisées au niveau de la géométrie mésoscopique plus pertinente pour répondre au besoin de résistance.

Le design des composants résistant aux chargements variables dans le temps est introduit en deux temps. D'abord, sous l'hypothèse de chargements proportionnels à amplitude constante, le phénomène de fatigue est pris en compte à l'aide d'un cas de charge statique de référence permettant d'évaluer les quantités d'intérêt intervenant dans les différents critères de résistance. Dans un deuxième temps, afin de prendre en compte des chargements plus complexes, le critère de Dang Van, d'usage courant dans l'industrie automobile française, est pris en compte. Ce dernier tient compte de l'état de contrainte au niveau du grain pour construire le critère de fatigue. La procédure en deux étapes du critère est

adaptée et une approche originale est proposée pour inclure la contrainte de résistance à la fatigue dans un cycle d'optimisation topologique.

Acknowledgments

This thesis is the culmination of four years of research within the Automotive Engineering group of the University of Liège. It is now time to thank all of those who have contributed to its success.

First of all, I would like to thank my academic advisor, Prof. Pierre Duysinx. In spite of the many reshuffles and the change in direction from the originally stated goals of this work, he knew how to get me back on track and he helped me remaining committed to finishing the different assigned tasks no matter how difficult they were. Thank you also for the good mood, the enthusiasm, the advice and the guidance, which allowed me to reach this point in my academic career.

During this thesis, I was offered the opportunity and privilege to undertake two research stays abroad in Italy and the United States. I would like to express my deepest gratitude to Dr. Matteo Bruggi for his great hospitality at Politecnico di Milano, his kindness and his availability since the very beginning of my PhD journey. I would also like to thank Prof. Julian Norato and his team for welcoming me so warmly in their group at the University of Connecticut. The exchanges allowed me to learn a lot and to share useful ideas, which made these stays even more memorable.

I am grateful to the members of the thesis committee who participated in the review and evaluation of this manuscript. Thanks to Davide Ruffoni, Jean-Philippe Ponthot, Michaël Bruyneel, Piotr Breitkopf, Mattias Schevenels and Matteo Bruggi.

This research work was made possible thanks to the financial support of the Belgian National Fund for Scientific Research through a F.R.I.A grant., which is gratefully acknowledged as well.

The completion of this work would not have been possible without the support and cheerfulness of my dear friends and colleagues of the Aerospace and Mechanical Engineering Department. In particular, I would like to thank Simon Bauduin, Pablo Alarcon, Eduardo Fernandez, Kim Liégeois, Kevin Bulthuis and Joffrey Coheur but also Lise Noël and Emmanuel Tromme for the unforgettable great moments of fun we had together during the breaks. I would also like to thank Asmaa El Khadri in particular for her presence, for listening in times of doubt and for giving me the motivation to keep moving forward.

A big thanks goes to the Shell Eco Marathon team without whom this experience would not have been so memorable. I wish to express my thanks in particular to Antonio Martinez for always knowing how to bring a good mood since my involvement in this wonderful project.

Finally, last but not least, I would like to thank all the members of my family and friends who have never stopped supporting me since the beginning of this research work but also in any of my endeavors.

Contents

Chapter 1

Introduction

Contents

1.1 Context of the study

Today climate concerns bring together new developments aiming at preserving the environment. A significant amount of human pollution comes notably from greenhouse gas emissions in the transport area and represented 14% of global emissions in 2014 [IPCC(2014)]. Actions are therefore needed to reduce energy consumption. In the particular case of the automotive and aerospace industries, many efforts are being made to offer alternative fuel but also to reduce vehicle mass. For example, in aircraft propulsion, the new LEAP®(*Leading Edge Aviation Propulsion*) engine is 450 kg lighter than the previous CFM56®which enables to spare 15% of fuels [Safran(2010)]. In the automotive industry, when it comes to conventional diesel or gasoline fuel vehicles, a 10% weight reduction can shorten energy consumption by 6% [Duysinx(2016)]. It is even further important for future electric vehicle (EV) where the reduction of the structural mass allows reducing the battery weight. The challenge of designing mechanical parts efficiently and reducing the number of trials and errors could not be achieved without the help of new design tools based on optimization. The latter must allow for accounting the manufacturing restrictions, e.g., static resistance, fatigue resistance, reduction of vibrations level, etc., that the components have to meet during their service life.

Since the end of the *80ies*, structural optimization, and in particular topology optimization, has been developed to achieve this goal. Its purpose is to offer the designers the ability to formulate the design automatically by handling the design problem, usually multi-constrained, in a mathematical framework. Many industrial tools like those distributed by Altair [1] Siemens [2] or Dassault Systems [3] now integrate the topology optimization method to deal with industrial problems in daily life. Although viable for large size problems, topology optimization still suffers

[1] www.altairhyperworks.com
[2] www.plm.automation.siemens.com
[3] www.fe-design.de

from deficiencies when static strength or fatigue failure criteria are required. The assurance that a component will withstand the stresses to which it will be subjected is an essential element in its certification before being put on the market. More advanced criteria than those abundantly used, i.e., maximum stiffness criteria, must be introduced into the optimization process in order to be able to solve practical industry problems and thus make the design chain more efficient. The literature now abounds with various methods that introduce strength criteria into the design problem. However, no fair comparison is available and it becomes difficult to get a clear picture of their relative performance under various conditions.

In order to design even lighter components and under the developments of additive manufacturing techniques, lattice structures and architectured materials can be introduced into mechanical components thanks to their mechanical properties to weight ratio. Topology optimization can also be used to design such structures but again a cruel lack of consideration of their resistance is observed.

This research work aims at extending the topology optimization techniques available in the literature in order to take into account the resistance criteria in the context of the automotive and aerospace sectors. First by considering the criteria of static failure and then in a second time the fatigue failure.

1.2 Origin and literature review

Structural optimization has been receiving increasing interest in engineering for many years since the founding work on truss structures initiated by [Schmit(1960), Dorn et al.(1964)]. In the continua, the topology optimization method defined by [Bendsøe and Kikuchi(1988)] constitutes a major breakthrough in the design process. The method aims at finding the optimal material distribution within an enclosed space, i.e., the design domain, to which boundary conditions and loads are applied in order to define prescribed performance criteria. Topology optimization is an extremely powerful tool that has found applications in many fields of engineering thanks to its great versatility and its solid mathematical foundations. For more details on the various usage of the method, interested readers may refer to [Deaton and Grandhi(2014)] for a comparison of available approaches and [Bendsøe and Sigmund(2003), Eschenauer and Olhoff(2001), Rozvany(2009), Sigmund and Maute(2013)] for a comprehensive review.

Today, the automotive and aerospace industries aim at using the topology optimization tool in their design chain. However, most of the problems that can be solved are formulated as maximum stiffness problems. Certification of mechanical parts aslo require to meet some strength criteria. If not considered in the problem definition, the solution of the optimization requires long post-processing phases of the results to meet the expected specifications. This causes additonal time that not only requires substantial human ressources but also financial costs, and finaly delays the marketing of final products. Moreover, the redesign phases degrade the optimized solution obtained and lead to sub-optimal end products. It is necessary to prevent component failure at any point of the structure during the preliminary design phase using topology optimization as indicated in [Duysinx et al.(2008)]. These strength problems involve both static and fatigue failure, i.e., mechanical failure of components subjected to time varying amplitudes loads.

Early stress constrained optimization works on truss structures, see e.g., [Dorn et al.(1964), Sved and Ginos(1968), Kirsch(1989), Kirsch(1990)], have established that stress–based problems are subjected to many challenges. The work by [Duysinx and Bendsøe(1998)], initially dedicated to laminated materials of rank-1, rank-2 and, to materials ruled by the Solid Isotropic Material with Penalization (SIMP) law ([Bendsøe(1989), Rozvany et al.(1994)]), on continuous media, confirmed the work carried out on discrete structures. The series of works that fol-

lowed, see e.g., [Duysinx and Sigmund(1998), Stolpe and Svanberg(2003), Peirera et al.(2004), Guilherme et Fontseca(2007), Svanberg et Werme(2007), Paris et al.(2009), Holmberg et al.(2013), Verbart(2015)] or more recently [Lian et al.(2017)], have once again illustrated the challenges underlying stress constraints in topology optimization while providing original solutions to those problems. The latter are classified into three main categories: 1) the singularity phenomenon of the stresses, 2) the high computational time, and 3) the non-linear behaviour of the stresses. For the latter, as discussed in [Le et al.(2010)], the stress values are highly dependent on individual design variables and this dependency is closely related to the proximity of the element to singular areas of the design domain such as reentrant corners, load application points or boundary conditions. This can be managed by a rational use of non-linear programming techniques like the *Method of Moving Asymptotes*, see [Svanberg(1987), Svanberg(1995), Svanberg(2007)].

Singularity phenomenon: The problem of structural optimization, whether with discrete elements, e.g., bars or beams, or in the continua, is subjected to the issue of singularity of the stress constraints, early highlighted by [Sved and Ginos(1968)], when non-linear gradient–based algorithms are used [Kirsch(1989), Kirsch(1990)]. It has been shown that a change in connectivity leads to a change in the compatibility conditions governing the problem and therefore the solution can get stuck in a local optimum. Afterwards, the work of [Achtziger and Kanzow(2008)] extended the concept of singularity to any optimization problem presenting *vanishing constraints*. Research conducted by [Cheng and Jiang(1992), Kirsch(1989), Kirsch(1990), Rozvany and Biker(1994), Rozvany(1996), Rozvany(2001)] has determined that the global optimum of the system is located in a degenerated subspace, i.e., of lower dimensionality, of the design space. This prevents mathematical programming algorithms to reach the global optimum and to be stuck in a suboptimal solution of the design space. As the optimization progresses, the cross sections of the bars or beams (resp. the density of the elements) decrease and *de facto* the stress level increases to reach the prescribed limit value. The immediate consequence is the impossibility to remove some members of the structure or to keep large grey areas filled with elements of intermediate density. To overcome this difficulty, several solutions have been proposed in the literature. The works of [Kirsch(1989), Kirsch(1990)] rewrite the initial problem with non-linear constraints into a linear problem and solve it using appropriate algorithms. Indeed, linear problems are known to be free from the issue of non-convexity. However, this approach is only valid in the case of a statically determined structure where the compatibility conditions are neglected, see [Rozvany and Biker(1994)]. The idea was later extended in [Stolpe and Svanberg(2003)] where a discrete 0-1 approach is followed. The disadvantage of the method is the long computational time required and therefore the impossibility of using it in industrial applications. In order to penalize the asymptotic behavior toward large values of the stresses as the design variables decrease to zero, [Cheng and Jiang(1992)] proposed to use a *qualification function*. The drawback with such an approach is that the design space remains identical to the original one and that the singularity phenomenon is not eliminated. An identical idea, removing the singularity, is put forward by [Rozvany and Sobieszczanski(1992)] advocating the use of a *smooth envelope* of the stresses on the set of variation of the design variables. Stress relaxation has been popularized by introducing a positive perturbation parameter ε into the definition of the constraints, see [Cheng and Guo(1997)]. This method known as ε-relaxation consists of giving a high value to the disturbance parameter ε and establishing a *continuation strategy* to gradually reduce it to get as close as possible to the initial unperturbed problem. Although the singularity is effectively removed, [Stolpe and Svanberg(2001a)] have shown that convergence towards the global optimum is not ensured. Moreover, this method is similar to the continuous envelope approach as discussed in [Rozvany(2001)]. In the context of SIMP materials, [Bruggi and Venini(2008), Bruggi(2008)] introduced the concept of *qp*-relaxation by noting that a different penalization exponent for the stiffness and

the stresses induces a shape modification of the constraints in the design space leading to the expected relaxation of the problem. However, as with the ε-relaxation, convergence towards the global optimum is not guaranteed. As discussed in [Verbart(2015)], qp-relaxation penalizes densities over the entire space of variations of their values. In the same way, ε-relaxation penalizes densities more locally, i.e., in the vicinity of low values, making it less adapted to gradient–based methods. The contribution of [Le et al.(2010)] introduces the notion of relaxed stresses. The principle consists in multiplying the stress matrix by a *relaxation function* whose properties maintain the stress values at full density and cancel them out at zero density. This approach, although purely mathematical, has been widely used in subsequent works, see e.g., [Holmberg et al.(2013), Lee et al.(2012), Zhang et al.(2017)]. Finally, the work of [Verbart et al.(2017)] unifies aggregation and relaxation methods by noticing that a lower bound aggregation function distorts the shape of the constraints allowing the expected relaxation effect. However, the authors have also noticed that large grey regions remain in the optimized layout.

High computational time: The major difficulty of the introduction of stress constraints in topology optimization lies in the significant increase in computational time required. In order to control the stress level within the structure and to ensure structural integrity, each point of the structure must have an equivalent stress below a prescribed limit. Numerically this amounts to controlling at each of the element centroïds or each Gauss points the value of the equivalent stress constraint. This inevitably leads to huge scale optimization problems that are difficult to manage for industrial applications. The founding work of [Duysinx and Bendsøe(1998)] dealt with local constraints, referred in the following as *the local approach*, and proposed to reduce the amount of calculation required using an appropriate selection of the most dangerous constraints. This method is later referred to as the local approach with active-set selection strategy. In the continuity of local methods with active-set, [Bruggi and Duysinx(2012)] have introduced alongside the local constraints, a global compliance constraint that helps significantly reduce the computational time. This method has been used in several subsequent research studies, see e.g., [Collet et al.(2015), Collet et al.(2017)]. In order to reduce as much as possible the computational effort, [Duysinx and Sigmund(1998)] have proposed to aggregate all the local constraints into a single one using a p-norm or p-mean function. This type of method is later referred to as *the global approach* of the problem with stress constraints. While the main advantage of this strategy is the considerable time saving, one of its drawbacks is the introduction of additional unwanted non–linearties into the optimization process which involves an increased dependency on the selected numerical parameters. These non-linearities, if not managed properly, can outweigh the benefits obtained when reducing the number of constraints. An alternative aggregation function based on the Kresselmeier-Steinhauser (KS) function is proposed in [Yang and Chen(1996), Paris et al.(2009), Luo et al.(2013)] with the same advantages and disadvantages as those found in [Duysinx and Sigmund(1998)]. At the intersection of the local and global approach, a third category referred to as the *regional approach* has been introduced. The principle consists in aggregating the local constraints not into a single set but into several ones to keep a small number of constraints to be passed to the optimizer. This approach, introduced by [Paris et al.(2010)], allows a more localized control of the stress values. In the latter contribution, a division of the design domain is performed into blocks and each block is aggregated by a KS function. The method has demonstrated its effectiveness when compared to a pure local approach while it is not the case when it comes to competing with the global approach. Nevertheless, it allows reducing the undesirable effects generated by the latter. In [Paris et al.(2010)], the method described can be considered as a regional approach with block aggregation based on the geometry. Subsequently, other methods based on an algebraic block decomposition, i.e., the blocks are constituted following algebraic conditions on the value of

the stress level within the elements, were proposed. [Le et al.(2010)] considered a p-norm as an aggregation function and added a scaling parameter to project the value of this p-norm to the maximum of the local constraints within each of the blocks. Finally [Holmberg et al.(2013)] proposed to modify the block setting of local constraints and used a p-mean function for the aggregation. Like global approaches, regional methods are more effective than the local approach regarding the CPU time but require more adjustments of numerical parameters. Moreover, the number of blocks influences the final solution. This adds an additional parameter to be managed by the user.

Non linearity of the stresses. Today, this issue is well mastered and has been since the first works with stress constraints on truss-structures solved with non-linear programming algorithms, see e.g., [Sved and Ginos(1968), Kirsch(1989), Kirsch(1990), Kirsch(1993)]. Using topology optimization in the continua implies that stress constraints are implicit functions of the design variables making the problem difficult to solve. The Sequential Convex Programming (SCP)([Fleury(1982)]) allows circumventing this issue. Here, the initial implicit optimization probelm is replaced by a sequence of approximated subproblems by expending the constraints and the objective around the current design points. As discussed in [Duysinx(1997)], convex approximations are needed to provide a reliable and conservative approximations of the structural constraints. Several structural approximations were developed such as the first or second order approximation CONLIN ([Fleury and Braibant(1986), Fleury(1989a), Fleury(1993)]), the second order approximations such as the Broyden-Fletcher-Goldfard-Shanno (BFGS)([Duysinx et al.(1995), Duysinx(1997)]) or the Method of Moving Asymptotes and extensions ([Svanberg(1987), Smaoui et al.(1988), Svanberg(1995), Svanberg(2007), Bruyneel et al.(2002)]). The convex subproblems are then solved resorting to either dual methods ([Fleury(1979a)]), Sequential Quadratic Programming ([Schittkowski(1985)]) or Interior point methods ([Byrd et al.(1999)]). The contribution of [Duysinx and Bendsøe(1998)] used the CONLIN approximation to solve the local stress constrained problem. However, as discussed in [Duysinx(1997)], the CONLIN approximation introduces fixed curvatures that lead to slow or unstable convergence. To alleviate this issue, the MMA scheme is often used due to its set of mobile asymptotes that modify the curvature and fit better the characteristics of the problem. In addition, the MMA scheme is a generalization of the CONLIN scheme. Finally, some authors, see e.g., [Kirsch(1989), Stolpe and Svanberg(2003)], have advocated a full linearization of the constraints in order to turn to Linear Programming (LP) methods. The advantage lies in the possibility to benefit from the robustness of the algorithms while guarding the problem from the singularity phenomenon discussed above. The major disadvantage of this approach is the small size of the problems that can be solved.

Fatigue: Fatigue failure, which is one of the most dangerous failure modes in many industrial mechanical applications, can be described in different ways depending on the number of loading cycles. For a low number of cycles, typically less than 10^3, the design is perfomed taking into account plastic deformations. For a high number of loading cycles, i.e., more than 10^3, stresses are used as design criteria. In this work, a large number of cycles is considered. Considering the latter, the extension of topology optimization with stress constraints embedding the phenomenon of fatigue failure is a natural procedure. As indicated in [Holmberg et al.(2014)], little information is available about fatigue strength using topology optimization. Yet, regarding shape optimization, their use in industrial processes seems promising and deserves to be highlighted, see [Grunwald and Schnack(1997) , Mrzygold and Zielinski(2006), Mrzygold and Zielinski(2007)] or [Kaya et al.(2010)]. The work of [Achtziger and Bendsøe(1995), Achtziger and Bendsøe(1999)] introduced fatigue strength into truss-like structures by successive degradations of the Young's modulus in accordance with [Bendsøe and Diaz(1998)] where the homogenization technique of a rank-2 material is used. [Jeong et al.(2014)] introduced fatigue using a modified signed Von

Mises criterion to account for its non differentiability. Static and dynamic failure are considered in the previous contribution and an aggregation method is used to manage the local stress field. Continuing along his work on static strength requirements, [Holmberg et al.(2014)] considered fatigue failure by aggregating local damage determined with a probabilistic fatigue model. A Weibull law ([Weibull (1939)]) allows in the work of [Svärd(2015a)] to construct a weak link model to achieve topology optimization taking fatigue failure into account. It has been observed that the Weibull's law has similarities with a p-norm function. More recently the contributions of [Collet et al.(2015), Collet et al.(2017)] have used the criteria of Sines, Crossland and, Goodman to design fatigue strength components under proportional loads, while [Oest and Lund(2017)] have compared the effective stress method with the cumulative damage method using the rainflow counting technique ([Dowing and Socie(1982)]). Some authors, see [Witteveen et al.(2009), Sherif and Irschif(2010)], have proposed industrial schemes to solve the problem based on the equivalent static loading (ESL) technique defined by [Park and Kang(2003), Kim and Park(2010)].

Material tailoring using topology optimization: Today, the growing development of additive manufacturing techniques allows offering new possibilities in component fabrication and introducing into mechanical parts regions made of porous architectured structures, widely spread in nature due to their efficiency to withstand various loads. The use of topology optimization as a design tool to propose innovative concepts exploiting these particular architectured structures, in the remaining of this manuscript referred to as *architectured materials*, enables to design innovative structures by specifying the desired final properties. Porous materials have been at the heart of topology optimization since the seminal work of [Bendsøe and Kikuchi(1988)] so has the theory of homogenization, see e.g., [Besoussan et al.(1978), Sanchez-Palencia (1983), Suquet(1982), Guedes and Kikuchi(1990), Mlejnek and Schirrmacher (1993), Torquato(2002), Andreassen and Andreasen(2014)], which has played a key role in the computation of the material effective properties. Interested readers can refer to the works of [Hassani and Hinton(1997), Hassani and Hinton(1998a), Hassani and Hinton(1998b)] for a review of topology optimization with homogenization techniques. Although these methods have been a little disregarded today, they are of growing interest, as shown by e.g., [Xia(2015), Andreassen et al.(2015)]. The use of topology optimization in the design of architectured materials was initiated by [Sigmund(1994), Sigmund(1995)]. In these seminal contribution, the author seeks to achieve prescribed values of macroscopic material properties, i.e., cubic compressibility modulus or negative Poisson's ratio, using the SIMP law to model the porous microscopic material and use the homogenization to extract equivalent properties. In [Bendsøe and Sigmund(1999)], the homogenization theory along with topology optimization is used to synthesize a design that represents the SIMP material. Subsequently, extensive research has been conducted in many application areas ranging from classical mechanics to acoustics or thermics, see [Sigmund(1999), Sigmund and Torquato(1999), Gibiansky and Sigmund(2000), Guest and Prévost(2006), Jensen and Sigmund(2011), Jia et al(2017)] and [Cadman et al.(2013)] for an exhaustive review. Few works are devoted to the consideration of resistance in the design of architectured materials. The works of [Lipton and Stuebner(2006), Lipton and Stuebner(2007)] are an exception. The authors used homogenization in a reverse procedure to identify the material gradient that provides the specified structural response while ensuring control over the local value of the stress field in the vicinity of the singularities between the structural elements. The method considers a local stress amplification in the porous microstructure using multi-scale quantities. Let us quote the works of [Noël and Duysinx(2017)] which introduces the stress constraints at the microstructural scale in the field of the Level-set method coupled to the XFEM. Benchmarks from the literature as well as an original example with several inclusions were analyzed and have validated the approach, demonstrating its robustness and flexibility.

1.3 Motivations, hypotheses and objectives

The main goal of this thesis is to continue and extend the developments encountered in the literature regarding topology optimization with static and fatigue strength criteria. All the developments are carried out considering an elastic response of the structures for which the laws of continuum mechanics are applicable. In addition, a material interpolation following the SIMP law is used to link its mechanical properties to the design variables, i.e., the densities.

The first objective is to perform a large review of the methods to introduce the concept of stress constraints and to carry out a fair comparison of the different approaches by proposing a series of benchmarks that will serve as a basis for future works. Given the wide variety of available methods, an exhaustive comparison is obviously impossible. Therefore, our investigations will be limited to methods built upon a founding idea. Furthermore, the methods as they are presented in their original version are not strictly compared because of the lack of information available. The comparison is for that reason performed by getting inspired by the approaches, e.g., p-mean/p-norm/KS functions or several block aggregation techniques, developed to deal with stress constraints in topology optimization. The comparison is fair in this approach since it is based on the same code and benchmarks.

In a second phase, the work will focus on the introduction, within the optimization problem dedicated to architectural materials, of stress constraints based on an equivalent Von Mises stress limitation. The hypothesis of the separation of scales is at the heart of the investigations in order to be able to apply the theory of homogenization used to extract the equivalent material properties on the studied Representative Unit Cells (RUC). These are considered small enough with respect to the actual structural scale but large enough with respect to a microscopic scale, i.e., the scale of the porous SIMP material, so that the definition of a Von Mises criterion can be defined while allowing the use of homogenization. Test average fields are applied since we don't know the exact far field at the macroscopic scale.

The third objective of this research work is to embed fatigue resistance into the optimization process. In order to tackle the problem in the context of the automotive industry, fatigue is studied for a high level of loading cycles, i.e., more than 10^3. Constraints are *de facto* used as design criteria. For this purpose, this third point is made in two steps. First, fatigue is introduced for proportional loads using global criteria, based on invariants, i.e., Goodman, Sines and Crossland. Then, more complex loads are considered using the Dang Van criterion built around a critical plan approach.

The general overview of the research work presented in this manuscript is illustrated in Figure 1.1 which represents the organization chart of the various works described in the following chapters.

All the theoretical developments presented in this thesis have been numerically implemented in Matlab®. The optimization algorithm used is the Matlab®version of the Method of Moving Assymptotes (MMA) [Svanberg(1987)]. The meshes are also generated using Matlab®functions.

1.4 Overview of the research work

Following this introduction, the remaining of this manuscript is organized as follows. Chapter 2 contains the main theoretical concepts used in the course of this research work. In particular, Sections 2.1. and 2.2 summarize the formulation of the density–based topology optimization problem as well as the general procedure for its resolution. Section 2.3 discusses stress constraints in topology optimization and in particular how they are introduced into porous materials. The relaxation procedure as well as the aspect of resolution effectiveness are also discussed.

In Section 2.5 the fatigue criteria used in this thesis are presented. The design of architectured materials is then discussed in Section 2.6. Chapter 3 reviews all the developments carried out during the research work and presents the main results. Chapter 4 provides a summary of the various written articles on which this manuscript is based. Finally, a general conclusion, summarizing all the discussions, and the perspectives for future work are held in Chapter 5.

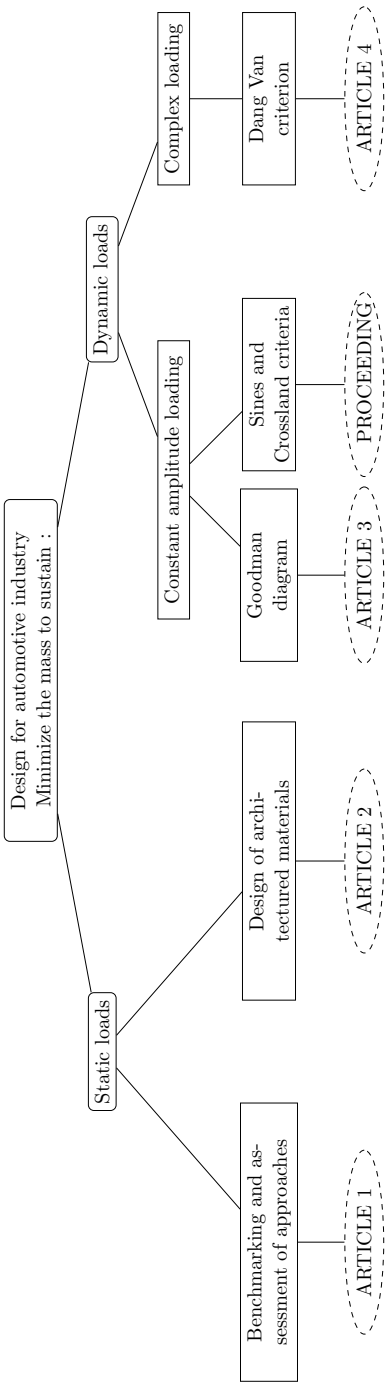

Figure 1.1: Overview of the thesis.

Chapter 2

Fundamental tools

Contents

This research work deals with the extensions of topology optimization techniques with stress and fatigue constraints whose implementation is described in Chapter 3. The present chapter focuses on the presentation of the fundamental concepts related to the research of optimal structures subjected to given requirements. In particular, a reminder regarding the fundamentals of optimization and, more precisely, of topology optimization is detailed. The basic principles of the method, the sensitivity analysis computation and the methods for updating the design variables are presented. The difficulties attributed to the introduction of strength specifications in topology optimization are next explained. The fatigue theory of components, which is necessary

for understanding the concepts contained within Chapter 3, is also discussed. Finally, the use of topology optimization in the context of material tailoring and, in particular, the numerical homogenization technique closes the theoretical presentation covered in this chapter.

2.1 Structural optimization

Since the late *1960's*, structural optimization has proven to be an extremely powerful tool to assist engineers and designers in their quest for optimized components. This approach considerably reduces "trials and errors" efforts and *de facto* makes the industrial process of bringing better products onto the market more efficient. Over the years, optimization methods have been improved to reach today a level of maturity adapted to industrial use. Structural optimization can be divided into three classes represented in Figure 2.1. The distribution into classes depends mainly on the nature of the design variables, i.e., the variables which can modify the design. The degree of design freedom increases with the degree of complexity and generality of the variables involved.

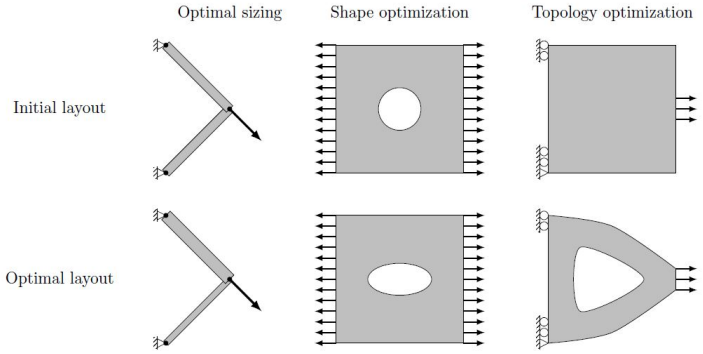

Figure 2.1: Illustration of structural optimization classes [Noël(2016)].

Size optimization. Structural optimization was originally applied to structures made of discrete elements such as beams, bars or shells. Design variables such as the thicknesses or the cross sections of these elements are automatically selected in order to obtain the most performing structure to meet the prescribed design requirements. Although historically important, this size optimization suffers from a lack of generality inherent to the structural elements that are considered. Indeed, the initial topology, i.e., the connections between the different elements, as well as the shape of the beams or bars cannot be modified. The design freedom is therefore limited and expected performance improvements are rather small. However, in engineering fields such as civil engineering and aeronautical structures, size optimization can be a valuable asset due to their extensive use of classical structural elements.

Shape optimization. The second class of optimization aims at improving the approach of size optimization by allowing changes in the structural shape for a given topology. The work initiated by [Zienkiewicz and Campbell(1973)] opened up new horizons in the field of optimal component design. Here, the design variables are linked to the components boundaries, i.e., their contours, via the nodal position of the finite element mesh or, better, using the description of the parametric curves of a Computer Aided Design (CAD) model. The shape modification of the

structure enables to improve the design of existing components in order to make them further able to meet the prescribed specifications. However, while reducing more substantially the design objective, the disadvantage of this class is the *a priori* knowledge of the initial topology of the component which cannot be modified by the optimization process.

Topology optimization. The last class of structural optimization problems overcomes the limitations inherent in the two previous ones. Indeed, topology optimization enables to define a new design concept based on a limited set of information such as boundary conditions, applied loads, characteristic dimensions of the final component and material data. The principle is to seek an efficient material distribution within the design domain in order to get a structure in accordance with given design criteria prescribed by the engineer. Design variables here are related to the presence or absence of material on specific regions of the design domain.

It is obvious that topology optimization offers a much greater design freedom but it also allows proposing layouts without any *a priori* knowledge about their initial appearance. Topology optimization is exploited in this research work.

The literature distinguishes classically two broad classes of topology optimization:

- Density–based methods as in ([Bendsøe and Kikuchi(1988)]).
- Level-set–based methods as in ([Osher and Sethian(1988), Allair et al.(2002)]).

The density–based methods are considered in this thesis and are described in more details in this manuscript. The Level-set methods, although having some advantages, are not developed here and interested readers can refer to dedicated contributions, see e.g., [van Dijk et al.(2013)] for a review.

2.1.1 Structural optimization and parametrization of the optimization problem

The density–based topology optimization approach which is considered in this thesis, was introduced in the late *1980's* with the founding work of [Bendsøe and Kikuchi(1988)]. Since then, the method has been continuously developed and is now sufficiently mature to be implemented as an industrial design tool. For a comparative and comprehensive review of the method, the reader may refer to the works of [Deaton and Grandhi(2014)] and [Sigmund and Maute(2013)] respectively.

In the following, the general principles of topology optimization with densities are summarized. Then a mathematical description of the structural optimization problem and various possible solution methods are given.

2.1.2 Density–based topology optimization

The objective of topology optimization, whatever the method, i.e., density or Level-set, is to find an optimal material distribution within a closed subspace of simple geometric form called the design domain. For density-based methods, the structural indicator function is discretized over the design domain using finite elements and assigns a design variable, x_e, to each one of them to reflect the presence or absence of material. Mathematically this is expressed by the following condition:

$$x_e = \begin{cases} 1, & \text{Material is present} \\ 0, & \text{Void is present} \end{cases} \tag{2.1}$$

The binary problem is often referred to as the black and white approach, i.e., black being the presence of material and white being the void. In order to introduce the concept of presence or absence of material, the design variables are assigned to the effective material properties of the components to be studied. In this research work, a linear elastic behavior is considered. Under these conditions, the design variable x_e can be introduced into the finite element analysis via the *Young's modulus* of the material within each element e as:

$$E_e(x_e) = x_e E_e^0, \tag{2.2}$$

where E_e^0 stands for the Young's modulus of the base material within the element. The analysis of Eqn. (2.2) illustrates that if the void (resp. the solid) is enforced on the element e the latter does not participate (resp. participates) to the total stiffness of the structure. Consequently, the mass of the element is given in terms of the design variable as:

$$m_e(x_e) = x_e m_e^0, \tag{2.3}$$

with m_e^0 the mass of the element.

However, the binary approach as described above is particularly difficult to solve leading to a large scale discrete non-linear optimization problem. Specific algorithms must be used. When a more accurate description of the structural boundaries is desired, a large number of design variables must be taken into account. Moreover, as mentioned in [Duysinx(1996)], this problem is poorly stated. As a result, the obtained numerical solutions are sensitive to the selection of some modeling parameters, namely, mesh size and element types. In addition, they unfortunately do not converge to an identical final layout with the mesh refinement. It is observed that composite structures made up of a mixture of void and solid tend to appear with increasingly finer mesh sizes. Let us cite however the work by [Beckers(1999)] which proposes a topology optimization procedure with discrete variables using an efficient dual method. A specially designed computer program has been developed allowing to deal with 2D and 3D discrete problems and to ensure the existence of the solution, the perimeter of the solid part is bounded.

To overcome the drawbacks mentioned above, it is advisable to relax the optimization problem by adding an intermediate phase to the two-phase material which is so far mentioned in this manuscript. In other terms, this is equivalent to consider porous materials between 0 and 1. This validates the idea that convergence is expected only in the larger set of structures made of composite materials with micro-perforations. In order to model these microstructures, the homogenization theory is used and will be discussed in detail in Section 3.1.4.

Besides to relaxing the design problem, the use of a porous material also allows eliminating the undesirable difficulty due to the discrete nature of the problem. In [Bendsøe(1989)], a very simple way to proceed is to use a power law to relate the mechanical properties of the material to the design variables as stated in Eqn. (2.4). This law, referred to as Solid Isotropic Material Interpolation law (SIMP)([Rozvany et al.(1994)]), allows intermediate densities to be taken into account while enforcing them towards solutions made of void or solid.

$$E_e(x_e) \quad = \quad x_e^p E_e^0, \tag{2.4}$$

In Eqn. (2.4), the exponent p is such that $p > 1$ and it is commonly chosen between 2 and 4 ([Bendsøe and Sigmund(2003)]). In this thesis, example are proceeded using a SIMP model, with an interpolation exponent of the stiffness equal to 3. Unlike the introduction of a microstructure, the use of this law no longer ensures a mathematical relaxation of the design problem and therefore the convergence of the solution with mesh refinement cannot longer

be guaranteed. However, there are many benefits to using this SIMP model. The material introduced is isotropic, i.e., only a single design variable is required, unlike homogenization methods with microstructures in which several variables are necessary. The simple numerical implementation effort and its reduced computational costs have greatly contributed to its success. Finally, the fact that the material can be used in many design criteria makes it robust and fairly general. Implementing SIMP model within a finite element code to perform topology optimization requires additional artifacts. Indeed, as stated above, the densities x_e can reach zero values to represent void. From a numerical point of view, this will induce zero stiffness terms within the stiffness matrix of the system and hence lead to its singularity so that its inversion is no longer possible. To circumvent this issue, a lower bound on the density value is generally imposed as follows: $x_e \in [x_{min}, 1]$ with $x_{min} = 10^{-3}$. Alternatively, note that if we want to impose a zero minimum gauge density, the SIMP law of Eqn. (2.4) can be modified as:

$$E_e(x_e) = E_{min} + x_e^p(E_e^0 - E_{min}), \tag{2.5}$$

with $E_{min} \in [10^{-9} - 10^{-6}]$. This law is referred to as the modified SIMP law and it exhibits certain advantages as discussed in [Sigmund(2007)]. Other interpolation laws are reported such as the RAMP law (Rationnal Approximation of Material properties) proposed by [Stolpe and Svanberg(2001b)] or the sinus hyperbolic model law by [Bruns(2005)]. In this work, SIMP law approach as described in Eqns. (2.4) and (2.5) is considered.

Finally, let us recall that the interpolation approach of the material properties as advocated above is subjected to mesh dependency. Several regularization techniques can be used to overcome this issue. Among others, filtering techniques are the most popular ones and a non-comprehensive comparison of these can be found in [Sigmund(2007)]. Filtering techniques have proven to be particularly attractive. The filter types used can be divided into *sensitivity filtering* and *density filtering* techniques. The difference between these two approaches as well as their respective mathematical expression are provided below. The essence of both regularization scheme is to construct the filtered quantities with respect to a weighted average of the information available in a given neighborhood around a particular element e. This neighborhood can be graphically illustrated considering an element e of a finite element mesh as pictured in Figure 2.2. The construction of the filtered densities (resp. sensitivities) are expressed in Eqn. (2.6) and Eqn. (2.7)

$$\frac{\tilde{\partial f}}{\partial \rho_e} = \frac{\sum_{i \in N_e} w_i \frac{\partial f}{\partial \rho_i}}{\rho_e \sum_{i \in N_e} w_i}, \quad \text{(sensitivity–based filtering)} \tag{2.6}$$

$$\tilde{\rho_e} = \frac{\sum_{i \in N_e} v_i w_i \rho_i}{\sum_{i \in N_e} v_i w_i}, \quad \text{(density–based filtering)} \tag{2.7}$$

where f stands for the objective or constraint(s) function(s), v_i for the element volume and w_i is a weighting factor. The latter can be determined using several expressions, see [Sigmund(2007)], but in this thesis, we consider the most usual formulation based on the distance rule:

$$w_i = r_{min} - |x_i - x_e|, \tag{2.8}$$

with r_{min} the prescribed radius filter and $|x_i - x_e|$ the distance between the centroïd of element i and e as illustrated in Figure 2.2. Let's note that N_e defines the number of elements in the neighborhood of the element e :

$$N_e = \{i, |x_e - x_i| \leq r_{min}\}, \tag{2.9}$$

The sensitivity filtering modifies the problem by smoothing out the design sensitivity whereas in the density filtering technique, the design variables, i.e., element densities, are mapped into physical ones. Performing a density-based filtering technique modifies also the design sensitivity, as for the the sensitivity filtering, but also the sensitivities of the constraints since the optimization process uses the new physical variables. Obviously, the corresponding sensitivities can be obtained by applying the chain rule relation.

Depending on the interpolation law, we note that in Eqn. (2.6) ρ_e should be defined as:

- If we use the SIMP law: ρ_e is the element density
- If we use the modified SIMP law than $\rho_e = \max(\varepsilon, \rho_e)$ with $\varepsilon = 10^{-3}$ in order to avoid a division by zero.

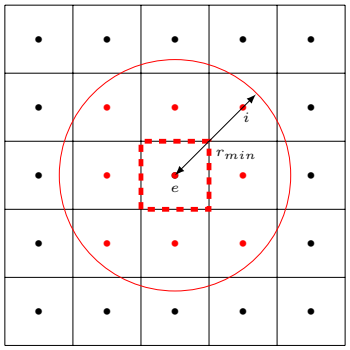

Figure 2.2: Illustration of the filtering radius on a finite element mesh.

2.1.3 Formulation of the optimization problem

After introducing the basic concepts of topology optimization, the structural optimization problem can be formulated under the general form, using the notations from [Duysinx(1997)], as:

$$\begin{array}{lll} \min\limits_{\boldsymbol{x}} & g_0(\boldsymbol{x}), & \\ s.t. & g_j(\boldsymbol{x}) & \leq 0, \\ & \underline{\boldsymbol{x}}_i \leq \boldsymbol{x}_i \leq \overline{\boldsymbol{x}}_i, & \end{array} \tag{2.10}$$

In (2.10), the objective function is denoted by $g_0(\boldsymbol{x})$ and the constraints by m design inequalities $g_j(\boldsymbol{x})$ with $j = 1, \cdots, m$ which are implicit functions of the n design variables, i.e., the densities $\boldsymbol{x}_i \in [0, 1]$ with $i = 1. \cdots, n$. Physically, the constraints $g_j(\boldsymbol{x})$ represent design restrictions, e.g., limitation in the stress level or volume constraints, while the lower and upper bounds ($\underline{\boldsymbol{x}}_i$ and $\overline{\boldsymbol{x}}_i$) are side constraints that limit the variation range of the design variables and which are generally tackled in a different manner by solution algorithms.

Note that this form is valid both for the density–based approaches considered here but also for the alternative Level-set methods. A discussion on how to solve the problem of Eqn. (2.10) is provided in the following sections.

2.2 Solution of the optimization problem

In the previous section, the problem of density–based topology optimization has been introduced. Once the problem has been defined, it has to be solved in the most effective way possible. Historically, the use of ***optimality criteria*** (OC) was the first approach employed to update the design variables following an iterative procedure. The advantage of the OC approach lies in its great efficiency in achieving the optimum in a few iterations. OC are based on a rigorous expansion of the Karush-Khun-Tucker optimality conditions (KKT). However, this type of approach is not free of disadvantages. Indeed, they are generally dependent on the problem under study and the convergence towards the optimum is not guaranteed ([Ma et al.(1993), Zhou and Sigmund(2017)]). Moreover, OC algorithms are generally adapted to cases where a single constraint is considered, which is not generally the case. In the context of stress constraints in structural optimization, the most famous optimality criterion is the *Fully-stressed Design* (FSD) ([Haftka and Gürdal(1992)]) which was interpreted as a low order expansion of stress constraints by [Fleury(1979b)].

Because of several difficulties encountered by the use of optimality criteria, a variety of different methods can be considered. A first category advocates an approach based on ***genetic algorithms*** (GA) ([Kennedy and Eberhart(1995), Mitchell(1996), Barnier and Brisset (1999), Eiben and Smith(2003), Simon(2013)]). There are many variations of GA methods but their fundamental principle is to mimic the process of natural selection to improve the performance of a population of potential solutions. First, an initial population of solutions is generated and a measure is associated with each of these responses according to the objective to be achieved. Generally one wants to minimize a quantity and therefore the smallest measure is the best. In a second stage, only the best candidate solutions are retained while the others are either discarded or recombined to generate new potential candidate solutions. This process is repeated as many times as needed until convergence, generating important computational time effort. Although this can be an obstacle, these methods find their limited interest in structural engineering problems where the information related to the gradients to be calculated is unavailable.

Alternatively, methods aiming at replacing the large size problems with small meta models are considered in ([Roux et al.(1998), Myers et al.(2009), Koziel and Leifsson(2013)]). Optimization is then carried out on these surrogate models for which approximation corrections can be provided during the optimization process in order to match closer to the original high fidelity model.

Finally, a widespread strategy is based on ***gradient-based Mathematical Programming*** techniques (MP). As seen in the previous section, the optimization problem defined by its objective function and its constrained function(s) is often implicit with respect to the design variables. In order to limit a too high computational burden, one solution consists in replacing the implicit original problem into a sequence of explicit problems for which the approximation of the functions can be handled by efficient MP methods. Generally, the functions take on a convex character. This method is known as ***Sequential Convex Programming*** ([Fox(1965), Fleury(1973), Schmit(1976), Fleury and Braibant(1986), Svanberg(1987), Fleury(1989a)]). The latter approach is considered in this thesis and presented in more detail hereafter.

2.2.1 Mathematical programming approach

The main reason to consider the MP approach is first its great flexibility and then its strong mathematical foundations to ensure convergence towards an optimum. Moreover, the ability to manage a large number of constraints is particularly attractive when it comes to study structural optimization for instance with many local constraints, e.g., stress constraints. However, it should be noted that this type of approach can be costly in terms of calculation time because of the

large scale nature of the problem ([Fleury(2007)]).

In what follows, we summarize the concept of structural approximation in convex sub-problems and their solution process is given. Subsequently, the theoretical foundations of a famous approximation scheme such as the Method of Moving Asymptotes (MMA) ([Svanberg(1987)]) are presented. In order not to weigh down this manuscript, only MMA scheme will be detailed because of its intensive usage in the numerical examples of Chapter 3.

2.2.2 Concept of convex approximation

The structural optimization problem of Eqn. (2.10) reveals an implicit dependency between the functions to be calculated and their design variables. The evaluation of these highly non-linear functions requires a significant computational cost which should be reduced. The convex approximation method can help meet this need and is based on two concepts. First, the implicit problem (2.10) is replaced by a sequence of explicit convex sub-problems around the current optimization point $\boldsymbol{x_0}$ as follows:

$$\begin{array}{lll} \min\limits_{\boldsymbol{x}} & \tilde{g_0}(\boldsymbol{x}), & \\ s.t. & \tilde{g_j}(\boldsymbol{x}) & \leq 0, \\ & \underline{\boldsymbol{x}}_i \leq \boldsymbol{x}_i \leq \overline{\boldsymbol{x}}_i, & \end{array} \tag{2.11}$$

where $\tilde{g_0}(\boldsymbol{x})$ and $\tilde{g_j}(\boldsymbol{x})$ are the convex approximations of $g_0(\boldsymbol{x})$ and $g_j(\boldsymbol{x})$ respectively. Note that in many applications, the lower and upper bounds ($\underline{\boldsymbol{x}}_i$ and $\overline{\boldsymbol{x}}_i$) are generally completed by *move-limits*, α_i and β_i as $\underline{\boldsymbol{x}}_i - \alpha_i \leq \boldsymbol{x}_i \leq \overline{\boldsymbol{x}}_i + \beta_i$ which further restrict the variations of the design variables in order to stabilize convergence.

Once the problem of Eqn. (2.10) is transformed into Eqn. (2.11), the sub-problems can be solved efficiently using dual methods ([Fleury(1979a)]), Sequential Quadratic Programming (SQP) methods ([Schittkowski(1985)]), or interior point methods ([Byrd et al.(1999)]).

As discussed in [Duysinx(1997)], the convex approximation has several advantages. First of all, this approach is adapted to a large variety of formulations of design problems and can also manage problems with one to a large number of constraints. Second, the direct consequence of restoring to convex functions allows optimal use of dual resolution methods that automatically select active constraints and reduce the size of the problem to the sub-space of non zero Lagrange multipliers. Finally, various structural approximations can be used.

2.2.3 Approximation schemes

An essential ingredient of the approximation is its accuracy while ensuring convex, explicit and ideally separable structure in order to take the most out of solution algorithms based on a dual approach. In addition, the complexity of implementing the approximation scheme should be kept to a minimum. Many schemes are available in the literature and differ from each other in their effectiveness, their formulation, i.e., the type of information required, or their implementation.

Among the most famous ones, are the first order methods with monotonic approximation based on reciprocal variables such as CONLIN (Convex Linearization) ([Fleury and Braibant (1986)]). The principle is to describe the functions by a Taylor development, truncated to the first order, around the current design point $x_i^{(k)}$ where (k) is the current iteration. Depending on the sign of the derivative, the reciprocal variables $(1/x_i^{(k)})$ are used instead of the direct variables $(x_i^{(k)})$. If the derivative is negative (resp. positive), the reciprocal variables (resp. direct variables) are selected. This allows writing a convex approximation of the response functions.

[Starnes Jr and Haftka(1979)] have shown that this method leads to the most convex approximation made of direct and reciprocal variables. However, CONLIN has a major drawback due to the constant curvature of the approximation. In order to overcome this inconvenience and to better represent the characteristics of the problem, [Svanberg(1987)] generalized the CONLIN scheme by introducing two mobile asymptotes in the approximation allowing to adapt to the curvature of the problem at the current point of design $\boldsymbol{x}^{(k)}$. This method is used in the present work. To introduce mobile asymptotes, two types of intermediate reciprocal variables are considered namely, $1/(U_i^{(k)} - x_i)$ and $1/(x_i - L_i^{(k)})$ leading to writing:

$$\tilde{g}_j(\boldsymbol{x}) = g_{0j} + \sum_{i=1}^{n} \left(\frac{p_{ij}^{(k)}}{U_i^{(k)} - x_i} + \frac{q_{ij}^{(k)}}{x_i - L_i^{(k)}} \right), \tag{2.12}$$

where $g_{0j} = g_j(\boldsymbol{x}^{(k)}) - \sum_{i=1}^{n} \left(\frac{p_{ij}^{(k)}}{U_i^{(k)} - x_i^{(k)}} - \frac{q_{ij}^{(k)}}{x_i^{(k)} - L_i^{(k)}} \right)$. The parameter $U_i^{(k)}$ and $L_i^{(k)}$ represent the upper and lower values of the asymptotes related to the variable x_i, and respect the property $L_i^{(k)} \leq x_i \leq U_i^{(k)}$. The coefficients $p_{ij}^{(k)}$ and $q_{ij}^{(k)}$ are never simultaneously non-zero and their setting to zero is conditioned by the following laws:

$$\begin{aligned} p_{ij}^{(k)} &= max\left\{0, \left(U_i^{(k)} - x_i^{(k)}\right)^2 \frac{\partial g_j}{x_i}\right\}, \\ q_{ij}^{(k)} &= max\left\{0, -\left(x_i^{(k)} - L_i^{(k)}\right)^2 \frac{\partial g_j}{x_i}\right\}, \end{aligned} \tag{2.13}$$

From Eqn. (2.13), setting $p_{ij}^{(k)}$ and $q_{ij}^{(k)}$ to zero depends on the sign of the derivative and means that only a single asymptote is enabled at a time leading to the monotonous behavior of the approximation.

Later, in order to create non-monotonic approximations, [Svanberg(1995), Svanberg(2002)] proposed to extend MMA by giving it a globally convergent character making use of the two asymptotes. Finally the update of the asymptotes is given by the relations:

$$L_i^{(k)} = x_i^{(k)} - s_i \left(x_i^{(k-1)} - L_i^{(k-1)}\right), \tag{2.14}$$

$$U_i^{(k)} = x_i^{(k)} + s_i \left(U_i^{(k-1)} - x_i^{(k-1)}\right), \tag{2.15}$$

where s_i is a parameter evaluated as a function of the variations of the design variables. Note that the same asymptotes are used for each constraint of the optimization problem. Adaptations can be made to perform approximations more specific to the constraints that are considered ([Bruyneel et al.(2002)]).

More elaborate schemes using information from the second derivative are also reported in the literature, see e.g., [Han(1976), Schittkowski(1981), Schittkowski(1985)] for the *Sequential Quadratic Programming* (SQP) method or [Fleury(1989b)] for a diagonalized version of the SQP. A second order version of MMA can be found in [Smaoui et al.(1988)] while [Duysinx(1997)] makes use of a sparse Broyden-Fletcher-Goldfard-Shanno (BFGS) formula to generate a sequence of diagonal Hessian matrices. A comparison of the performance of the different approaches is given in [Duysinx(1997)].

2.2.4 Sensitivity analysis

A key information when using structural approximations is the sensitivity of the constraints and objective functions with respect to the design variables. An accurate evaluation of the

derivatives is required in order to build a precise structural approximation of the original problem and not bias the optimization process. In the gradient method considered in this work, it is known that the computation of the sensitivities represents a significant part of the total computational effort. A judicious choice of the used approach is essential in order not to alter the efficiency of the process.

Generally, the considered functions in the optimization problems of this thesis, e.g., g_j with $j = 0, \cdots, m$, are of the form:

$$g_j = g_j(\boldsymbol{x}, \mathbf{U}(\boldsymbol{x}))), \tag{2.16}$$

where $\mathbf{U}$ is the unknown of the state equation. The total derivative is then written:

$$\frac{dg_j}{dx_i} = \frac{\partial g_j}{\partial x_i} + \frac{\partial g_j}{\partial \mathbf{U}} \frac{d\mathbf{U}}{d\boldsymbol{x}}, \tag{2.17}$$

In Eqn. (2.17), the term $\frac{\partial g_j}{\partial x_i}$ and the factor $\frac{\partial g_j}{\partial \mathbf{U}}$ are easy to evaluate and do not constitute a particularly expensive computational cost. The difficulty lies in evaluating the factor $\frac{d\mathbf{U}}{d\boldsymbol{x}}$. To evaluate the latter, different methods are available and are recalled below. Note that extensive and more complete reviews of the different approaches are given by [Haftka and Adelman(1989), Adelman and Haftka(1993), Tortorelli et Michaleris(1994), Van Keulen et al.(2005)]

Finite difference: The finite difference method is the simplest approach for numerically evaluating the derivatives of a function. The principle consists in writing a truncated Taylor series expansion to order one of g_j perturbed by an increment Δx_i :

$$g_j(\boldsymbol{x} + \boldsymbol{\Delta x}_i) = g_j(\boldsymbol{x}) + \boldsymbol{\Delta x}_i \frac{dg_j}{dx_i} + \mathcal{O}(\Delta \boldsymbol{x}_i), \tag{2.18}$$

By neglecting the terms $\mathcal{O}(\Delta \boldsymbol{x}_i)$ the derivative being searched is expressed by:

$$\frac{dg_j}{dx_i} \approx \frac{\Delta g_j}{\Delta x_i} = \frac{g_j(\boldsymbol{x}_i + \Delta \boldsymbol{x}_i) - g_j(\boldsymbol{x})}{\Delta x_i}, \tag{2.19}$$

where $\Delta \boldsymbol{x}_i = [0, \cdots, 0, \Delta x_i, 0, \cdots, 0]$. To reduce the truncation errors, it appears that the smaller the increment $\Delta \boldsymbol{x}_i$, the more accurate the approximation. However, too small disturbance values may impair the quality of the solution due to numerical rounding errors ([Green and Haftka(1991)]). In addition to these errors, precision discretization can also be problematic and lead to inaccuracies ([Moin(2010)]).

The main advantage of the finite difference method is its great versatility, i.e., it can be used for any type of problem, and it is easy to implement. However, these come at the cost of a significant computational effort. Indeed, to evaluate the derivative of g_j with respect to each design variable, a successive perturbation of the latter must be performed. Numerically this means that for each disturbance, a new finite element analysis, i.e., a stiffness matrix assembly procedure ($\mathbf{K}(\boldsymbol{x})$) and a static problem solution (2.20), must be realized.

This method is not advised for large scale problems but is an undeniable asset when concepts need to be validated or when it comes to verify whether the sensitivity computation by an alternative method is correct.

Direct differentiation: The direct differentiation method enables the evaluation of the factor $\frac{d\mathbf{U}}{d\boldsymbol{x}}$ of Eqn. (2.17) by differentiating the state equation of the optimization problem with respect to the design variables. In this thesis, this considered state equation is the static equation of equilibrium given by the following expression (2.20):

$$\mathbf{K}(\boldsymbol{x})\mathbf{U}(\boldsymbol{x}) = \mathbf{F}(\boldsymbol{x}), \tag{2.20}$$

Evaluating the derivative of Eqn. (2.20) with respect to the design variables, it comes:

$$\frac{\partial \mathbf{K}}{\partial x_i}\mathbf{U} + \mathbf{K}\frac{\partial \mathbf{U}}{\partial x_i} = \frac{\partial \mathbf{F}}{\partial x_i}, \tag{2.21}$$

This allows isolating the quantity of interest $\frac{\partial \mathbf{U}}{\partial x_i}$:

$$\mathbf{K}\frac{\partial \mathbf{U}}{\partial x_i} = \frac{\partial \mathbf{F}}{\partial x_i} - \frac{\partial \mathbf{K}}{\partial x_i}\mathbf{U}, \tag{2.22}$$

Rearranging the terms of Eqn. (2.22) brings up a *pseudo static problem* in which the *pseudo load* is given by $\frac{\partial \mathbf{F}}{\partial x_i} - \frac{\partial \mathbf{K}}{\partial x_i}\mathbf{U}$ and the *pseudo response* by the amount of interest $\frac{\partial \mathbf{U}}{\partial x_i}$. After solving the problem of Eqn. (2.22), the solution is introduced in Eqn. (2.17) to calculate the complete derivative of g_j.

This method, although more efficient than the finite difference method due to the use of the same stiffness matrix $\mathbf{K}(\boldsymbol{x})$, has a major drawback. Indeed, it requires the solutions of as many pseudo-problems (2.22) as the number of design variables x_i.

Adjoint approach: The purpose of the adjoint approach is to eliminate the term $\frac{\partial \mathbf{U}}{\partial x_i}$ from the derivative evaluation $\frac{dg_j}{dx_i}$. The principle is to construct the augmented function $\widehat{g_j}$ using the state equation as follows:

$$\widehat{g_j} = g_j(\boldsymbol{x}, \mathbf{U}(\boldsymbol{x})) + \boldsymbol{\lambda}^T(\mathbf{K}(\boldsymbol{x})\mathbf{U}(\boldsymbol{x}) - \mathbf{F}(\boldsymbol{x})), \tag{2.23}$$

where $\boldsymbol{\lambda}$ is an arbitrary Lagrange multiplier vector associated with the g_j constraint. Note that proceeding as indicated in Eqn. (2.23) comes down to adding to the original constraint g_j a null term and consequently does not modify the initial problem. Indeed, as soon as the static problem is solved, the condition $\mathbf{K}(\boldsymbol{x})\mathbf{U}(\boldsymbol{x}) - \mathbf{F}(\boldsymbol{x}) = \mathbf{0}$ is fulfilled and the second term of Eqn. (2.23) is null leading to the equality $\widehat{g_j} = g_j$. Differentiating, Eqn. (2.23) with respect to the design variables x_i and reorganizing the terms, it comes:

$$\frac{d\widehat{g_j}}{dx_i} = \frac{\partial g_j}{\partial x_i} + \boldsymbol{\lambda}^T\left(\frac{\partial \mathbf{K}(\boldsymbol{x})}{\partial x_i} - \frac{\partial \mathbf{F}(\boldsymbol{x})}{\partial x_i}\right) + \frac{\partial \mathbf{U}}{\partial x_i}\left(\frac{\partial g_j}{\partial \mathbf{U}} + \boldsymbol{\lambda}^T\mathbf{K}(\boldsymbol{x})\right), \tag{2.24}$$

In the expression (2.24) above, the term of interest $\frac{\partial \mathbf{U}}{\partial x_i}$ is still present and unknown. In order to set it to zero, a judicious choice of the $\boldsymbol{\lambda}$ vector has to be made, the latter being arbitrary. Doing so, the second term of expression (2.24) is cancelled for $\boldsymbol{\lambda}$ given by:

$$\boldsymbol{\lambda}^T\mathbf{K}(\boldsymbol{x}) = -\frac{\partial g_j}{\partial \mathbf{U}}, \tag{2.25}$$

Expression (2.25) is known as the *adjoint problem* in which the term $-\frac{\partial g_j}{\partial \mathbf{U}}$ is called the *adjoint load*. The Lagrange multiplier, $\boldsymbol{\lambda}$, is usually referred to as the *adjoint vector*. The evaluation of the desired derivative is obtained once the solution of the associated adjoint problem has been determined. The benefits and the efficiency of the adjoint approach lie in the fact that it is only required to solve one adjoint problem per constraint g_j. The stiffness matrix is identical and should not be reassembled as for the direct differentiation. It appears that if the number of constraints tends towards the number of design variables, then the adjoint method and the direct differentiation method become equivalent. The adjoint method is therefore particularly well indicated to the case where the number of constraints is lower than the number of design variables.

In this thesis, the adjoint approach is considered to evaluate the sensitivities of the constraints with respect to the design variables. The methods used to solve the various examples illustrated in Chapter 3 imply a number of constraints to be considered that are always smaller than the number of design variables. The adjoint approach is therefore generally more effective than a direct approach and will be particularized in the case of stress and fatigue constraints in the next chapter.

2.2.5 Solution procedure of the sub-problems

In the previous sections, the concept of structural approximation and sensitivity analysis was introduced. All the tools are now in hand to solve the optimization problem of Eqn. (2.10)

The general procedure can be summarized as follows:

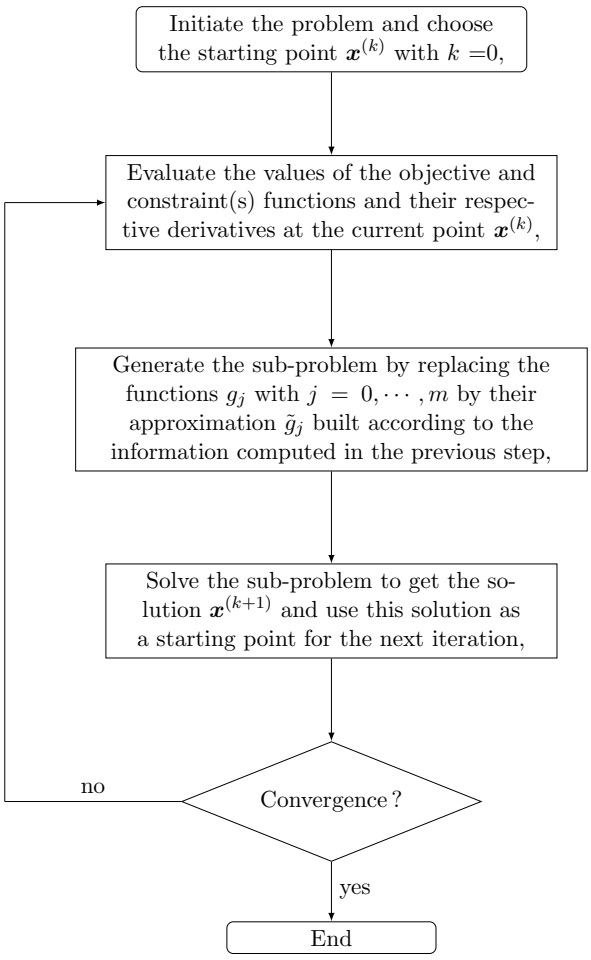

Figure 2.3: General procedure of an optimization loop.

Remember that point 4 of the procedure strongly depends on the scheme used. For example, a separable convex scheme should better be handled by a dual approach because of its high efficiency ([Fleury(1993)]). To check convergence, several stopping criteria are used and reported in the literature. The most usual ones are based on either evaluating the design changes between two successive iterations or the changes of the objective values. A maximum

number of iterations can also be specified as well as a verification of the stabilization of the KKT optimality conditions. Regardless of the chosen stopping criterion, the latter must be specified when presenting optimized solutions. In this work, we choose to check the difference between two successive designs, i.e., we evaluate the variation of the density maps between two iterations that should be lower than a prescribed threshold.

2.3 Stress constraints in topology optimization

The core of this research work is the concept of stress constraints introduced into the structural optimization process. As indicated in [Duysinx et al.(2008)], it is essential to consider material failure in the formulation of the optimization problem because of the particular solution behavior and in order to minimize as much as possible the post-processing operations. Indeed, when different materials are considered, when the tensile and compressive yield strengths are different or in the presence of several load cases, the optimized topology may look very different from the one given by a maximum stiffness. Over the years and since the first work on truss structures, various contributions on the subjected have highlighted the challenges of this type of problem. Indeed, stress constraints are part of the so–called *vanishing constraints* [Achtziger and Kanzow(2008)] and are subject to the *singularity problem* ([Kirsch(1989,1990)]) preventing gradient–based algorithms to reach near the optimum. Later, the introduction of strength criteria into the topology optimization for continua ([Duysinx and Bendsøe(1998)]) raised the significant computational burden associated with this type of problems. Indeed, it is desirable from an engineering point of view to maintain the level of the stresses all over the structure under a prescribed value. Solving this problem in the continua by the finite elements method implies that the value of the stresses must be controlled at each discrete points where the stresses are evaluated. This inevitably leads to a large scale optimization problem with a large number of restrictions that quickly becomes difficult to manage for industrial applications. Finally, due to their intrinsic nature, stress constraints represent non-linear functions that must be treated accordingly using adapted solution algorithms.

Beside the various contributions aiming at addressing the posed challenges, numerous research projects have made possible to extend the use of the stress constraints in topology optimisation. For example, we can cite the introduction of strength requirements in thermal problems ([Deaton and Grandhi(2013), Takezawa et al.(2014)]). In the work of [De Leon et al.(2015)], the authors are interested in the effects of mechanical strength in compliant mechanisms design. The work of [Lee et al.(2012)] introduced stress constraints into problems involving the self–weight of the structures. The contribution of [Amir(2017)] proposed an approach to deal with stress constraints based on an elastoplastic model and the contribution of [Zhang et al.(2017)] allowed to design structures made by the assembly of discrete elements such as beams or bars. Finally, topology optimization and shape optimization with stress constraints are combined in [Lian et al.(2017)] and [Kuci(2018)].

In this section, various theoretical aspects and issues related to stress–based topology optimization are recalled. First, the choice of the stress criterion within the porous SIMP material is presented. Then, the concept of *relaxation* of the problem is widely discussed and illustrated. Finally, the so-called aggregation techniques, essential for dealing with large scale problems, are introduced and a brief discussion of their behavior is given. As for the non-linear aspects of stress constraints, it can be managed by using optimization algorithms based on a structural approximation, see Section 2.2, and will not be further discussed. Note that the developments in this chapter are intended to be as general as possible and the particular aspect of the numerical implementation will be carried out in Chapter 3.

2.3.1 Choice of a suitable stress criterion

Stress computation with the finite elements method

This section aims at illustrating how the stress computation is performed in this work. The purpose is not to recall the complete theory of the finite elements method but rather to formalize the approach in order to allow the reader to get used with the notations used in the following chapter.

As stated previously, the linear static equation is considered in this work. Its discretized expression written into the finite elements formalism is reminded in Eqn. (2.26)

$$\mathbf{KU} = \mathbf{F}, \tag{2.26}$$

where $\mathbf{K}$, $\mathbf{U}$ and $\mathbf{F}$ represent the structural stiffness matrix, the structural displacement vector and the load vector respectively. Once the solution of the static problem is known, it is possible to calculate the value of the stresses within the elements. To do this, let us consider an element e of the first order with bilinear interpolation shape functions , i.e., element of type Q4, represented in figure 2.4.

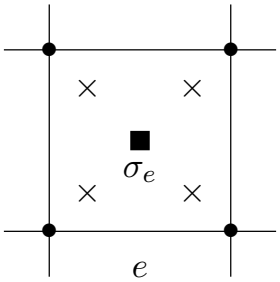

Figure 2.4: Illustration of a Q4 type element and the location of stress evaluation.

In the finite element theory, see e.g., [Neto et al.(2015)], the strain over the element e is linked to the element displacement ($\mathbf{U}_e$) through the following relationship:

$$\boldsymbol{\varepsilon}_e = \mathbf{B}_e \mathbf{U}_e, \tag{2.27}$$

with $\mathbf{B}_e$ the strain-displacement matrix evaluated at the Gauss points of the elements. The value of the stress, generally displayed during the post-processing phase, represents the mean of the equivalent Von Mises stress evaluated at each Gauss point. In the particular case of the Q4 element, this equivalent stress is directly accessible by evaluating it at its centroïd represented by the black square in Figure 2.4. Thus, in order to speed up the computational procedure, only one evaluation is required per element. This option is used in the remainder of this manuscript. From a topology optimization point of view, doing so means that only one sensitivity analysis is required per element, which greatly reduces the computational burden of the optimization process. Doing so, the remaining of the discussion will focus on the stress evaluation at the centroïd of the element e. Assuming a linear elastic behavior, one can relate the strain to the stresses by Hooke's law:

$$\boldsymbol{\sigma}_e = \mathbf{E}_e \boldsymbol{\varepsilon}_e = \mathbf{E}_e \mathbf{B}_e \mathbf{U}_e = \mathbf{T}_e^0 \mathbf{U}_e, \tag{2.28}$$

where $\mathbf{E}_e$ stands for the matrix of elasticity coefficients defined on element e and $\mathbf{T}_e^0$ is the stress matrix. Knowing the vector of constraints $\boldsymbol{\sigma}_e$ enables to calculate the equivalent Von Mises

stress at the centroïd of the element. Following the notations of [Duysinx and Sigmund(1998)], the latter is written:

$$\sigma_e^{\text{VM}} = \sqrt{\mathbf{U}_e^T \mathbf{M}_e^0 \mathbf{U}_e}, \tag{2.29}$$

where $\mathbf{M}_e^0 = \mathbf{T}_e^{0,T} \mathbf{V} \mathbf{T}_e^0$ with $\mathbf{V} = \begin{pmatrix} 1 & -1/2 & 0 \\ -1/2 & 1 & 0 \\ 0 & 0 & 3 \end{pmatrix}$.

Let's note that the displacement formulation, adopted in this work, is known to suffer from a lack of accuracy in approximating the stress field. In addition, inaccuracies of the stress field evaluation in the context of density-based topology optimization is also due to the jagged nature of the optimized structure. Mesh refinement can be used to overcome this issue, but significantly increases the CPU time required. Although conventional discretization methods cannot predict the exact value of stress concentrations, they are able to detect their location and mitigate them through the optimization process. Several research projects focus on solving these inacurate problems in the context of stress-based topology optimization. For example, [Bruggi and Venini(2008), Bruggi and Cinquini(2009), Bruggi(2016)] used the stresses as primary variables, while [Svärd(2015b)] proposed an extrapolation of the inner value of constraints across the design boundary.

Stress criterion inside the porous material

In [Duysinx and Bendsøe(1998)], the authors developed an approach to consider stress constraints within a topology optimization problem in the continua, i.e., approach with densities. In their founding contribution, they considered a strength criterion within porous laminated materials of rank-1 and rank-2. This type of rank-N material relaxes the problems and leads to a well–posed formulation (from a mathematical point of view) ensuring a mesh independent solution and simultaneously circumvent the binary nature of the problem by providing continuous variables. However, from an implementation point of view, porous materials such as SIMP are preferable so the introduction of a consistent strength criterion within this SIMP material law is desirable. The goal is to link the macroscopic stress $\langle \sigma_e \rangle$ to the actual microscopic stress state σ_e within the porous material as sketched in Figure 2.5.

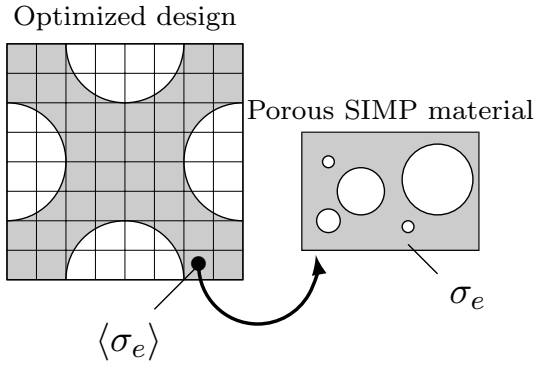

Figure 2.5: Schematic of a SIMP material within an optimized structure.

In the particular case of SIMP materials, the stress within an element e can be written:

$$\langle \sigma_e \rangle = \langle E_e \rangle \langle \varepsilon_e \rangle = x_e^p E_e^0 \langle \varepsilon_e \rangle, \tag{2.30}$$

The relationship between $\langle\sigma_e\rangle$ and σ_e is given by:

$$\langle\sigma_e\rangle = A(x_e)\sigma_e, \tag{2.31}$$

with $A(x_e)$ the localization tensor depending on the microstructure. One seeks for a localization tensor $A(x_e)$ that should meet the following specifications:

- Be as simple as possible to facilitate implementation.
- Provide a finite stress value for densities tending towards zero.

Inspired by the requirements of the strength criterion on rank–2 laminated materials, the first condition is met by choosing $A(x_e) = \frac{1}{x_e^q}$, with q the stress interpolation parameter. Thus the microscopic stress within the SIMP material can be written as:

$$\sigma_e = \frac{\langle\sigma_e\rangle}{x_e^q} = x_e^{p-q} E_e^0 \langle\varepsilon_e\rangle, \tag{2.32}$$

the second condition is satisfied if $p = q$ in order to ensure physical consistency. We finally have:

$$\sigma_e = E_e^0 \langle\varepsilon_e\rangle, \tag{2.33}$$

Although the stated conditions are met, the model presented above is in breach. Indeed, it appears that stresses are not zero for zero densities and dependent of the strain value within the element. The latter can be huge and is at the origin of the singularity problem discussed in Section 2.3.2. As we shall see, the definition of the strength criterion within the SIMP material law remains applicable provided that precautions are taken to circumvent the stress singularity problem.

2.3.2 Singularity of the stress–based optimization problem

The early work on optimization of truss structures ([Sved and Ginos(1968)]) highlighted the difficulty of dealing with stress constraints. Indeed, the use of gradient–based algorithms does not allow to reach the global optimum of the problem. This phenomenon referred to as the *singularity phenomenon* by [Kirsch(1989), Kirsch(1990)] has been the subject of many research investigations to determine its origin, see e.g., [Cheng and Jiang(1992), Rozvany and Biker(1994), Rozvany(1996), Rozvany(2001)]. In many applications, it was shown that the global optimum is located in a degenerated sub-domain, i.e., lower-dimensional, than the dimensions of the original problem, preventing the optimization algorithm from reaching it and leading the optimization process to a region of the design space with local optima. In concrete terms, the singularity problem occurs when unnecessary small elements of the structure, which quickly reach the prescribed stress limit, cannot be removed while obviously they should be suppressed from the optimized solution. In case of a truss frame, for a given load, stress is inversely proportional to cross-sectional area. When the optimization tends to decrease their cross section, stresses within bars (or beams) increase a lot and reach their maximum allowable value, which is difficult, if not impossible, to be removed. In the density approach, as density within an element decreases, the strain undergone by that element increases as well and so does the stress. The final structure eventually exhibits large grey areas.

The purpose of this section is to illustrate the effect of the relaxation scheme in stress constrained topology optimization using simple structure, i.e., a truss made of bar elements.

Altough different methods are available to relax the stress constraints and to solve the problem using gradient–based algorithms, we discuss here, only two methods, commonly called ε-relaxation and *qp*-relaxation. The choice of these two methods is motivated by the fact that the ε-relaxation is historically the first one to popularize the relaxation of the constraints. As for the *qp*-relaxation approach, it allows an easy implementation while providing the relaxation effect. The *qp*-relaxation exploits the fact that using different interpolation exponents of the stiffness (p) and the stresses (q) with $q < p$, see Eqn. (2.32), provides the expected relaxation. A third method has been recently very popular in recent contributions, see e.g., [Le et al.(2010), Holmberg et al.(2013), Holmberg et al.(2014), Lee et al.(2012), Zhang et al.(2017)], and consists in multiplying the stress matrix ($\mathbf{T}_e^0$) by a so-called relaxation function ($\eta_T(x)$) whose properties are given below

$$\eta_T(x) = \begin{cases} 1, & \text{Material is present} \\ 0, & \text{Void is present} \end{cases} \tag{2.34}$$

The function must preserve the constraints at full density and suppress them at zero density. This approach defined as the *relaxed constraint* ([Le et al.(2010)]) generally uses a relaxation function $\eta_T(x) = x^{1/2}$ which is a special case of *qp*-relaxation. Its effect on the design space is therefore similar. Many functions can be used to achieve the desired relaxation effect, and providing a complete comparison of their capabilities would be beyond the scope of this work.

To illustrate the effect of the relaxation scheme, the popular example of the three-bar truss, see [Stolpe and Svanberg(2001a), Bruggi(2008)], is revisited and its geometry and boundary conditions are represented in Figure 2.6. Nodes II, III, IV are fixed while two load conditions are applied at node I. All bars are made of the same material, i.e., Young modulus $E_i = 1$,Poisson's ratio $\nu_i = 0.3$, stress limit $\sigma_{y,t}^0 = \sigma_{y,c}^0 = 3$, have the same cross section areas, i.e., $A_{0,i} = 1$ and the following respective lengths $L_1 = L_3 = \sqrt{2}$ and $L_2 = 1$ with $i = 1, \cdots, 3$. The two loads are defined by : $F_1 = (0, 1.5)^T$ and $F_2 = (1, 0)^T$.

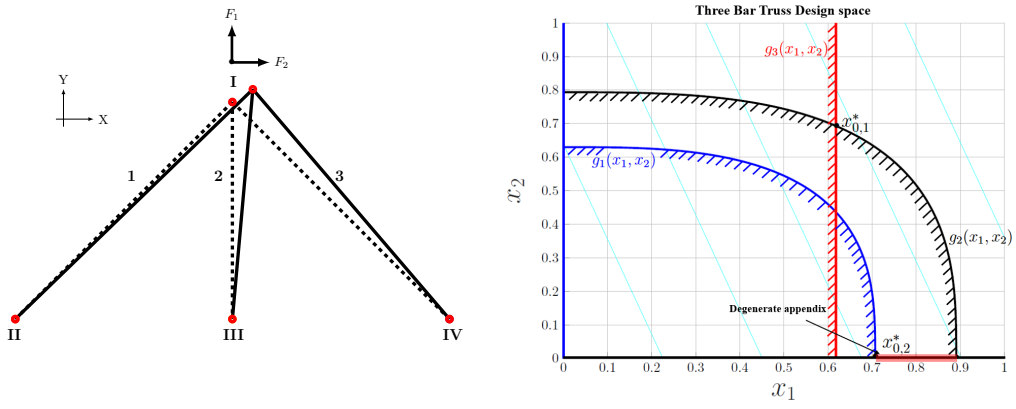

(a) (b)

Figure 2.6: Illustration of the three-bar truss problem: (a) Geometry (b) Design space of the three-bar truss.

As highlighted in [Bruggi(2008)], a rigorous comparison of the relaxation approaches can only be made when the design variables are written in terms of the densities. Indeed, a truss problem uses the cross sections of the bars as design variables. So, we can write the latter as $x_i A_{0,i}$ where $A_{0,i}$ is the nominal cross section. Design variables are given by densities x_i with $i = 1, \cdots, 3$. Let's consider only symmetric designs so that $x_1 = x_3$ and, for convenience,

only x_1 and x_2 are kept in the optimization problem. It comes that the topology optimization problem of Eqn. (2.35) can be written as:

$$\begin{cases} \underset{x_1,x_2}{min} & 2\sqrt{2}x_1 + x_2, \\ s.t. & g_1(x_1,x_2) \leq 0, \\ & g_2(x_1,x_2) \leq 0, \\ & g_3(x_1,x_2) \leq 0. \end{cases} \tag{2.35}$$

where the three constraints, i.e., g_1, g_2, g_3, are calculated using a finite elements analysis. The final expressions of the constraints using ε-relaxation and *qp*-relaxation are provided in Table 2.1. The full developments made to derive these are described in details in Appendix C.

	ε-relaxation	*qp*-relaxation
$g_1(x_1,x_2)$	$\left(\frac{0.75}{\frac{x_1^p}{\sqrt{2}}+x_2^p} - 3x_1^p\right) - \varepsilon/x_1,$	$\frac{0.75}{\frac{x_1^p}{\sqrt{2}}+x_2^p} - 3x_1^q,$
$g_2(x_1,x_2)$	$\left(\frac{1.5}{\frac{x_1^p}{\sqrt{2}}+x_2^p} - 3x_2^p\right) - \varepsilon/x_2,$	$\frac{1.5}{\frac{x_1^p}{\sqrt{2}}+x_2^p} - 3x_2^q,$
$g_3(x_1,x_2)$	$\left(\frac{1}{\sqrt{2}} - 3x_1^p\right) - \varepsilon/x_1,$	$\frac{1}{\sqrt{2}} - 3x_1^q,$
	$\varepsilon^2 \leq x_1, x_2 \leq 1\ ,$	$0 \leq x_1, x_2 \leq 1,$

Table 2.1: Stress constraints for the example of the three-bar truss in the context of the ε-relaxation and the *qp*-relaxation.

Figure 2.6(b) represents the design space of problem (2.35) with the isolevel curves of the objective function and the trace of the constraints, i.e., $g_i = 0$ with $i = 1, \cdots, 3$, represented in bold lines. Let's note that those curves are pictured for $p = 3$. On this picture, two optima can be distinguished. A local optimum $x^*_{0.1} = (0.617, 0.700)^T$ and a global optimum $x^*_{0.2} = (0.708, 0.00)^T$. This example perfectly illustrates the singularity problem of the stress constraints for which the global optimum is located in a degenerate sub-space of the design space.

To solve this problem, the constraints are modified to be able to access to the region in which the global optimum is located. The traces of the relaxed stress constraints obtained, after the implementation of the relaxation methods, are represented with dotted lines in Figure 2.7. As discussed in [Verbart(2015)], the ε-relaxation perturbs the constraints more locally than the *qp*-relaxation, which is clearly visible in this example.

Figure 2.8 shows the shape of the constraint $g_2(x_1, x_2)$ for various relaxation parameter values and for both considered approaches. Note that the choice of this constraint is arbitrary. Similar behaviors are observed when considering the other constraints. As expected, for increasing values of the q parameter (resp. decreasing values of the ε parameter), the original singular aspect of the constraint is recovered. As seen in Figure 2.8(b), once a high value of the q parameter is reached, here $q = 2.9$, the global optimum is difficult to reach by minimization sequence generated by gradient–based algorithms. Numerical experiments have confirmed that in most cases, the value of q should be such as $2.5 \leq q \leq 2.8$ in practice. Nevertheless, this rule is not valid in the case of the ε-relaxation as illustrated in Figure 2.8(a) where even for small values of the relaxation parameter, the global optimum remains accessible. However, tests have shown that a low value of this parameter can lead to instabilities in the convergence process. In order to get a weakly disturbed problem, it is common to assign the ε-relaxation of a continuation procedure, e.g., $\varepsilon = 0.01 \longrightarrow 0.001$ in the course of optimization. Although this

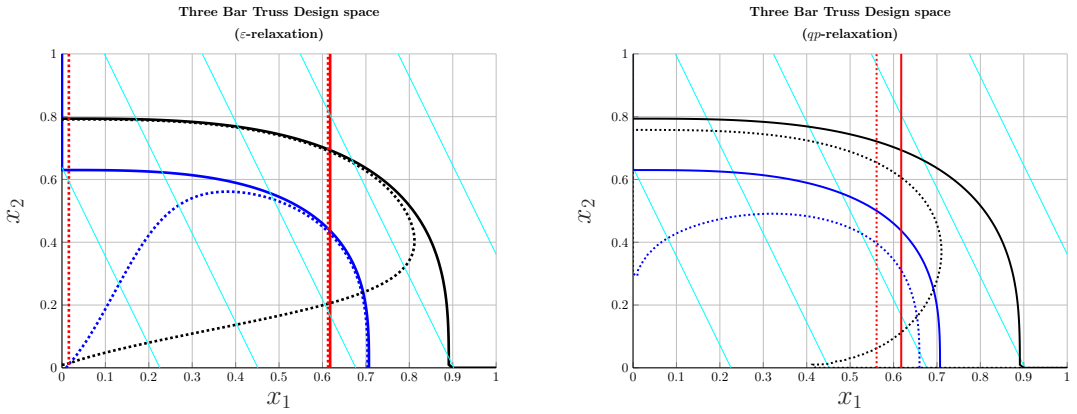

(a) (b)

Figure 2.7: Illustration of the relaxation of the design space: (a) ε-relaxation ($\varepsilon = 0.01$), $p = 3$ (b) qp-relaxation ($q = 2.5$), $p = 3$.

is justified, doing so increases the convergence time, see [Duysinx and Sigmund(1998)]. With respect to the use of a continuation process for qp-relaxation, its overall disruptive effect does not require such a procedure. It can however be considered as we will see in the next chapter and in particular as discussed in the PROCEEDING. In his Phd, [Verbart(2015)], looked at the detailed comparison of the relaxation methods described above. His observations revealed, that even though both methods provide the expected relaxation effect, the qp-relaxation perturbs the original constraints in the entire density range which is beneficial for gradient–based optimization algorithms as considered in this work. This last comment is the main reason why in the remainder of this research, the qp-relaxation approach is adopted in the numerical examples of Chapter 3.

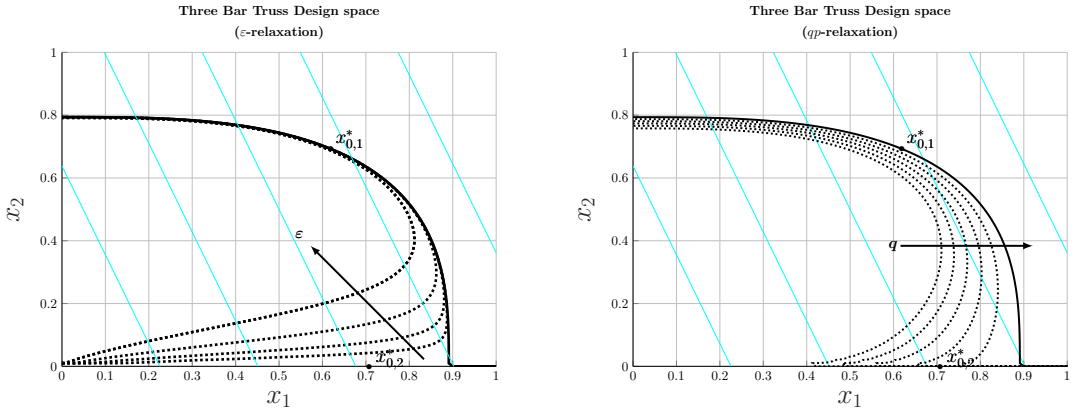

(a) (b)

Figure 2.8: Shape of constraint $g_2(x_1, x_2)$ for different values of the relaxation parameters: (a) ε-relaxation with $\varepsilon = 10^{-1}, 10^{-2}, 10^{-3}, 10^{-4}, 10^{-4}, 10^{-5}$, $p = 3$ (b) qp-relaxation with $q = 2.5, 2.6, 2.7, 2.8, 2.9$, $p = 3$.

2.3.3 Aggregation methods for large scale problems

One of the major challenges associated with the introduction of stress constraints, and which still remains up to now an open question, is the high computational time required to solve the stress constrained problem. When tackling large scale problems, the solution of the state equation(s), e.g., the problem of static equilibrium, should not be dissociated from the treatment of design variables and their update. Conventional direct solvers are no longer suitable and the large size of the problems implies considering specific solution methods such as iterative solvers, parallel computing techniques or alternative condensation models. Such techniques are not considered in this manuscript and interested readers can refer to the following works for further information [Saad(2003), Golub et Van Loan(1996), Vassilevski(2008)].

Once the solution of the state equation has been found, the optimization problem can be solved. When considering local constraints, i.e., stress restrictions in each finite element, one has to deal with a huge optimization problem to solve. To circumvent this issue, one should reduce the number of constraints. For instance, one useful strategy is to select the local constraints in order to keep only the most critical ones under a prescribed limit. This method is referred to as the *local approach with active-set* initiated in [Duysinx and Bendsøe(1998)]. Additional performance can be gained if a global compliance constraint is added to the problem as described in [Bruggi and Duysinx(2012)]. Although interesting results are obtained using methods exploiting an active-set selection strategy, its usage for industrial applications remains limited. To overcome this difficulty, [Duysinx and Sigmund(1998), Yang and Chen(1996), Paris et al.(2009)] proposed to aggregate the set of local constraints, using continuous aggregation functions, in order to get a single value which is a representation of the maximum local value. Many types of aggregation functions are reported in the literature. This work considers only three of them, namely the p-norm/p-mean functions and the Kresselmeier-Steinhauser(KS) function whose analytical expressions are summarized in Table 2.2 below.

p-norm (σ_{PN})	p-mean (σ_{PM})	KS (σ_{KS})
$\left(\sum_e^{NE} \sigma_e^r\right)^{1/r}$,	$\left(\frac{1}{NE}\sum_e^{NE} \sigma_e^r\right)^{1/r}$,	$\frac{1}{r} ln\left(\sum_e^{NE} e^{r(\sigma_e)}\right)$,

Table 2.2: Mathematical expression of the p-norm, p-mean and KS aggregation functions.

In these mathematical expressions, e represents the element index, r the aggregation parameter and NE the total number of elements to be aggregated.

To illustrate the behavior of such functions with increasing aggregation exponent, let's consider a distribution of local constraints represented in Figure 2.9(a). The aggregation of this local field by the aggregation functions of Table 2.2 and for various values of the aggregation parameter r is represented in Figure 2.9(b).

As can be seen, the p-norm and the KS approaches approximate the maximum value by excess whereas the p-mean approaches by below. This different behaviors of the aggregation functions have a direct impact on the final topology and the resulting optimized local stress field. Indeed, an approach by excess (resp. by below) leads to a stress field whose real local value is lower (resp. higher) than the admissible stress limit. In addition, for any function, it should be noted that the larger the aggregation exponent, the closer it is to the actual

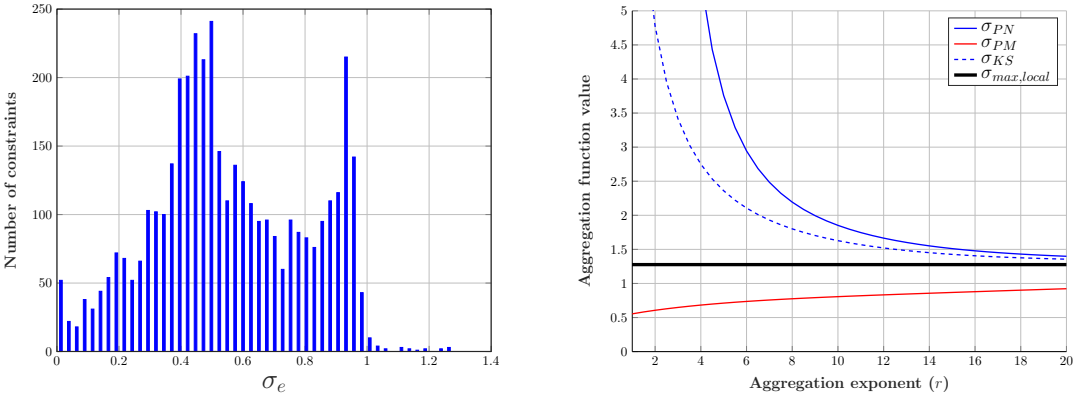

(a) (b)

Figure 2.9: Illustration of the value of the agglomeration functions as a function of the value of the agglomeration parameter: (a) Local sample to be agglomerated (b) Aggregation for various values of the aggregation parameter.

maximum value. Numerically, a high exponent value introduces additional non-linearities into the optimization problem that can lead to significant convergence issues. However, the global approach as described above requires a rather high value of the exponent in order to capture at best the maximum value while avoiding as much as possible the oscillations caused by a too non-linear behavior. Stabilization procedures, e.g., use of move-limits or more conservative MMA approximations, are therefore required. Finally, note that a default p-mean approach makes the aggregation method less sensitive to mesh refinement as discussed in [Fernandez et al.(2018)].

To overcome the problems encountered in the global approach, the works of [Paris et al.(2010), Le et al.(2010), Holmberg et al.(2013)] proposed to aggregate local constraints into several subgroups. The main advantage of these methods is the possibility to use lower aggregation exponents and thus to reduce non-linearities. The disadvantages lie in the definition of these subsets as well the choice of the number of them which can have a direct impact on the final solution.

Because of the wide range of available methods in the literature, only a non-comprehensive comparison inspired by the main most usual approaches could be reported in this research work. This comparison, as well as a theoretical reminder of the stress constrained density–based topology optimization, can be found in ARTICLE 1 of this thesis.

2.4 Fatigue resistance

A major contribution of this research work is to consider fatigue resistance criteria into the optimization problem. In this section, we present the general concept of fatigue before focusing on specific methods used in the optimization problems of Chapter 3. In particular, a reminder of the *Wöhler curve*, the *Haigh diagram* and their extension to *multiaxial fatigue* is provided.

2.4.1 Introduction

A large majority of failures, typically between 50 and 90% according to [Stephens et al.(2010)], in mechanical industry occurs when parts are subjected to time varying loads. Components failure occurs for stress levels way below the material ultimate tensile stress (S_{ut}). This type of failure is referred to as mechanical *fatigue failure*. For metallic materials, under the effect of cyclic stresses, the disslocations slide through the crystal network resulting in the formation of microcracks that can lead to the collapse of the structure. The process of preventing fatigue failure of a mechanical part should be taken into account as soon as the preliminary design phases in order to guarantee its durability. Techniques for studying fatigue durability can be classified into two categories depending if prevention or verification are considered.

If a crack is detected within a component, then the fracture mechanics theory is relevant to check the stability of the crack propagation. This process is a very usual tool in the aeronautical industry where components are expensive and do not always need to be completely replaced. An estimate of the crack propagation enables to decide if the parts can, and for how long, remain in service, thus preventing unnecessary manufacturing and costs. However, this approach is not followed in this manuscript. Advanced investigations are available for information in [Weiβgraebe et al.(2016)] among others. In this research work we follow the mechanical design approach. Fatigue resistance of a mechanical part is introduced with a view of prevention. Indeed, in order to guarantee the propensity of a component to resist fluctuating mechanical stresses, it must be designed to reduce the formation of cracks. The work of prevention has its roots with the works carried out by August Wöhler in the middle of the 19th century, see e.g., [Schütz(1996)], subsequent to the first railway accidents. Prevention techniques have continued to be developped over the decades leading today to a multitude of available methods with their advantages, disadvantages and also their own field of validity. Several authors propose a critical review of fatigue design methods, see e.g., [You and Lee(1995), Papadopoulos et al.(1997), Wang and Yao(2004), Schijve(2003), Papuga(2011)].

2.4.2 Design tools

After a series of railway accidents in the mid-19th century, August Wöhler's early work laid the foundations for modern knowledge of fatigue failure. The S-N curve, or Wöhler curve, was used to characterize the fatigue behavior of materials in standardized test specimens subjected to rotating bending for different levels of applied stress.

Wöhler curve: Let's assume that the samples are subjected to a time varying load represented in Figure 2.10(a) which generates fluctuating constraints as illustrated in Figure 2.10(b).

The S-N curve is constructed by plotting the nominal stress in terms of the number of cycles (often in logarithmic scale) that conducted to failure. A representation of such a curve is illustrated in Figure 2.11.

It is observed experimentally that under a certain stress level, no failure occurs even for an infinite number of cycles. This stress limit, noted S_e is called the *endurance limit*. Any other stress level where failure is detected for a given number of cycles N is referred to as *fatigue limit*

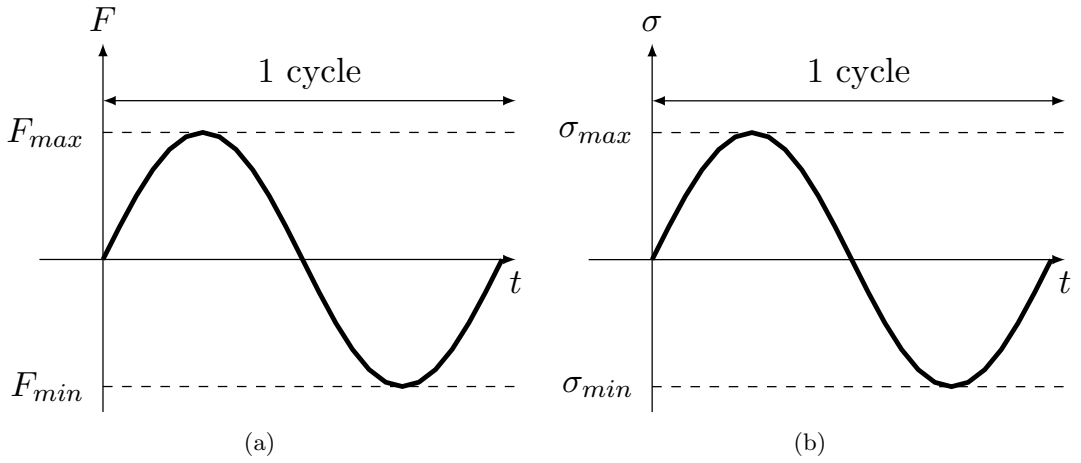

Figure 2.10: Alternating loading and resulting fluctuating stress within the sample: (a) Load (b) Nominal stress.

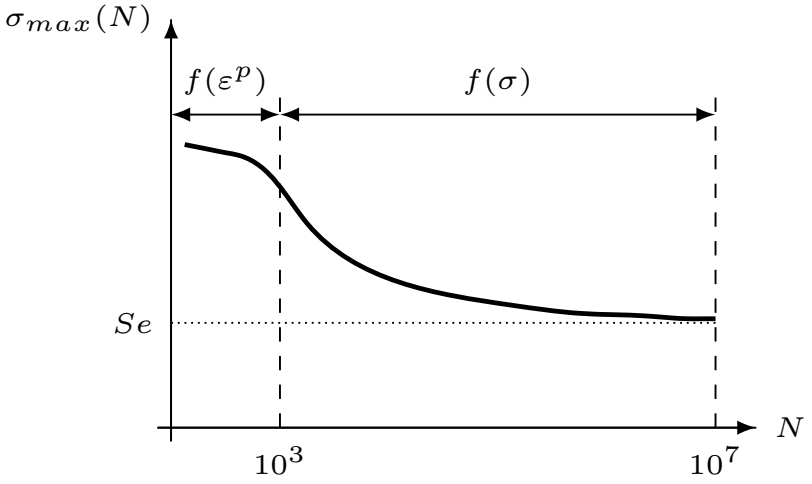

Figure 2.11: Illustration of a Wöhler curve.

at N cycles, noted $\sigma_{max}(N)$ or $\sigma_f(N)$. By taking a close look to this representation, two distinct areas can be observed. For a low number of cycles, i.e., typically less than 10^3, the stress level is high and large plastic regions are observed both at the macroscopic and microscopic scales. Fatigue failure, qualified as *oligocyclic*, is studied using the plastic deformations ($f(\varepsilon^p)$) following Manson-Coffin's work ([Gillis(1966)]). This approach depends on the specific properties of the material (type of material, forming process, etc.) as well as the ability to calculate the history of plastic deformations ([Norton(2000)]). This part of the diagram is not considered in the following of this work.

For a number of loading cycles greater than 10^3, we are in a high cycle fatigue regime. The fatigue failure ($f(\sigma)$), referred to as *polycyclic*, is ruled by the stresses. The strength of the approach lies in its capacity to give a suitable sizing of a structure in the first design stages of mechanical components, because it does not require a thorough knowledge of the characteristics of the material. In addition, large databases are available, facilitating its use.

The main hypothesis related to the approach is that it is restricted to a macroscopic linear elastic behavior, i.e., for low stress levels. In other words, no macroscopic plastic strain should be observed. Note that because of the large number of experiments required to draw the curve in Figure 2.11 and due to the statistical scattering of the results, the Wöhler curve corresponds to the plot of the points whose given probability of failure is typically 50%.

Many parameters influence the fatigue resistance of a mechanical part. These can be metallurgical in nature such as grain size, strain hardening rate, heat treatment(s) performed or the presence of defects, e.g., cracks. Other parameters are of a geometrical or mechanical nature such as the type of loading, the geometrical discontinuity, i.e., the presence of angular corners or changes in the cross sections, as well as the surface finish quality following machining operations for instance. In order to take these different aspects into account, corrections or safety factors are used to modify the stress state and/or the endurance limit (S_e) [Dang Van and Papadopoulos(1999), Budynas and Nisbett(2011), Norton(2000)].

An essential parameter of the fatigue life, not accounted for by the Wöhler curve, is the influence of the mean load component. This can have an impact on the service life of the structure, especially if the mean stress generated is high with respect to the alternating stress. A compressive stress increases the service life of the structure while an average tensile stress decreases it. An example of loading with a non-zero mean component and the corresponding generated stress are given in Figure 2.12.

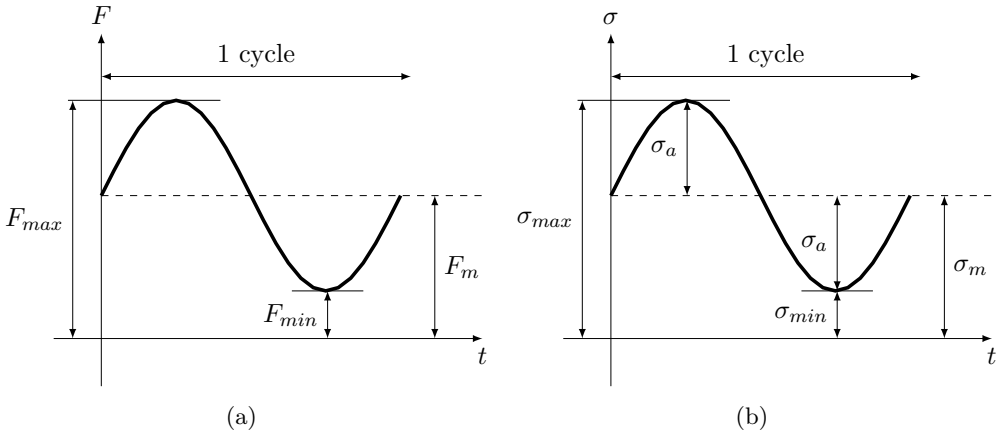

Figure 2.12: Effort with non-zero mean stress: (a) Load(b) Stress.

Figure 2.12(b) allows introducing the concepts of alternating constraint (σ_a) and mean constraint (σ_m) which will be key elements in the following. A widely used tool to take into account the effect of the mean stress is the Haigh diagram, see e.g., [Bannantine et al.(1990), Lalanne(1999)].

Haigh diagram : This graph represents the amplitude of the alternating stress as a function of the amplitude of the average stress for a given number of cycles. The material properties used are the endurance limit (S_e) for a purely alternating case (endurance limit identified on a Wöhler diagram) and the ultimate tensile strength of the material (S_{ut}). The Haigh diagram, illustrated in Figure 2.13 for $\sigma_m > 0$ can be represented by several models when knowing the endurance limit and the yield stress (σ_y^0). The equations of the most famous models are gathered in Table 2.3.

Numerous experimental tests have been conducted to validate the different approaches and they have shown that the Gerber curve is generally the most appropriate. However, Goodman's

Goodman	Gerber	Soderberg
$\sigma_a = S_e\left(1 - \frac{\sigma_m}{S_{ut}}\right)$,	$\sigma_a = S_e\left(1 - \left(\frac{\sigma_m}{S_{ut}}\right)^2\right)$,	$\sigma_a = S_e\left(1 - \frac{\sigma_m}{\sigma_y^0}\right)$,

Table 2.3: Expression of the models represented on the Haigh diagram.

line is often preferred, particularly in the aeronautic field, because of its linear character and because of it is more conservative behavior, placing the design on the safe side. Similarly, the Soderberg's line is also safer than the Gerber curve and the Goodman's line but its over-safety aspect makes it a little-used tool in practice.

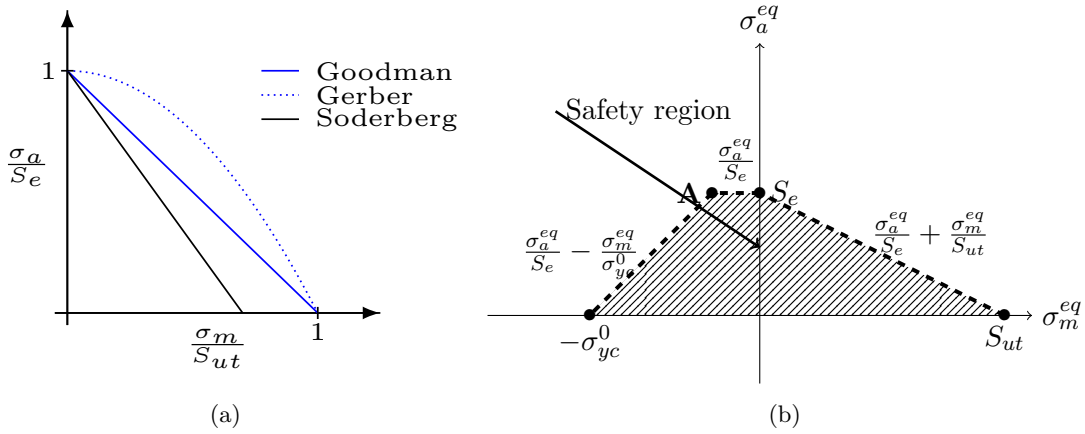

Figure 2.13: Fatigue resistance diagram including mean stress: (a) Haigh diagram (b) Augmented Goodman criterion.

In this research work, Goodman's line is selected to approximate the Haigh diagram as commonly seen in the aeronautical field. However, according to [Norton(2000)], an extension is admitted to consider the case where σ_m <0. Graphically the modification made is represented in Figure 2.13(b) by a second line which is given by the following equation:

$$d_2(\sigma_a^{eq}, \sigma_a^{eq}) = \frac{\sigma_a^{eq}}{S_e} - \frac{\sigma_m^{eq}}{\sigma_{yc}^0}, \tag{2.36}$$

This is truncated by a third line $d_3(\sigma_a^{eq}, \sigma_a^{eq}) = \frac{\sigma_a^{eq}}{S_e}$, to emphasize the conservativeness of the criterion as discussed in [Norton(2000)]. The piece-wise criterion gathering the three restrictions is used in the present topology optimization approach as exposed in Section 3.2.1 of Chapter 3. The Haigh diagram, and in particular the Goodman diagram considered here is valid for infinite life sizing. If considering a finite life, the endurance limit S_e used in the criterion should be replaced by a fatigue limit for a given number of cycles, noted $\sigma_f(N)$.

Finally, it is important to note that so far fatigue design tools require the ability to assess the stress state within the structure. In the case of a uniaxial stress state, the application is straight forward. On the other hand, in the case of a multi-axial stress states, i.e., at least two principal stresses are non-zero, which is widely encountered in practical mechanical design, adaptations are necessary to evaluate the equivalent alternate and mean components in mutliaxial stress state. To extend the one dimensional theory, different methods exist. The Sines approach, see

e.g., [Norton(2000)], is considered in this manuscript and for a two dimensional problem, it is given by: [1]

$$\sigma_a^{eq} = \sqrt{\sigma_{x_a}^2 + \sigma_{y_a}^2 - \sigma_{x_a}\sigma_{y_a} + 3\tau_{xy_a}^2}, \quad (2.37)$$

$$\sigma_m^{eq} = \sigma_{x_m} + \sigma_{y_m}, \quad (2.38)$$

The definition of equivalent quantities generalizing 1D results is a key element for the implementation of stresses in fatigue criteria. According to the definition of Eqn. (2.38), the alternating equivalent stress (σ_a^{eq}) is the square root of the second invariant of the deviatoric stress tensor ($\sqrt{3J_2}$), i.e., the Von Mises stress, whereas the mean equivalent stress corresponds to the first invariant of the stress tensor (I_1), i.e., three times the hydrostatic pressure. As illustrated above in Section 2.3.1, the formalism adopted to calculate the equivalent stresses is perfectly adapted to the evaluation of stress constraints.

2.4.3 Multiaxial fatigue criteria

Prediction of fatigue resistance can also be done using multiaxial fatigue criteria. The relevant literature abounds with such criteria making any attempt to provide a comprehensive review a daunting task. It is thus out of the scope of this manuscript. Comparisons of the different criteria are available in [Weber(1999), Koutiri(2011)] among others. For the sake of brevity, Figure 2.14 gathers different approaches that will be presented later on in this thesis.

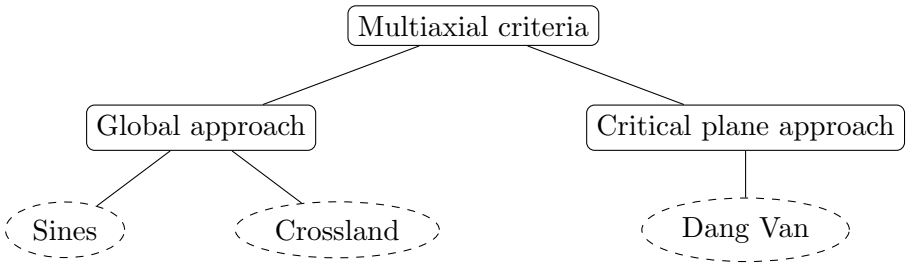

Figure 2.14: Families of multiaxial criteria selected in this work.

The global approach brings together all the criteria using the invariants of the stress tensor or its deviatoric part. They allow representing the stress state using a scalar quantity conferring a global character to the considered criteria. In this thesis, two criteria are studied, namely the criterion of *Sines* ([Sines(1959)]) and *Crossland* ([Crossland(1956)]). An alternative approach is to consider the criterion using a critical physical plane where the stress state is likely to lead to crack initiation. This critical plane corresponds to the crystallographic plane around which local plasticity is likely to appear leading to the initiation of micro-cracks. One of the most famous criteria exploiting this theoretical approach is the Dang Van criterion ([Dang Van et al.(1973), Dang Van et al.(1989), Dang Van(2010)]). In this thesis, the latter is introduced into the optimization process because of its intensive use in the automotive sector in Europe ([Morel et al.(2010), Koutiri(2011)]).

[1] In the three-dimensional case, the extension is naturally done as:

$$\sigma_a^{eq} = \sqrt{\frac{(\sigma_{x_a} - \sigma_{y_a})^2 + (\sigma_{y_a} - \sigma_{z_a})^2 + (\sigma_{z_a} - \sigma_{x_a})^2 + 6(\tau_{xy_a}^2 + \tau_{yz_a}^2 + \tau_{zx_a}^2)}{2}},$$

$$\sigma_m^{eq} = \sigma_{x_m} + \sigma_{y_m} + \sigma_{z_m},$$

This section aims at presenting the criteria that will be considered in this work and in particular to discuss the physical quantities involved in their description. The practical implementation of fatigue strength will be explained in Chapter 3.

Sines and Crossland criteria: The first family of criteria studied in this thesis involves the global fatigue resistance approach. In this, the criteria exploit global stress state quantities, e.g., invariants.

The Sines ([Sines(1959)]) and Crossland ([Crossland(1956)]) criteria are relatively similar in their formulation so they will be handled simultaneously. The respective expressions of these are given in Eqn. (2.40).

$$\sigma^{eq}_{sines} = \frac{\sqrt{J_{2,a}} + a \cdot P_H}{b} \leq 1, \tag{2.39}$$

$$\sigma^{eq}_{crossland} = \frac{\sqrt{J_{2,a}} + a \cdot P_{H,max}}{b} \leq 1, \tag{2.40}$$

where P_H and $P_{H,max}$ stand for the *hydrostatic pressure* and *the maximum hydrostatic pressure* respectively. The following definition of material parameters a and b are gathered in Table 2.4.

	a	b
Sines	$\kappa = \frac{6\tau}{f_0} - \sqrt{6}$ or $\kappa = \frac{3\tau(S_{ut}+\mu)}{\mu S_{ut}} - \sqrt{6}$	τ
Crossland	$\frac{3\tau}{\mu} - \sqrt{3}$	τ

Table 2.4: Definition of material constants from Sines and Crossland criteria.

where τ, μ and f_0 stand for the fatigue limit in alternate torsion, the fatigue limit in rotation bending, the fatigue limit in repeated bending respectively.

Dang Van criterion: Dang Van criterion belongs to the second family of fatigue resistance criteria. The latter is based on a critical plane research approach in which localized plastic regions appear and in the vicinity of which mirco-cracks are likely to be initiated. The complete presentation of the theory of this type of approach would be beyond the scope of this work, so this section is devoted to presenting the broad outlines necessary to understand the concepts presented in Chapter 3.

Let's consider a mechanical structure and a small volume element, whose characteristic size is such that it is small enough but sufficiently large enough to contain a representative sample of the crystallographic structure of the mechanical component. This small volume element is located at the macroscopic point P as shown in Figure 2.15. Within the latter, the stress state is defined at local point Q (see Figure 2.15), where the *microscopic stress* state is evaluated. Considering that the volume element at point P satisfies the assumptions and that it is subjected to an average stress field evolving over time ($\boldsymbol{\Sigma}(t, P)$), the microscopic stress ($\boldsymbol{\sigma}(t, Q)$) at point Q can be related to the average stress acting on the elementary volume by (Hill-mandel):

$$\boldsymbol{\sigma}(t, Q) = \boldsymbol{A}(P, Q)\boldsymbol{\Sigma}(t, P) + \boldsymbol{\rho}(t, Q), \tag{2.41}$$

where $\boldsymbol{A}(P, Q)$ and $\boldsymbol{\rho}(t, Q)$ are respectively the *localization tensor* and the *residual stress tensor*. The latter represents the local plastic zones that can be initiated and brings a correction

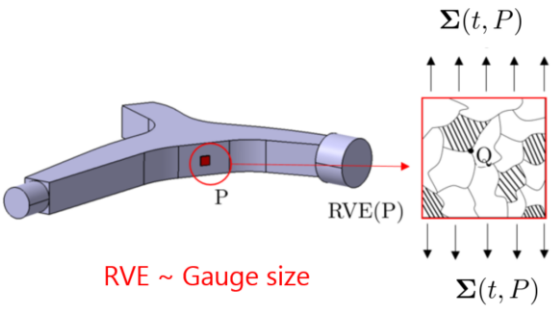

Figure 2.15: Illustration of macroscopic and microscopic scale separation within a mechanical component.

to the stress measure. In HCF regime, parts are designed to have a stress state below the fatigue limit. Near this limit, the observed stresses are low and it is reasonable to consider the structure in a state of *elastic shakedown*. Based on this assumption and working with the Melan's theorem, the residual stress field is stabilized and is no longer time-dependent. As far as the localization tensor is concerned, a good approximation is to take this one equal to the unity because its evaluation is difficult. Actually, the latter depends on the local properties and orientations of the grains. Eqn. (2.41) becomes:

$$\boldsymbol{\sigma}(t,Q) = \boldsymbol{\Sigma}(t,P) + \boldsymbol{\rho}^*(Q), \tag{2.42}$$

Working in the deviatoric space and by rewriting the stress tensors in their deviatoric and hydrostatic part[2], Eqn. (2.42) is simplified as:

$$\boldsymbol{s}(t,Q) = \boldsymbol{S}(t,P) + dev(\boldsymbol{\rho}^*(Q)), \tag{2.43}$$

Eqn (2.43) assumes that the hydrostatic term of the microscopic and macroscopic stress are identical, i.e. $P_H = p_h$. Moreover, as the hydrostatic part does not influence the plastic yielding, the residual stress tensor can be considered as purely deviatoric. In what follows, the reference to position (P and Q) is dropped for the sake of clarity. From Eqn. (2.43), the problem amounts to finding the residual stress tensor value minimizing the propensity of the grain to yield. Working in deviatoric space and similarly to what is done in plasticity theory, [Mandel et al.(1977)] showed that the stabilized residual stress tensor can be interpreted as the center of the smallest hypersphere, in the five-dimensional space, surrounding the load path as illustrated in Figure 2.16(b). Mathematically, this comes down to solving the min-max problem:

$$dev(\boldsymbol{\rho}^*) = \arg\min_{\boldsymbol{\rho}} \quad \max_{t}(J_2(\boldsymbol{S}(t) - dev(\boldsymbol{\rho}))), \tag{2.44}$$

The maximum operation must be taken on t to ensure that the entire load path is enclosed within the hypersphere but with the smallest residual stress tensor value. In practical terms,

[2]The decomposition into the deviatoric and hydrostatic components reads:

$$\begin{aligned} \boldsymbol{\Sigma} &= \boldsymbol{S} + P_H\boldsymbol{\delta}, \\ \boldsymbol{\sigma} &= \boldsymbol{s} + p_h\boldsymbol{\delta}, \\ \boldsymbol{\rho}^* &= dev(\boldsymbol{\rho}^*) + hyd(\boldsymbol{\rho}^*), \end{aligned}$$

this means that the hypersphere is not only allowed to move in the deviatoric space, but also to grow in size until the load path lies entirely within the hypersphere. The behavior of the grains is therefore assumed to obey both the kinematic and isotropic hardening law. Several methods are available in the literature to solve problem (2.44), see [Dang Van et al.(1989), Bernasconi(2002), Bernasconi and Papadopoulos(2000)]. When the solution to the "min-max" problem is known, the microscopic stress is constructed following Eqn. (2.42). Then the Tresca's microscopic shear stress, defined as $\tau(t) = \max_{IJ} 0.5|s_I(t) - s_J(t)|$ where $s_I(t)$ and $s_J(t)$ stand for eigenvalues of the microscopic stress state $\boldsymbol{s}(t)$, is finally evaluated before its insertion into the Dang Van criterion given by ([Ballard et al.(1995)]):

$$\max_t \left(\tau(t) + aP_H(t)\right) \leq b, \tag{2.45}$$

where a and b are material parameters computed respectively as $a = \frac{\tau - \mu/2}{\mu/3}$ and $b = \tau$. After the construction of the criterion, it should be checked whether the material will be damaged or not as illustrated in Figure 2.17(b): In this example, two loading cases, γ_1 and γ_2, are considered. The principle of the graphical verification consists in representing the load path in the plane (τ,P_H) and to evaluate if all the points stay below the Dang Van's line. In our example, loading γ_1 will not lead to fatigue failure unlike loading γ_2.

The shear stress used in Eqn. (3.23) plays a prominent role in defining the fatigue strength criterion. The original form of the Dang Van criterion uses the Tresca shear stress which provides information about the critical facet on which plastic flow is likely to occur. In order to achieve topology optimization, the use of Tresca's shear stress would involve manipulating the stress eigenvalues in the sensitivity analysis which would bring an unecessary level of difficulty to the problem. Following Dang Van's proposal ([Dang Van(2001)]), the *Octahedral shear stress* ($\tau_{oct}(\boldsymbol{s}(t))$) is used instead of Tresca's to overcome this technical difficulty. The octahedral shear stress is defined as follows:

$$\tau_{oct}(\boldsymbol{s}(t)) = \sqrt{\frac{2}{3} J_2(\boldsymbol{s}(t))} = \sqrt{\frac{2}{9}} \sqrt{3J_2(\boldsymbol{s}(t))} = \sqrt{\frac{2}{9}} \overline{\sigma}_e^{\mathrm{VM}}(t), \tag{2.46}$$

In (2.46), $\sqrt{3J_2(\boldsymbol{s}(t))}$ represents the equivalent Von Mises stress measure. In the development of the following chapter, this shear stress measure is considered to define the Dang Van criterion.

Until now, the formalism followed is valid for a continuous representation of the applied load. However, to solve the problem numerically, it is necessary to handle the latter in a discreet manner. Note that the described procedure has to be repeated for each element e. The loading over time ($P(t)$), shown in Figure 2.16(a) is discretized into l samples P^l. Each of these load samples is then used to evaluate, by means of a static analysis, the associated stress field and in particular its deviatoric component $\boldsymbol{S}^l$. Then the continuous load path can be represented in the deviatoric space and the solution of the "min-max" problem can be solved in discrete form. Figure 2.16(b) represents the continuous load path in black and the corresponding discrete path after sampling of the load profile ($P(t)$) in dotted blue.

The complete procedure for calculating fatigue resistance for the time discretized problem is provided in Figure 2.17(a). Let's recall that this procedure is performed for each individual element e.

Finally, it should be noted that the approach described above is not free from some difficulties. The criterion is not suitable for a highly out-of-phase loading conditions. These types of loads activate many slip systems so that there are more opportunities for crack nucleation.

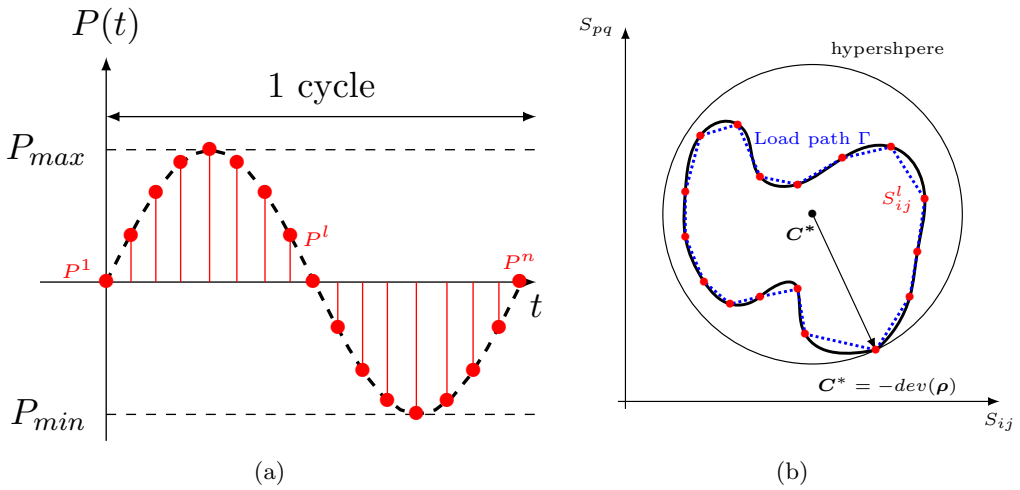

Figure 2.16: Illustration of the hypersphere and the loading path in the deviatoric space.

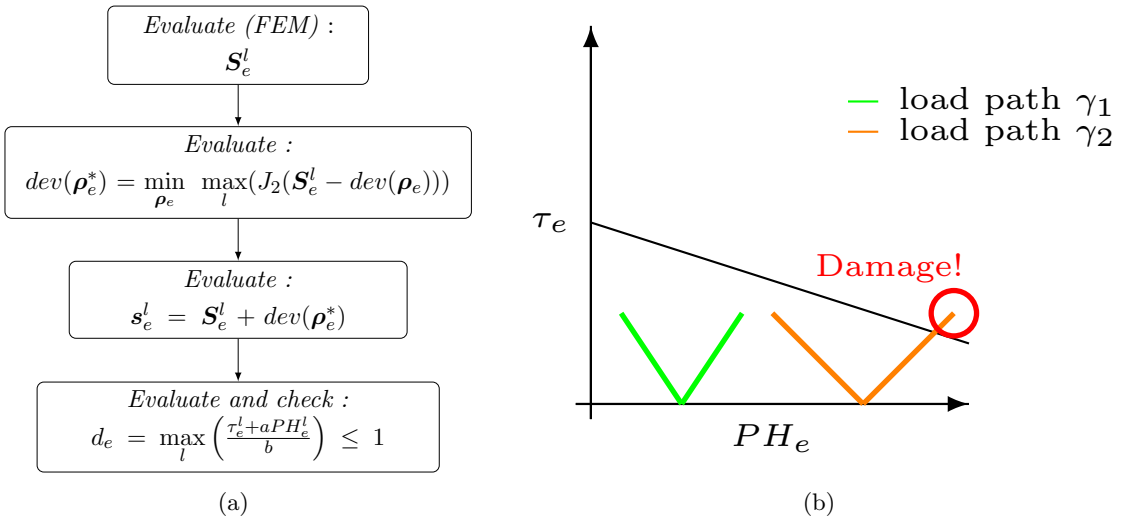

Figure 2.17: Illustration of the procedure for calculating the Dang Van criterion: (a) Discretization of the load in (b) Procedure for calculating the damage in the sense of Dang Van.

An alternative proposed in [Papadopoulos(1994), Papadopoulos(1995)] aims at bringing some degree of refinement to the original Dang Van criterion with very good agreement with tests results. However, the latter approach remains very difficult to use in practice.

2.5 Design of architectured materials

In the previous sections, it has been shown that topology optimization is able to handle efficiently design problems in engineering. Nowadays, the massive development of 3D printing techniques opens new perspectives to the design of optimal structures. The layer by layer manufacturing of mechanical components allows introducing areas made of lattice structures which can be used to propose alternative skeletons with a huge performance to weight ratio in many applications. More generally, nature tends to create such porous composite structures as in wood or bones,

see Figure 2.18.

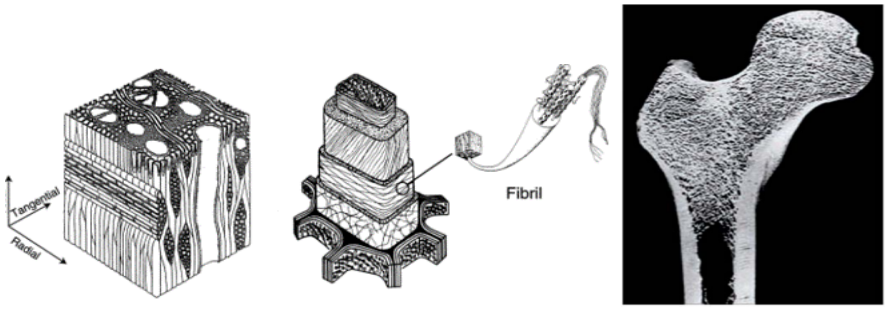

(a) (b)

Figure 2.18: Illustration of porous structure in (a) wood ([Greil et al.(1998)]) (b) bones([Lan Levengood and Zhang(2014)]).

Inspired by nature and benefiting from the latest advances in manufacturing, it is possible to to market industrial components with porous or graded materials as illustrated in Figure 2.19. This new way of designing components represents a revolution in industrial design where lattices are relevant. A typical example is surgical implants designed in such a way that the bone structure can grow back inside the lattice allowing for a better immersion of the implant.

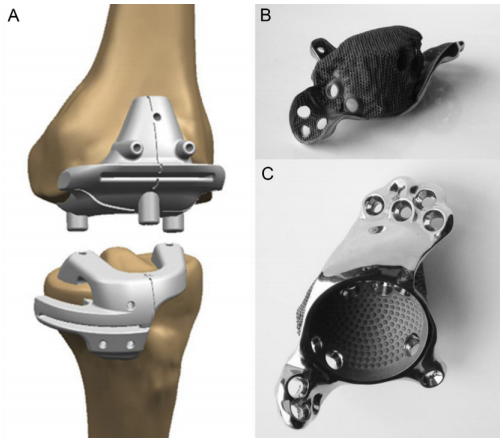

Figure 2.19: Practical example of the use of 3D printing with lattice structures [Mok et al.(2016)].

The use of topology optimization to design architectured materials was introduced by the works of [Sigmund(1994), Sigmund(1999)]. Many contributions have extended the scope of applications as discussed in [Cadman et al.(2013)]. Among others, we can quote the optimization of the electromagnetic and phonic properties ([Jensen and Sigmund(2011)]), optimization in the presence of several material phases ([Gibiansky and Sigmund(2000), Guest et Prévost(2006)]), optimization of tailored thermal properties ([Sigmund and Torquato(1999)]), optimization of vibratory properties ([Liu et al.(2016)]) or the optimization based on an asymmetry of the microscopic tension-compression field at the microstructural level([Jia et al.(2017)]).

The design of architectured materials is based on the homogenization method. Generally speaking, the latter theory has been developed to compute numerically or analytically the effective behaviour of complex microstructures. Although applicable to heterogeneous environ-

ments, periodic materials, constructed from the periodic repetition of a Representative Unit Cell (RUC) ([Aboudi et al.(2012)]) in the two directions of space are exploited and their homogenized effective properties are extracted, see e.g., [Besoussan et al.(1978), Sanchez-Palencia (1983), Suquet(1982), Torquato(2002)] for a description of periodic homogenization. The analytical evaluation of the effective properties can be performed for simple microstructure cases which are not that often encountered in practice. This is why numerical homogenization methods are used instead, see e.g., [Guedes and Kikuchi(1990), Mlejnek and Schirrmacher (1993), Andreassen and Andreasen(2014)].

In the following, the evaluation of the homogenized elastic properties (E_{ij}^H) and of the load vector ($\mathbf{f}_i^0$) which are necessary for the development of the optimization problem are recalled. Their implementation within the optimization problem is left for the next chapter.

In the two-dimensional case, which concerns the applications of this thesis, the equivalent elastic properties are determined using three independent unitary strain fields defined by : $\boldsymbol{\varepsilon}_1^0 = [1\ 0\ 0]^T$, $\boldsymbol{\varepsilon}_2^0 = [0\ 1\ 0]^T$ et $\boldsymbol{\varepsilon}_3^0 = [0\ 0\ 1]^T$, see e.g., [Sanchez-Palencia (1983)]. An efficient way to compute the homogenized elastic properties E_{ij}^H is detailed in [Bendsøe and Sigmund(2003)] and is given by Eqn. (2.47) :

$$\begin{aligned} E_{ij}^H &= \frac{1}{Y}\int_Y (\boldsymbol{\varepsilon}_i^0 - \boldsymbol{\varepsilon}_i)^T\ \mathbf{E}\ (\boldsymbol{\varepsilon}_j^0 - \boldsymbol{\varepsilon}_j)\ dY, \\ & i,\ j = 1,\ 2,\ 3, \end{aligned} \tag{2.47}$$

where Y is the volume of the RUC, $\boldsymbol{\varepsilon}_i^0$ are the prescribed unitary strain fields and $\boldsymbol{\varepsilon}_i$ are the strain fields resulting from the application of $\boldsymbol{\varepsilon}_i^0$. These unitary fields are applied within the RUC in each node. As mentioned above, solely structures with a periodic architecture are considered here and only one RUC is therefore studied by applying periodic boundary conditions. Working with regular meshes, boundary conditions are conveniently applied by removing redundant degrees of freedom (dofs), see for example [Sigmund(1994), Sigmund(1999), Andreassen and Andreasen(2014)]. In the case of non-regular meshes, specific procedures, based on the introduction of Lagrange multipliers [Michel et al.(1998), Miehe et Koch(2002)] or polynomial interpolations [Nguyen et al.(2012), Tyrus et al.(2007)] have been developed. Such cases are not considered here and will not be further discussed in this thesis.

In this work, the dofs removal strategy is adopted, as illustrated in Figure 2.20. The periodic boundary conditions are applied by removing redundant nodes located on either side of the RUC. Thus, the number of dofs associated with the RUC and consequently the size of the system to be solved are reduced. The analysis is first performed on the dashed area of Figure 2.20. The obtained displacements $\mathbf{u}_{\mathrm{P}}$ can be extended in a post-processing step to recover the initial size of the problem $\mathbf{u}_{\mathrm{NP}}$ and account for the periodicity of the RUC.

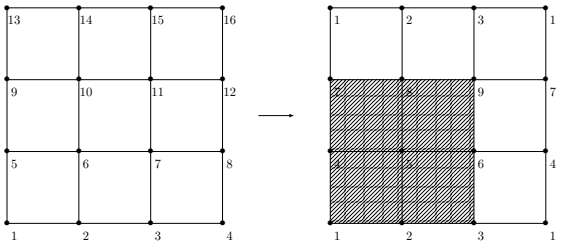

Figure 2.20: Enforcing periodic boundary conditions to a square RUC by applying a dofs deletion strategy: corresponding nodes are associated leading to the elimination of redundant dofs.

After the displacements at the nodes are determined following the application of unit test strain fields $\boldsymbol{\varepsilon}_0^i$, one has to introduce them into Eqn. (2.47) to calculate the homogenized elastic tensor as:

$$\begin{aligned} E_{ij}^H &= \frac{1}{Y}\int_Y (\mathbf{u}_i^0 - \mathbf{u}_i)^T \ \mathbf{B}^T \ \mathbf{E} \ \mathbf{B} \ (\mathbf{u}_j^0 - \mathbf{u}_j) \ dY, \\ &= \frac{1}{Y}(\mathbf{u}_i^0 - \mathbf{u}_i)^T \ \mathbf{K} \ (\mathbf{u}_j^0 - \mathbf{u}_j), \\ & \quad i, \ j = 1, \ 2, \ 3, \end{aligned} \tag{2.48}$$

where $\mathbf{B}$ is the strain-displacement matrix and $\mathbf{K}$ is the structural stiffness matrix associated with the RUC.

To evaluate the displacement field $\mathbf{u}^i$, the following static equation must be solved:

$$\mathbf{K} \ \mathbf{u}_i = \mathbf{f}_i^0, \qquad i = 1, \ 2, \ 3, \tag{2.49}$$

where $\mathbf{f}_i^0$ is the load vector consistent with the unitary strain field application $\boldsymbol{\varepsilon}_i^0$. The latter can be numerically evaluated using the following expression ([Andreassen and Andreasen(2014)]):

$$\begin{aligned} \mathbf{f}_i^0 &= \int_Y \mathbf{B}^T \ \mathbf{E} \ \boldsymbol{\varepsilon}_i^0 \ dY, \qquad i = 1, \ 2, \ 3, \\ &\approx \sum_{n_{gp}} w_{gp} \ \mathbf{B}^T \ \mathbf{E} \ \boldsymbol{\varepsilon}_i^0 \ \det(\mathbf{J}), \end{aligned} \tag{2.50}$$

where w_{gp} is the weight associated to each Gauss point, $\det(\mathbf{J})$ is the determinant of the Jacobian matrix. Note that the equivalent load vector $\mathbf{f}_i^0$ depends on the elastic properties which are functions of the design variables, i.e., densities. Thus, the optimization problem that will be defined in the next chapter is a design dependent load problem, which will have an impact on the computation of the sensitivity.

2.6 Chapter conclusion

In this chapter, the theoretical concepts necessary for the developments covered in Chapter 3 have been introduced. First, the concept of structural optimization and, in particular, density–based topology optimization has been presented.

This was then followed by a discussion on the available methods to solve the problem, with a particular focus on the concept of Mathematical Programming. Afterwards, the concepts of structural approximations and also the methods to compute the derivatives of the functions with respect to the design variables have been recalled.

In a third step, the definition of stress constraints and the related challenges within the optimization framework are described. Particular attention is paid to the concept of the singularity of stress constraints and on how the large scale nature of the problem can be managed to reduce the computational time through the introduction of aggregation methods.

Fatigue resistance is an important part of the contributions of this thesis. The underlying theory behind this problem being vast, the methods presented in this chapter have been chosen with the purpose of enabling their use in the industrial world.

Finally, the concepts of homogenization for the design of architectured materials closes the theoretical reminders of this chapter.

Chapter 3

Stress and fatigue constraints in topology optimization

Contents

This chapter summarizes the main developments made during this thesis. It is based on the papers written throughout this research work, see Appendices. In particular, the first part is dedicated to summarizing some specific characteristics of the stress-based topology optimization problem. Next, is provided and discussed, a comparison of usual approaches encountered in the

literature and developed to solve this type of problem. The work continues along with the introduction of stress constraints into the design problem of architectured materials. Finally, the introduction of fatigue criteria into the optimization process and related numerical results conclude this chapter.

3.1 Static stress constraints

Nowadays, topology optimization is being more and more considered as an industrial design tool as evidenced by the appearance of several dedicated softwares already mentionned in the introduction. However, most of the possibilities offered by the latter ones is to propose a problem formulation aiming at maximizing the stiffness of the optimized structure. This limitation is rather restrictive when the strength of the component is critical. As an illustration, let's consider a typical test case defined in Figure 3.1. The famous problem of the literature, see e.g., [Olhoff et al.(1993), Duysinx and Bendsøe(1998)], consists in a L-shaped design domain. The design domain is clamped along the AF edge and a load is applied in D. The latter is distributed over several nodes to avoid introducing any stress singularity at the point of application of the load. The number of elements constituting the mesh as well as the element edge size and the number of elements over which the load is distributed are referenced in Table 3.1. Let's note that no specific units are referred here as any of them can be used if the material parameters are set consistently.

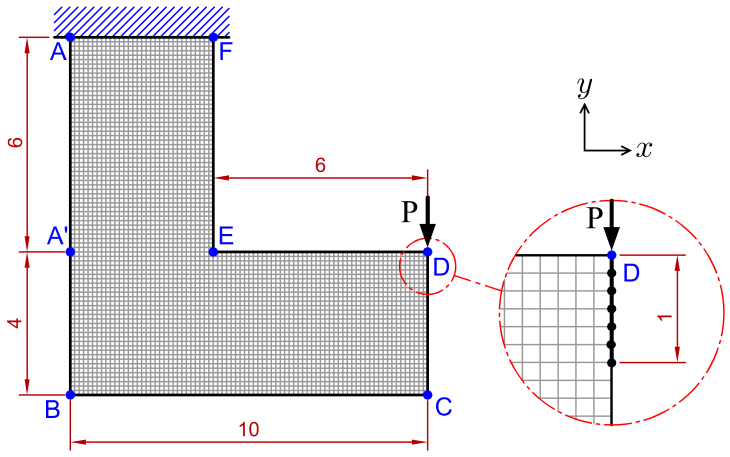

Figure 3.1: Design domain and boundary conditions definition of the L-shape benchmark.

Number of elements	4096
Element edge size	0.125
Number of elements for load distribution	6

Table 3.1: Mesh information of the L-shape benchmark.

The result of the compliance minimization, noted $\mathcal{C}$, under a volume constraint $\mathcal{V}^*$ is represented in Figure 3.2.

Particular implementation details related to the topology optimization process, e.g., filter size, element type, relaxation, etc., will be discussed later in the subsequent sections.

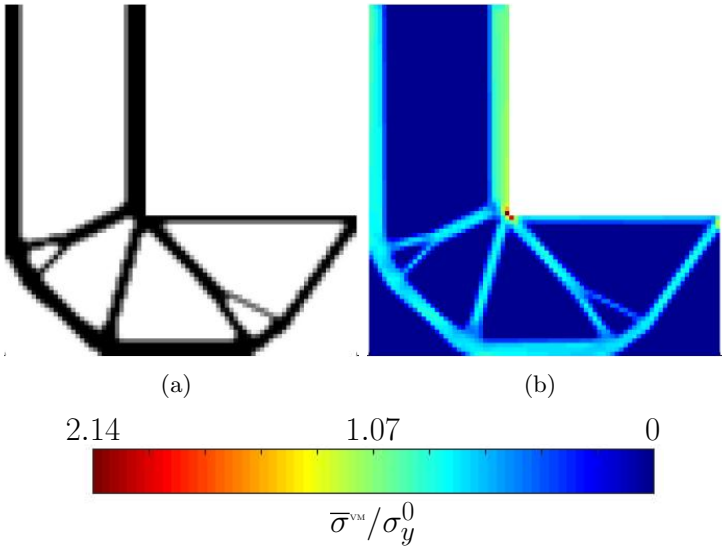

Figure 3.2: Compliance minimization solution of the L-shape benchmark: (a) Design (b) Stress map.

The optimized solution shown in Figure 3.2(b) exhibits localized high stress concentrations in the vicinity of the re-entrant corner E. In this thesis, equivalent Von Mises stresses under static loading within optimized structures have to be less or equal than a well-defined physical limit, e.g., the yield stress σ_y^0. Hence, normalizing the calculated stress within the design in Figure 3.2(a), and for the mesh size defined in this example, it appears that the maximum equivalent value is more than twice the prescribed limit σ_y^0. Subsequent redesign phases, following the optimization process, are necessary to adapt the optimized layout and result in additional engineering time costs. These could be avoided by including restrictions on the calculated stresses directly into the optimization process.

This first analysis introduces the main motivation to account for stress constraints within the optimization process. However, other results discussed in [Duysinx et al.(2008)] mention additional reasons to consider stress constraints. If several load cases are applied or if a different yield stress in tension and compression is detected, the optimized stress–based design may differ from the compliance optmimized layout. As shown in [Perdersen(1998)], designs with or without stress constraints can only be identical if the stress criterion used is consistent with the measured elastic energy. This condition is not met when using the Von Mises criterion ([Bendsøe and Sigmund(2003)]).

For the sake of comparison with compliance design in Figure 3.2, Figure 3.3 presents the results of the stress constrained optimization (prescribed stress limit $\sigma_y^0 = 6$). Both Figure 3.2 and Figure 3.3 have been obtained with the same final weight.

Optimized results of Figure 3.3 show the impact of stress constraints on the optimized design. First of all, the region around the re-entrant corner E is rounded off to reduce stress concentrations. Next, it can be seen that a large amount of the structural members are close to the prescribed stress limit even if the whole structure does not reach the maximum stress level. Although the final layouts are similar, the introduction of stress constraints enables to obtain a more consistent structure with regard to strength restrictions.

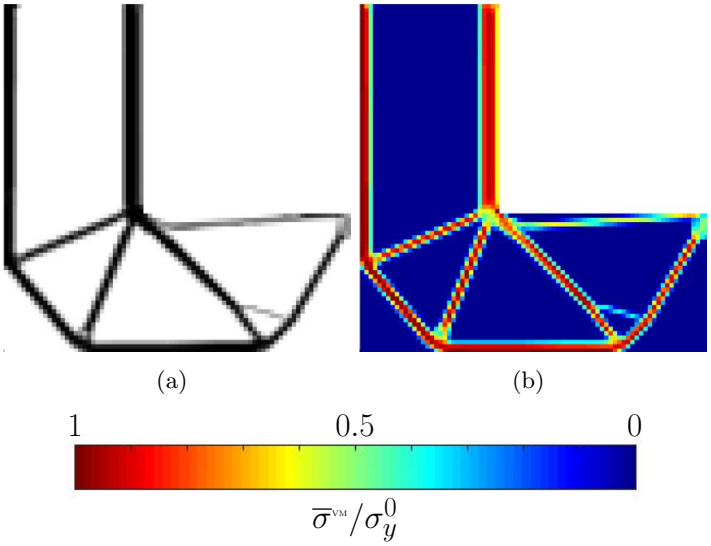

Figure 3.3: Optimized design and stress maps for the weight minimization problem under stress constraints: (a) Design (b) Stress map.

3.1.1 Sensitivity analysis of stress constraints

This research work focuses on structures made of SIMP materials. As described in [Duysinx and Bendsøe(1998)], it is assumed that the base material is isotropic and metallic and that the first point of plasticity can be predicted using the equivalent Von Mises stress criterion. Stresses are therefore controlled by defining a criterion constructed using the microscopic stresses within the material at a porous mesostructure level, i.e., which is dependent on design variables.

As proposed by [Bendsøe(1989)], and described in the previous chapter, the SIMP interpolation scheme is adopted and links the properties of the elasticity tensor $\mathbf{E}(x)$ to the design variables by:

$$\mathbf{E}(x) = x^p \mathbf{E}^0, \tag{3.1}$$

where $\mathbf{E}^0$ represents the stiffness properties of the solid material, and p the interpolation exponent generally taken equal to 3 [Bendsøe and Sigmund(1999), Bendsøe and Sigmund(2003)].

Recalling the stress computation within a finite elements formalism, held in Section 2.3.1 of the previous chapter, and accounting for Eqn. (3.1) the equivalent Von Mises stress writes:

$$\langle \sigma_e^{\text{VM}} \rangle = x_e^p \sqrt{\mathbf{U}_e^T \ \mathbf{M}_e^0 \ \mathbf{U}_e} = x_e^p \ \overline{\sigma}_e^{\text{VM}}, \tag{3.2}$$

Following [Duysinx and Bendsøe(1998)], a consistent failure criterion at the mesoscale level must be defined. The microscopic stresses $\boldsymbol{\sigma}$ within the porous material can be written as:

$$\boldsymbol{\sigma} = \frac{\langle \boldsymbol{\sigma} \rangle}{x_e^q}, \quad \text{with } q > 1. \tag{3.3}$$

This finally allows writing the final form of the Von Mises equivalent stress constraint defined in the porous material, at the e element level as :

$$\frac{\sigma_e^{\text{VM}}}{\sigma_y^0} = \frac{\langle \sigma_e^{\text{VM}} \rangle}{x_e^q \ \sigma_y^0} = x_e^{p-q} \ \frac{\overline{\sigma}_e^{\text{VM}}}{\sigma_y^0} \leq 1, \tag{3.4}$$

where σ_y^0 is the prescribed stress limit below which local stresses must be maintained, i.e., stresses standardized by the stress limit must be less than or equal to 1. Note that in this manuscript, the stress singularity is circumvented by the use of qp-relaxation and hence $p \neq q$ with $q < p$, see [Bruggi(2008)]. When not specified, the default value of the q parameter is set to 2.5.

Now that the expression of the relaxed stress is defined, the sensitivity of these with respect to the design variables, i.e., $\frac{\partial \sigma_e^{\mathrm{VM}}}{\partial x_j}$, is easily obtained by differentiating the expression (3.4):

$$\frac{\partial \sigma_e^{\mathrm{VM}}}{\partial x_j} = (p-q)\ x_e^{p-q-1}\ \overline{\sigma}_e^{\mathrm{VM}}\ \delta_{ej} + x_e^{p-q}\ \frac{\partial \overline{\sigma}_e^{\mathrm{VM}}}{\partial x_j}, \tag{3.5}$$

In Eqn. (3.5), the term $\frac{\partial \overline{\sigma}_e^{\mathrm{VM}}}{\partial x_j}$ is the one that requires numerical evaluation using a direct or an adjoint sensitivity approach. In this thesis, a selection of the most critical constraints is first made by an active–set selection strategy so that the number of constraints to be treated is lower than the number of elements. Hence, the use of the adjoint approach, see Eqn.(2.24) and Eqn.(2.25) in Chapter 2, is often recommended. Adapting it to the most general case (2.24) with stress constraints, one can write:

$$\frac{\partial \overline{\sigma}_e^{\mathrm{VM}}}{\partial x_j} - \boldsymbol{\lambda}^T \left(\frac{\partial \mathbf{K}}{\partial x_j}\mathbf{U} - \frac{\partial \mathbf{F}}{\partial x_j} \right) + \left(\frac{d\overline{\sigma}_e^{\mathrm{VM}}}{d\mathbf{U}} - \boldsymbol{\lambda}^T \mathbf{K} \right) \frac{d\mathbf{U}}{dx_j} = 0, \tag{3.6}$$

where $\boldsymbol{\lambda}$ is the adjoint vector

The implicit part of (3.6) is eliminated by defining an adjoint vector such that:

$$\frac{d\overline{\sigma}_e^{\mathrm{VM}}}{d\mathbf{U}} - \boldsymbol{\lambda}^T \mathbf{K} = 0, \tag{3.7}$$

The desired derivative is then obtained by inserting the solution of (3.7) in (3.6)

$$\frac{\partial \overline{\sigma}_e^{\mathrm{VM}}}{\partial x_j} = \boldsymbol{\lambda}^T \left(\frac{\partial \mathbf{K}}{\partial x_j}\mathbf{U} - \frac{\partial \mathbf{F}}{\partial x_j} \right), \tag{3.8}$$

An evaluation of the adjoint vector $\boldsymbol{\lambda}$ is required for each active constraint and one has to solve:

$$\mathbf{K}\ \boldsymbol{\lambda} = -\left[\frac{\mathbf{M}_e^0\ \mathbf{U}_e}{\sqrt{\mathbf{U}_e^T\ \mathbf{M}_e^0\ \mathbf{U}_e}} \right]^T, \tag{3.9}$$

Note that the derivative of the stiffness matrix with respect to the design variables is easily obtained given the simple structure of the SIMP law:

$$\frac{\partial \mathbf{K}}{\partial x_j} = p\ x_j^{p-1}\ \mathbf{K}_e^0, \tag{3.10}$$

Except for the developments held in Section 3.1.4, it is assumed that the applied loads are design independent, i.e., are not functions of the design variables, so that most of the time we have $\frac{\partial \mathbf{F}}{\partial x_j} = 0$. In the numerical procedure of Section 3.1.4 however, the value of this derivative is not null and will be provided accordingly.

The derivatives of global stress constraints with respect to the design variables are attached in Appendix A.

3.1.2 Specific character of stress constraints in topology optimization

An interesting point is to compare the optimized solution from density–based topology optimization with results produced with Michell trusses, see e.g., [Rozvany(1996b)] and [Lewiński and Rozvany(2008)] among others. The solutions to the analytical problem present a series of characteristics reminded below. First of all, the weight of this optimal solution is minimal. Then, the size of its structural members are adapted to fit the Fully Stressed Design (FSD) state, see e.g., [Haftka and Gürdal(1992)]. As discussed in [Rozvany(2001b)] for truss structures, this particular state is only reached under very special conditions such as the presence of a single load case, a single material limit or if no minimum gauge constraint is applied. These conditions are difficult to meet in practice and one should not expect to obtain a FSD state for optimized layout when accounting for stress constraints. Additionally, as discussed in [Berke and Khot(1974), Kirsch(1993), Zhou and Sigmund(2017)], the FSD state does not always lead to the most optimal solution. For the continua, the works of [Perdersen(2000)] and [Zhou and Sigmund(2017)] bring an additionnal condition to reach the FSD state. In the latter, it is shown that the structural members of the optimized layout reach the prescribed stress limit only if the design boundaries are unconstrained, i.e., are free from geometrical singularities. In the case of the L-shape problem, this last condition is not fulfilled due to the presence of the re-entrant corner. Reaching the FSD state for more general cases should not be expected. For illustration purposes, the design obtained under Michell's conditions for the L-structure is provided in Figure 3.4 and was determined in [Lewiński and Rozvany(2008)].

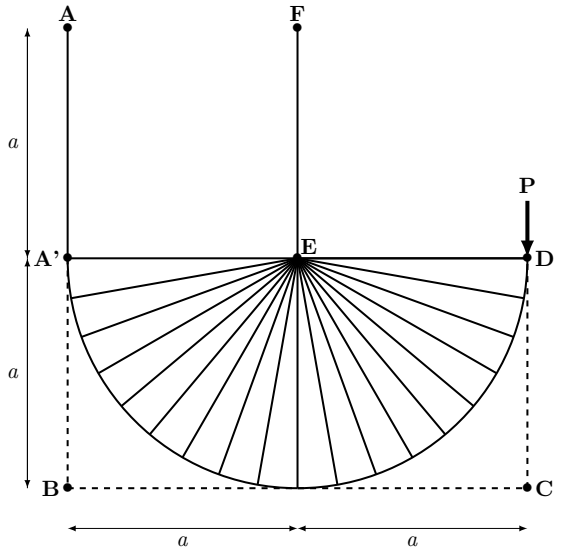

Figure 3.4: Analytical solution of the L-shape benchmark in the framework of Michell's structure.

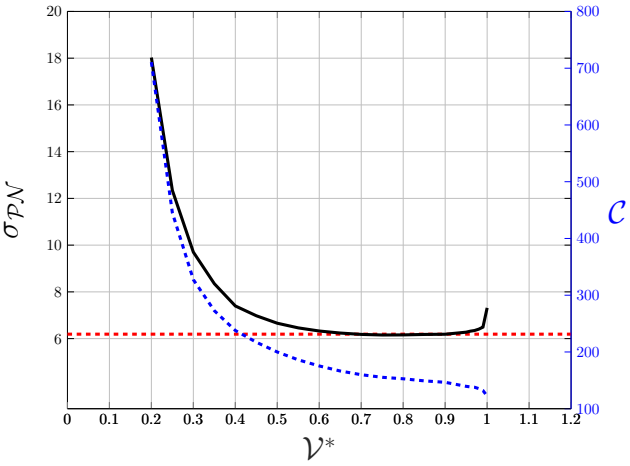

Figure 3.5: Variation of the P-norm value for various remaining volume fraction.

Besides the non-FSD behavior as discussed previously, other differences between the solution obtained in Figure 3.3 and the theoretical solution in Figure 3.4 are observed. First of all, many bars in the A'BCD region are present and meet at E. The design in Figure 3.3 has its corner rounded off and presents a limited number of reinforcement members. The large number of bars in the theoretical solution enables to reduce the intensity of the stresses by distributing the flow among them. The obtained layout is stiffer but seems unattractive from a good engineering practice point of view. This comparison highlights that topology optimization with stress constraints goes against what might be expected to reduce stress concentrations.

Indeed, optimization adds holes, in wisely chosen places, instead of adding unnecessary material. This example shows the interest of this design method.

As discussed in ARTICLE 1, an interesting aspect of the stress–based problem is the non-monotonicity of the maximum stress with respect to the remaining volume fraction of material. Indeed, in absence of body load, the problem of minimizing the compliance under a volume constraint is known to present a monotonic decreasing behavior of the objective function with respect to the requested remaining volume fraction. The evolution curve of such a behavior is illustrated in Figure 3.5. This means that, in theory, for any remaining volume fraction of material, there will always be a separate solution for each $\mathcal{V}^*$ value. Given this observation, it is legitimate to investigate the behavior of the problem including stress constraints. To this end, we studied several problems of minimizing the maximum stress under a volume constraint. The maximum stress is represented by a p-norm function, noted $\sigma_{\mathcal{PN}}$, due to the non differentiability of the "max" function. The resulting curve is shown in Figure 3.5. It is observed that the obtained behavior is quite different from the one of the compliance minimization problem. Indeed, for low volume fractions, the lower the volume of remaining material, the bigger the maximum stress. This is explained by the fact that smaller structural members constitute the structure and that consequently the stress state begins to increase. Then for larger values of material, the value of the maximum stress reaches a stable value, here around 6, for a wide range of remaining volume fraction. This indicates that reaching designs with stress values below the stabilized one can lead to great convergence efforts for the optimizer since it would become difficult to fulfill this requirement. We conclude that, the problem with stress constraints is therefore less flexible than the compliance problem. In the case of a problem with strength restrictions, several scenarios are distinguished. On the one hand, if the objective is to reduce the maximum stress value for a low volume target, it appears that the optimization process will lead to a solution that violates the material limit, e.g., the yield stress. On the other hand, if the objective is to lighten the structure as much as possible by imposing a limit that can not be exceeded by the stress, several cases are possible. Firstly, if the stress limit to be reached is feasible, i.e., the value to fulfill is around the stabilized one or bigger, the optimization process will work correctly since the problem is well posed. Secondly, if the admissible limit is too restrictive, i.e., below the stabilized value, the optimization problem is poorly stated and by virtue of the non-monotonic behavior, see Figure 3.5, the structure will not be lightened and admissible value of the stress will be violated in some points. From the point of view of the benchmark problems, the foregoing discussion implies that a monotonic behavior of the maximum stress with respect to the volume fraction cannot be expected.

Studies conducted over the years on compliance minimization problems have shown that the topology optimization process requires regularization procedures to obtain a well–posed problem. Indeed, several numerical issues have been observed such as the checkerboard pattern or the mesh dependency of the solution, see e.g., [Diaz and Sigmund (1995)]. When Q4 elements are used, the checkerboard pattern appears because it exhibits artificially very high stiffness and is therefore privileged by the optimizer. The mesh dependency comes from the chosen interpolation law, e.g., the SIMP model, which, although allowing to relax the problem as explained in the previous chapter, leads to a badly mathematically posed optimization procedure, i.e., no unique solution exists. For stress–based topology optimization, the mesh dependency and checkerboard problem are also encountered. Several procedures are available to overcome the aforementioned issues and the most commonly encountered way of dealing with both aspects at the same time is the filtering techniques, see e.g., [Sigmund and Peterson(1998), Sigmund(2007)]. The filters as they are defined in the previous chapter act like a so–called length scale control on the size of the structural members of the optimized layouts. The two most commonly encountered types of filters are presented in Section 2.1.2 of the previous chapter. For the problem with

stress constraints, each type of filter leads to a well defined optimized structure. However, as shown in ARTICLE 1, the density filter is more adapted than the sensitivity filter because the latter leads to important oscillations both in the evolution of the objective function and in the Karush-Kuhn-Tucker (KKT) optimality conditions. It is therefore advised to use the density filter for stress–based problems. In the remaining of this manuscript, the presented results are always obtained using the density filter as it has been the case for all the results shown so far. It should also be emphasized that all the numerical parameters related to the filtering scheme have to be referred when presenting numerical examples as the solutions can be strongly dependent on the chosen values. Let's mention that a recent work from [Amir and Lazarov(2018)] uses the stress information in order to build a new filtering technique to provide length scale control to the optimized solution while controlling the stress level. The authors shows that the proposed procedure is a promising alternative to the classical stress–based topology optimization problem.

Finally, to conclude this section, it should be reminded that topology optimization with stress constraints is a non-linear problem in which the choice of the starting point might influence the performance of the optimized results. A recent work by [Yan et al.(2018)], in the context of optimal structures for heat conduction problems, has highlighted the importance of choosing well the starting point to get the optimized solution with the best performance. Indeed, it is shown that the tree structure, commonly obtained and accepted, in the literature is a sub-optimal solution coming from the chosen starting point that distributes the density field uniformly. In contrast, the aforementioned contribution shows that lamellar needles provide the optimal topologies illustrating the propensity for the optimization process of getting stuck in a local optimum only due to a bad choice of the starting point. As far as stress constraints are concerned, the various studies carried out by the author do not allow to answer with certainty the question of the optimal starting point. A complete study of the robustness of the methods solving such a problem as well as the influence of the starting point is beyond the scope of this work but mentioning it here is to remind how important it is to always specify the chosen starting point when an optimized result is presented.

3.1.3 Comparison of solution approaches for stress constrained topology optimization

Problem formulation

Topology optimization with stress constraints has been the subject of numerous publications since the founding work of [Duysinx and Bendsøe(1998)]. The major numerical problems described in the previous chapter, i.e., the singularity phenomenon and the high computational time, has attracted particular research attention over the years. The consequence is that nowadays the literature reports several methods claiming to be effective without any real and fair point of comparison.

Part of this thesis is dedicated to the comparison of usual approaches proposed to solve the weight minimization problem under stress constraints, mathematically formulated in Eqn. (3.11).

$$\min_{\boldsymbol{x}} \quad \mathcal{W}(\boldsymbol{x}) \tag{3.11a}$$

$$\text{s.t.} \quad \mathbf{K}(\boldsymbol{x})\ \mathbf{U} = \mathbf{F}, \tag{3.11b}$$

$$\sigma^* \leq 1, \tag{3.11c}$$

$$0 \leq x_e \leq 1, \qquad e = 1, \ldots, n_e \tag{3.11d}$$

In (3.11),

- (3.11a) is the objective function and represents the weight of the structure, noted $\mathcal{W}$, to be minimized.
- (3.11b) recalls the state equation of linear elastic structure to be solved. It represents the static equilibrium equation written into finite element discretization.
- (3.11c) represents the stress criterion introduced in the optimization problem.

In (3.11c) σ^* is a generic form of the stress measurement that depends on the considered approach. In this work, we prefer the term "approach" rather than "method" because some modifications in their original formulation have been made. The reasons which guided this choice relate in particular to the obsolescence of certain methods or the lack of information in the related papers that prevents to reproduce them identically. As an example, a method that originally used ε-relaxation to tackle of the singularity phenomenon has been implemented as part of the *qp*-relaxation more commonly encountered in recent publications. Besides updating an approach, this allows comparing the performance of the different schemes in the same framework. That being said, the essence of each of the selected methods has been retained. In this work, we compare nine different approaches reported in Table 3.2 for which the fundamental idea is also recalled. Their respective mathematical formulation are reported in ARTICLE 1.

Original paper	Idea of the method	Reference
[Duysinx and Bendsøe(1998)]	Reference solution (no drop in the CPU burden)	*local 1*
[Duysinx and Bendsøe(1998)]	Active-set strategy	*local 2*
[Bruggi and Duysinx(2012)]	Active-set strategy + compliance constraint	*local 3*
[Duysinx and Sigmund(1998)]	Aggregation by p-norm function	*global 1*
[Duysinx and Sigmund(1998)]	Aggregation by p-mean function	*global 2*
[Paris et al.(2009)]	Aggregation by KS function	*global 3*
[Le et al.(2010)]	Clustering + adaptive p-norm function	*regional 1*
[Holmberg et al.(2013)]	Clustering + p-mean function	*regional 2*
[Paris et al.(2010)]	Clustering + KS function	*regional 3*

Table 3.2: Approaches considered for comparison.

Details regarding the implementation of certain approaches, e.g., aggregation parameter, compliance constraint, active-set, etc., are provided in ARTICLE 1. To evaluate the performance of the approaches, we compare the total accumulated CPU time needed to solve the optimization problem (t_{tot}), the time spent in MMA (t_{MMA}) and the time spent evaluating the sensitivities (t_{sense}). In addition, the number of iterations to achieve convergence (It.), the final value of the objective (Obj) and the number of constraints treated by the optimizer at the end of the process (m) are also provided. Finally, the average time per iteration ($t_{mean/it}$) is referenced. Since static strength is the primary objective of our study, it is interesting to assess whether local stress values are above the prescribed stress limit once the optimization reaches convergence. The normalized maximum local stress, that is, the maximum local stress divided by the prescribed stress limit, σ_y^0, concludes the comparison data. We also introduce the quantity *pd* which measures how much the MMA parameters have been changed from their default value, see [Svanberg(1987)]. The latter are used to stabilize convergence and can be either *move-limits* (ml) or a modification of the MMA asymptotes update strategy. The change

of these is set using the parameter $\beta \leq 1$ which multiplies them and modifies their value if $\beta \neq 1$. The *pd* expression is given to the Eqn. (3.12) below.

$$pd = \frac{(1 - m_l) + (1 - \beta)}{2} \times 100, \tag{3.12}$$

It is needless to say that the expression in Eqn. (3.12) is only an indicator and other forms of measures can be proposed. The parameter values that will be presented in the following section do not necessarily correspond to optimal values and have been determined after trials and errors to ensure the convergence of the different solutions.

Numerical application

The example treated in this section is the L-shape design, represented in Figure 3.1. Table 3.3 gathers the move-limits and β parameter values used to obtain the optimized solutions, that will be later presented, as well as the resulting *pd* factor. The other parameters necessary for the optimization are referenced in ARTICLE 1. They correspond to the default values of the optimization algorithm (MMA), see [Svanberg(1987)]. The initial starting point (x_{ini}), representing a uniform density distribution all over the design domain, is also provided in Table 3.3.

The filter radius for this example is defined as $r_{min} = 1.5l_e$ with l_e being the size of the element edge. For local stress constraints approaches, no modification on the asymptotes value and no use of move-limits are necessary, as suggested in [Duysinx and Bendsøe(1998)].

	m_l	β	$pd[\%]$	x_{ini}
local 1	1.0	1.0	0.0	1.0
local 2	1.0	1.0	0.0	1.0
local 3	1.0	1.0	0.0	1.0
global 1	0.07	1.0	46	1.0
global 2	0.07	1.0	46	0.5
global 3	0.07	0.95	49	1.0
regional 1	0.3	0.95	37	0.5
regional 2	0.1	1.0	45	0.5
regional 3	0.07	1.0	46	1.0

Table 3.3: Remaining numerical parameters used to solved the L-shape problem.

As can be seen in Figure 3.6, the influence of the chosen approach on the final optimized structures is strongly perceptible. This clearly shows the presence of many local optima in the design space. For a given choice of parameters, that influences the conditioning of the optimization process, the optimization process is directed towards one or another descent direction. Although the achieved topologies show disparities, each of them meets design expectations in the sense that the re-entrant corner, region of high stress concentrations, is rounded off. Note however that some approaches avoid it with a more intense rounded shape, see Figure 3.6(b), Figure 3.6(e), Figure 3.6(e) and Figure 3.6(g). As shown in Table 3.4, the total time required to reach convergence for the reference solution, i.e., the approach *local 1*, is high. Moreover, in this case, most of the time is devoted to updating the design variables, i.e., the time spent in MMA. This is not surprising given that the optimizer used here is based on a dual approach, effective only for a number of constraints treated much less than the number of design variables, that is of elements. However, the number of iterations is relatively small. Finally, as expected, the structural integrity is strictly respected since the maximum local stress is equal

to the prescribed stress limit, i.e., $\frac{\sigma^{max}}{\sigma_y^0} = 1$. The other two local approaches, i.e., *local 2* and *local 3*, considerably reduce the computation time required by introducing a selection of handled constraints via an active–set selection strategy, described in ARTICLE 1. As shown in Table 3.4, the average time per iteration is drastically reduced due to the process of considering a fewer number of constraints. Using a global compliance constraint accentuates the reduction of the computational burden by further lowering the average time per iteration by a less important selection of constraints, in agreement with [Bruggi and Duysinx(2012)]. Finally, it should be noted that, as for the reference solution, the structural integrity is guaranteed in the approaches with an active-set and the final values of the objectives are quite close to the reference value, the approach *local 3* being slightly bigger. Finally, by observing the convergence curve of the objective function ($\mathcal{W}$), represented in Figure 3.7, it appears that some oscillations are encountered during the optimization but without having a significant impact on the process. No oscillations are observed for the approaches *local 1* and *local 2*, demonstrating their high robustness. Note also that few iterations are necessary before the value of the objective function reaches a plateau. The long plateau is due to the chosen convergence criterion chosen described in ARTICLE 1, which requires very small design changes. From a practical point of view, its presence implies that the process could have been interrupted before reaching the convergence specified in this work.

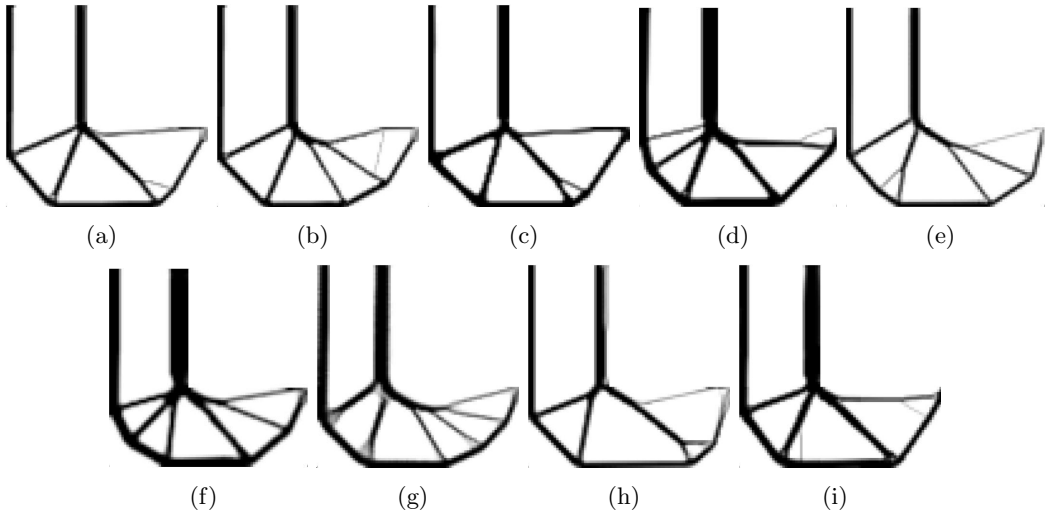

Figure 3.6: Achieved design using several stress–based approaches to solve the L-shape benchmark: (a) Pure local (b) Local + active set (c) Local + active set + compliance constraint (d) p-norm (e) p-mean (f) KS (g)Clustering with adaptive p-norm (h) Clustering with p-mean (i) Clustering with KS .

Looking further at Table 3.4, it is observed that global approaches generally reduce the computational time needed to solve the problem despite a greater number of iterations. Indeed, the average time per iteration is about half a second, giving these methods an undeniable efficiency of execution. However as shown in Table 3.3, the *pd* parameter is not negligible confirming the parameter dependency of aggregation–based approaches. As discussed in Section 2.3.3 of Chapter 2, approaches based on a p-norm (*global 1*) or KS (*global 3*) function overestimate the maximum local stress leading to much heavier structures than the reference solution. However, the structural integrity of the layouts is guaranteed because $\frac{\sigma^{max}}{\sigma_y^0} < 1$. The approach *global 2* has exactly the opposite effect because it is based on a p-mean function. Therefore, it underestimates the maximum stress leading to a structure whose objective is similar to the reference but

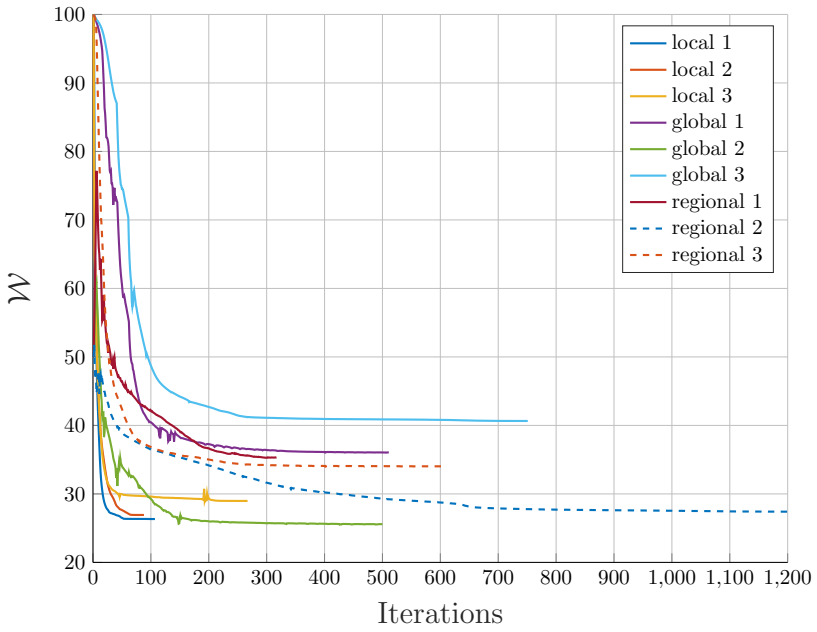

Figure 3.7: Evolution of the objective function for the L-shape benchmark for the studied approaches.

without guaranteeing structural integrity, i.e., $\frac{\sigma^{max}}{\sigma_y^0} > 1$. By observing Figure 3.7, oscillations are to be noted for each of the global approaches and this despite the use of move-limits or changes in the asymptotes values. It is also shown that the rate of descent is lower than local approaches due to the need of using stabilization procedures. The latter are essential in the case of approaches with an aggregation functions to ensure convergence. The stabilization of the objective function, symbolized by the presence of a plateau, appears only for a number of iterations higher than for local approaches, indicating that it is important to let the optimization process last longer. This remark highlights the major disadvantage of global methods but shows that once numerical stabilization has been achieved, they are particularly interesting in the context of an efficient optimization process from the point of view of computational time but especially concerning the average time per iteration.

Regarding regional approaches, although a reduction in time is indeed observed, due to the decrease in average time per iteration, the effectiveness of these approaches is quite relative compared to global approaches. Nevertheless, for the example discussed in this section, in the case of the approach *regional 1*, the number of iterations to achieve convergence is reasonable and the structural integrity is guaranteed ($\frac{\sigma^{max}}{\sigma_y^0} = 1$) making it the best alternative to solve the L-shape problem. However, the target value is higher than the reference value. For the approach *regional 2*, the number of iterations is large and the structural integrity is not granted, i.e., $\frac{\sigma^{max}}{\sigma_y^0} > 1$. Finally, the approach *regional 3* converges towards a heavier optimal solution than the reference solution but ensures that the maximum value of the local constraint is well below the prescribed limit. When observing the convergence curves in Figure 3.7, it is noted that, compared to global approaches, less intense oscillations appear. This effect is due to the clustering of local stresses which allows a more localized control of their value and a lower

aggregation exponent. However, it is again observed that the rate of descent is slower than for local approaches due to the numerical stabilization techniques essential for ensuring convergence. This is reflected by the appearance of the plateau for a greater number of iterations.

As a summary, for the example discussed here, it has been demonstrated that local approaches with active-set allow a significant reduction in computation time while guaranteeing the structural integrity of the structures and this for an acceptable number of iterations. For these approaches, the decrease in the objective function is fast and stabilizes quite early, as evidenced by the appearance of a plateau after a small number of iterations. In practical terms, this means that the optimization process could be stopped quickly if the designer's goal is to achieve only a stable value of the objective. Local approaches are really well suited when new developments have to be made in a first step before considering computational efficiency. In order to further reduce computational time, it was observed that global approaches are of undeniable interest. However, due to the use of numerical stabilization, the descent of the objective is slower. Furthermore, structural integrity is not guaranteed if the value of the maximum local constraint is underestimated, as in the case of the approach *global 2* (p-mean). For the approaches *global 1* (p-norm) and *global 3*(KS), the overestimation of the maximum stress leads to heavier structures than the reference solution but guarantees structural integrity. If the designer's goal is to obtain the most efficient process, it is appropriate to turn to this type of approach and choose whether the maximum local constraint should be respected or not. Finally, the regional approaches also proved to be effective compared to the reference solution but, with the exception of the approach *regional 1*, they do not bring any advantage compared to the global approaches. In Table 3.4, the line related to the reference solution is underlined and the best solution scheme is put in bold. Let's note that the CPU time values referred here are obtained when using a personal computer with the following specifications: Intel(R) Xeon(R) CPU E3-1505M v5 @ 2.8 GHz 32 Go RAM.

Figure	$t_{tot}[s]$	$t_{MMA}[s]$	$\%MMA$	$t_{sens}[s]$	$\%sens$	$t_{stat}[s]$	$\%stat$	It.	Obj	m	$t_{mean/it}[s]$	$\frac{\sigma_{max}}{\sigma_y^0}$
3.6(a)	22641	18608	82.19	1664	7.35	2.33	0.01	107	26.33	4096	211.60	1
3.6(b)	985.68	402.95	40.88	235.02	23.84	1.70	0.17	88	26.93	565	11.20	1
3.6(c)	495.26	168.70	34.06	123.73	24.98	5.19	1.05	267	28.97	98	1.85	1
3.6(d)	282.08	223.35	79.18	26.36	10.06	11.23	3.98	511	36.05	1	0.55	0.87
3.6(e)	226.13	175.07	77.42	24.30	10.75	10.30	4.55	500	25.58	1	0.45	1.25
3.6(f)	467.90	380.42	81.31	42.00	8.98	16.50	3.53	751	40.65	1	0.62	0.87
3.6(g)	**184.04**	**110.86**	**60.24**	**55.58**	**30.20**	**5.25**	**2.86**	**317**	**35.34**	**8**	**0.58**	**1**
3.6(h)	627.81	296.11	47.17	262.03	41.74	20.66	3.29	1200	27.40	10	0.52	1.40
3.6(i)	598.40	369.41	61.73	198.03	33.09	10.76	1.80	606	34.03	16	0.99	0.93

Table 3.4: Numerical performances of the studied approaches for the L-shape benchmark.

In ARTICLE 1, similar simulations to those illustrated above were performed on two other examples. The observations made on the L-shape have been confirmed in that global approaches are the best alternative to meet the need for CPU time reduction. Regional approaches also help to achieve this goal but do not contribute much when compared to purely global approaches. Moreover, because of their definition and the use of clusters, the implementation is more meticulous, which again is not in their favor compared to global approaches.

In conclusion, the studies carried out in ARTICLE 1 enable to restate the theory of stress constraints in topology optimization while allowing the definition of benchmarks that can be used to carry out a fair comparison of future methods to solve this problem. It is shown the importance of specifying all the numerical parameters used because they condition the entire optimization process.

3.1.4 Introduction of static stress constraints in the design of architectured materials

This section aims at illustrating the introduction of stress responses into the framework of periodic microstructural design using topology optimization, see e.g., [Sigmund(1994), Sigmund(1999)]. However, the term "microstructure" can be misleading because it has not to be understood in the context of metallurgy where it designates the granular distribution of material. The structures that are proposed to be designed have a higher length scale than the characteristic size of these grains. Hence, we will refer to the design of *mesostructures* or *architectured materials*. The emergence of novel additive manufacturing techniques encourages the search for innovative approaches to adapt the properties of materials. Indeed, it is now possible to manufacture parts with complex micro-geometry but also to introduce regions with graded material. These zones can be sized to withstand the stresses encountered by mechanical components while guaranteeing their lightness. Many examples in nature like wood and bones [Greil et al.(1998), Lan Levengood and Zhang(2014), Mattheck(1998)] present a complex architectured mesostructure to support the various loads to which they are subjected to. The manufacturing industry, driven by the possibilities offered by additive manufacturing techniques, is now taking inspiration from nature to fabricate tailored innovative components ([Mok et al.(2016)]).

In order to illustrate the goals of the study, let us consider the structure, discretized by finite elements, in Figure 3.8. The scale of this clamped beam subjected to a bending effort is referred to as the *macroscopic scale* or *structural scale*. By solving the static equations, it is possible to compute at each Gauss point, represented by the crosses, a macroscopic strain field ε^{macro}. A Representative Unit Cell (RUC) is associated to each of these Gauss points and sustains the previously computed strain field. This scale is referred to as the *mesoscopic scale*. Therefore, it is possible to introduce within the optimization process a two-level design procedure, e.g., FE^2 ([Feyel(2003)]), aiming at optimizing the structure at the macroscopic scale but, also, optimizing the mesoscale geometry and the material distribution. The objective is to design optimal components presenting regions constituted by architectured sub-structures similar to those encountered in nature.

In this thesis, the two-level procedure is not fully considered and our investigation focus solely on the mesoscopic scale. The far strain field, i.e. ε^{macro}, is therefore unknown so far and, to perform the optimization, arbitrary macro test fields are imposed on the RUC. The direct consequence of this approach is that material properties, such as the yield stress σ_y^0 not to exceed, do not really match the physical values of the base material but they are arbitrarily chosen. That being said, in the future, the procedure developed during this research work is directly transposable, at the price of minor modifications to cases where a two-level procedure is considered. The major contribution of the developments held in this work is to introduce stress

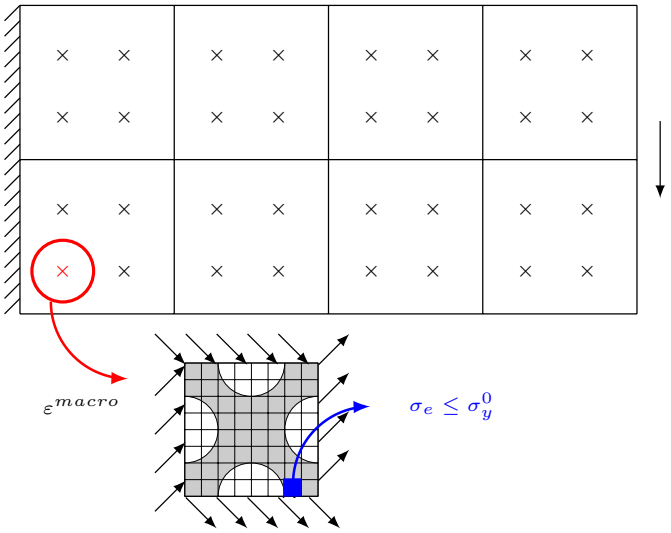

Figure 3.8: Fundamental idea of the microsctructural design problem of this thesis.

constraints into the design problem in order to reduce stress concentrations that may occur during the optimization. The goal is not to determine an equivalent criterion or first point of plasticity that can be used microscopically.

In the following, the various hypotheses underlying our formulation are defined and the optimization problem solved is presented and discussed. Then, typical results of the developed approach are illustrated. More details can be found in ARTICLE 2 attached in the Appendices.

Formulation of the architectured materials design problem

The design of architectured materials with topology optimization was introduced by [Sigmund(1994)] and has since been the subject of many extensions in various fields, see e.g., [Cadman et al.(2013)]. A usual formulation of the optimization problem is to maximize (resp. minimize) equivalent material properties ($f(E_{ij}^H)$), e.g., the equivalent bulk modulus or the equivalent shear modulus, under a volume constraint (V^*). In this thesis, we propose also to reduce the stress intensities by introducing additional constraints to the optimization problem conventionally encountered. A general mathematical formulation of the structural optimization writes:

$$\begin{aligned}
\min_{\boldsymbol{x}} \quad & f(E_{ij}^H) && i,\ j = 1,2,3 && \text{(3.13a)}\\
\text{s.t.} \quad & \mathbf{K}(\boldsymbol{x})\ \mathbf{u}_i = \mathbf{f}_i^0(\boldsymbol{x}), && i = 1,2,3 && \text{(3.13b)}\\
& \mathbf{K}(\boldsymbol{x})\ \boldsymbol{\chi}_s = \mathbf{f}_s(\boldsymbol{x}), && s = 1,\dots,n_s && \text{(3.13c)}\\
& x_e^{p-q}\ \overline{\sigma}_{e,s}^{\mathrm{VM}} \leq \sigma_y^0, && e = 1,\dots,n_e && \text{(3.13d)}\\
& && s = 1,\dots,n_s &&\\
& V(\boldsymbol{x}) \leq V^\star, && && \text{(3.13e)}\\
& 0 \leq x_{\min} \leq x_e \leq 1, && e = 1,\dots,n_e && \text{(3.13f)}
\end{aligned}$$

In (3.13),

- (3.13a) is the objective function depending on the homogenized elastic properties of the RUC, i.e., E_{ij}^H.
- (3.13b) is used to evaluate homogenized elastic properties, see (2.47) in Chapter 2.
- (3.13c) refers to load cases n_s applied to the RUC as external arbitrary strain fields. The loading vectors $\mathbf{f}_s$ are computed according to the same procedure as the one used for the evaluation of $\mathbf{f}_i^0$, see (2.49) in Chapter 2. These load cases generate stresses inside the unit cell and these will be controlled by the imposition of stress constraints.
- (3.13d) introduces $n_e \times n_s$ local stress constraints, where n_e is the number of elements. To reduce the computational effort associated with the large number of constraints, an active–set selection strategy is used and is recalled in ARTICLE 2. The number of constraints n_a is then less than the maximum number of constraints $n_e \times n_s$. Remember that in this equation, σ_y^0 defines an arbitrary chosen stress limit value that has not to be exceeded and does not correspond exactly to the actual yield stress of the material.
- (3.13e) enforces the volume of the final design to reach a given value V^*.
- (3.13f) introduces a $x_{\min}$ lower bound on the design variables. This one enables preventing the singularity of the stiffness matrix. The value of $x_{\min}$ is typically set to 10^{-3}, as recommended by [Bendsøe and Sigmund(2003)] for base materials with a Poisson coefficient of 0.3. Note that if the modified SIMP law as defined in [Sigmund(2007)] had been used and, x_{min} would have been imposed at 0. In the development of ARTICLE 2, the classic SIMP law has been used for the developments and therefore a non-zero minimum limit is imposed.

As mentioned above, the effective elastic properties are determined using the theory of homogenization, for which the theoretical background has been recalled in the previous chapter. In addition, we restrict the analysis to the case of periodic structures. The use of homogenization requires that the characteristic dimensions between the mesoscopic scale (l_{RUC}) are much smaller than those of the macroscopic scale (l_{macro}), i.e., $l_{RUC} \ll l_{macro}$ ([Besoussan et al.(1978), Sanchez-Palencia (1983), Suquet(1982)]). The latter relation is referred to as the separation of scales and we will assume that this is indeed the case in our analyses. Furthermore, the assumption that the structure is periodic may be incorrect under certain conditions, e.g., in the presence of localized actions such as strong gradients or edge effects. However, as discussed in [Kouznetsova et al.(2001)] as long as the separation of scales $l_{RUC} \ll l_{macro}$ is respected, the periodicity of the structure can be assumed.

As indicated in (3.13d), the limitation of the stress intensities is carried out by introducing stress constraints in the optimization problem whereas it is commonly accepted to use them as an objective, see e.g., [Noël and Duysinx(2017)]. However, it is legitimate to consider the stress constraints as described above. Indeed, the theory of homogenization is based on the separation of scale but does not require an infinitesimal dimension of the mesoscopic scale, see [Sanchez-Hubert and Sanchez-Palencia(1992), Hassani and Hinton(1997)]. Since the dimensions of the RUC are finite, we can suppose that the assumptions of continuum mechanics remain valid. Therefore, the equivalent Von Mises stress can be defined at each point similarly to the work of [Gurson(1977), Michel et Suquet(1993), Ponte-Castenada and De Botton(1992), Duysinx and Bendsøe(1998)]. Moreover, mathematically speaking, swapping the problem by placing the stress as restrictions and not as objective is equivalent as discussed in ARTICLE 2. With the density–based topology optimization approach, numerical experiments have shown that using the stresses as the objective and solving the "min-max" problem commonly defined

by the bound formulation ([Bendsøe and Sigmund(2003)]) is more difficult to handle in practice. Alternatively, replacing the "max" function by a continuous function reduces the computation time but introduces additional non-linearities that are detrimental to the stability of the process. Therefore, the approach followed in this work results from a good compromise between stability of the optimization and computational efficiency. The procedure used here is associated with an active-set strategy, i.e., a selection of the most dangerous constraints, to reduce the computational burden. More details are available in ARTICLE 2.

Finally, by observing (3.13b) and (3.13c), it appears that the equivalent loads are design dependent. Therefore, the term $\frac{\partial \mathbf{F}}{\partial x_j}$ in (3.8) is non-zero in the present case and must be accounted for in the sensitivity evaluation like in self-weight problems, see [Bruyneel et al.(2005)]. The latter is computed as:

$$\frac{\partial \mathbf{F}}{\partial x_j} = p\ x_j^{p-1}\ \mathbf{f}_e^0, \tag{3.14}$$

with $\mathbf{f}_e^0$ defined in Eqn.(2.49) of Chapter 2.

Numerical application

As explained in the previous paragraphs, the design problem in Eqn. (3.13) is investigated in ARTICLE 2. The approach is first evaluated on a classic example of the literature inspired from the work of [Vigdergauz(2001)]. This test case corresponds to a two-dimensional plate subjected to hydrostatic loading for which the optimal contour of a single inclusion is sought for. The optimized contour thus minimizes the elastic energy of the structure as well as the stress concentrations. The works of [Vigdergauz(2001)] and [Grabovsky and Kohn(1995)] show that the optimal contour is characterized by a family of "ellipses" whose final shape depends on the desired remaining volume fraction of material . For this optimal structure, the bulk modulus, denoted by $\mathcal{K}$, is optimal and saturates the theoretical lower bounds of [Hashin and Strickman (1963)]. Then solving Eqn. (3.13) where $f(E_{ij}^H) = \mathcal{K}$ and without Eqn. (3.13d) allows finding Vigdergauz's theoretical results to some precision errors due to the FE discretization and geometrical precision offered by the density maps. The introduction of the constraint (3.13d) has demonstrated its effectiveness by limiting the stress values within an arbitrarily prescribed limit. The comparison between the baseline results and the approach developed leads to a more square shape inclusion, better adapted to the reduction of stress concentrations. However, the value of the obtained bulk modulus $\mathcal{K}$ leaves a bit the theoretical Hashin-Strickman lower bound. These minor differences are due to the approach followed in this work because the initial problem of [Vigdergauz(2001), Grabovsky and Kohn(1995)] is not really solved. In this contribution, stress constraints assign a prescribed value of the stress value, making the problem more restrictive. This steers the optimization towards a less optimal solution of the design space regarding the achieved objective function value. However, one achieves a solution consistent with the theoretical approach and meeting the stress requirements .

The synthesis of a mesotructure with a negative Poisson's ratio as well as an original example aiming at supporting a piece of art while providing an insolation with respect to shear loads is in numerical applications of ARTICLE 2. These two test cases highlight different aspects of the optimization process developed during this research. In order not to weigh down this manuscript and because the complete results are available in the Appendices, we will illustrate, in the following, a single example: The synthesis of a material with a negative Poisson's ratio. In particular, the objective is inspired from the work of [Xia and Breitkopf(2015)] and is given by $f(E_{ij}^H) = E_{12}^H - \beta^k \left(E_{11}^H + E_{22}^H\right)$ with a constant β such as $\beta < 1$ and k the current iteration number. The objective function thus formulated enables at the beginning of the optimization

process to guarantee the structural integrity along the main axes. As the process goes on, the term β^k tends towards 0 then allowing minimizing the coefficient E_{12}^H and realizing a material with negative Poisson's ratio. The starting point of the test case is provided in Figure 3.9. It represents a square with a hole in its center. The result of topology optimization solving (3.13) without accounting for stress constraints is represented in Figure 3.10(a). The related stress field is represented in Figure 3.10(b) for an arbitrary ε_x field. As we can see, the optimized layout has a complex topology exhibiting thin structural members that quickly fail due to stress concentrations. Therefore, introducing stress constraints as recommended in this research and still applying the arbitrary field ε_x, leads to the optimized design shown in Figure 3.11(a). The corresponding stress field is illustrated in Figure 3.11(b). A drastic change in the optimized topology is observed in order to reduce the stress concentrations we observed previously. The weak structural members have been replaced by thicker parts allowing a better distribution of the stress flow within the mesostructure. Moreover, the study conducted in ARTICLE 2 showed that when the topology changes as in this case, a better value of the objective function can be reached. This illustrates the fact that the solved problem has many local minima and that, when stress constraints are accounted for, the optimization process may be steered towards better optima. Additional analyses were conducted to corroborate and confirm these observations. In ARTICLE 2, it is also shown that solving the problem (3.13) with stress constraints, without a change of topology, leads to a less optimal structure in terms of objective. This result is expected because for a solution with a similar topology, the more constrained the problem, the smaller the feasible space of solutions.

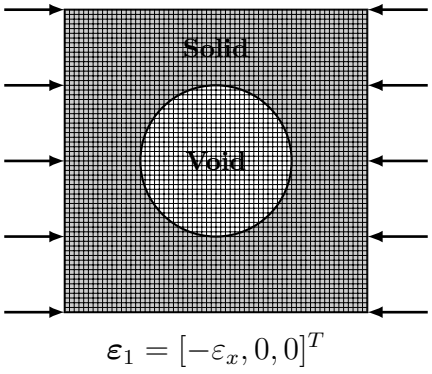

Figure 3.9: Initial geometry used to solve the problem (3.13) for the synthesis of negative Poisson's ration materials.

Additional investigations are conducted on an example with two load cases and identical observations were carried out. More information is available in ARTICLE 2.

3.2 Fatigue Strength Constraints

This section aims at illustrating the main results regarding the consideration of fatigue strength into the topology optimization process. As mentioned in Section 2.4 of the previous chapter, only high cycle fatigue is considered in this work. The use of stresses as quantities to construct the fatigue criteria is followed and the formalism adopted in the previous sections, e.g., relaxation of constraints, remains applicable.

First of all, an important element in fatigue design is the load modeling. The latter is briefly reminded. Second, the sensitivity analysis of each criterion used in this research work is

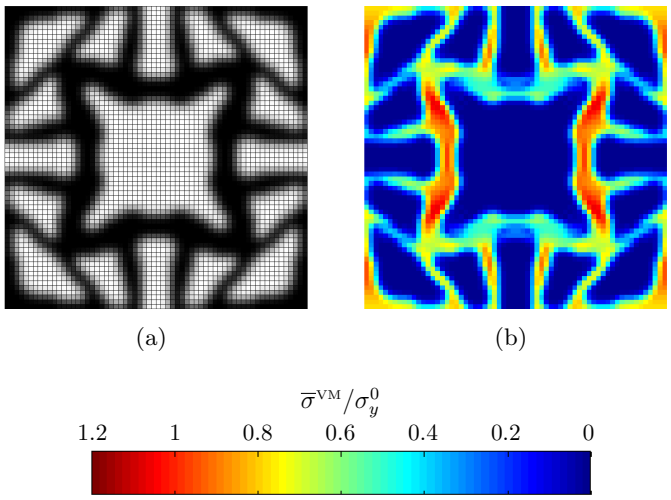

Figure 3.10: Material with negative Poisson's ratio without stress constraints: (a) Optimized design (b) Stress map.

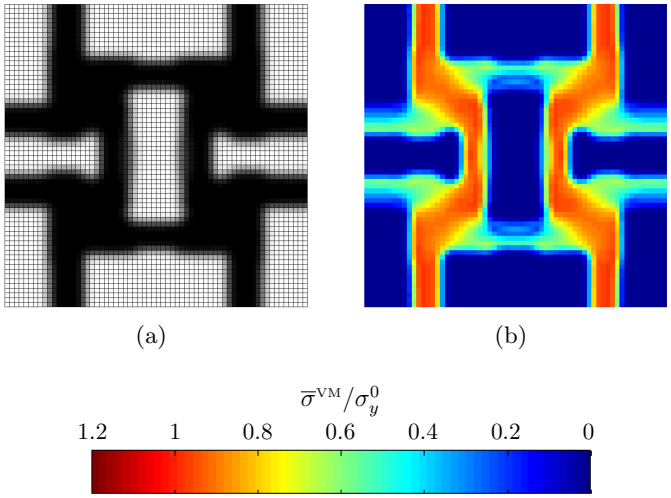

Figure 3.11: Material with negative Poisson's ratio with stress constraints: (a) Optimized design (b) Stress map

revisited. Again the L-shape benchmark, see Figure 3.1, is selected to illustrate the behavior of each fatigue criterion and the reader can refer to ARTICLE 3 and ARTICLE 4, as well as to the PROCEEDING for more numerical examples.

3.2.1 Goodman, Sines and Crossland criteria

The implementation of Goodman, Sines and, Crossland criteria is described and is carried out in ARTICLE 3 and the PROCEEDING. First of all, the structural optimization problem solved in the aforementioned contributions is given in Eqn.(3.15). The objective is to minimize the weight ($\mathcal{W}$) subjected to fatigue stresses and a global compliance constraint as suggested in [Bruggi and Duysinx(2012)]. For the considered examples of this section, the compliance constraint helps reducing the computational time by allowing fewer selection of the most dangerous

constraints. Indeed, as we have seen in Section 3.1.3, combining an active-set selection strategy with the global compliance constraint enables further reducing the average time per iteration by lowering the number of constraints to be addressed to the optimizer. That is why this procedure was chosen in these contributions. All the numerical parameters values can be found in the Appendices.

$$\min_{\boldsymbol{x}} \quad \mathcal{W}(\boldsymbol{x}) \tag{3.15a}$$

$$\text{s.t.} \quad \mathbf{K}(\boldsymbol{x})\ \mathbf{U} = \mathbf{F}, \tag{3.15b}$$

$$\sigma_f^* \leq 1, \qquad e = 1, \ldots, n_e \tag{3.15c}$$

$$\mathcal{C}(\boldsymbol{x}) \leq \alpha_c \mathcal{C}_0, \tag{3.15d}$$

$$0 \leq x_e \leq 1, \qquad e = 1, \ldots, n_e \tag{3.15e}$$

The numerical results presented below have been obtained with the procedure developed in ARTICLE 3 and the PROCEEDING but have been slightly modified. Indeed, the material interpolation law used in these original contributions is the classical SIMP law, while the numerical results presented in this work have been performed with the modified SIMP law explaining the null value that design variables can take at Eqn. (3.15e). Of course, this does not change the procedure developed in the published works.

Load Modeling

For this first part, time varying loads are assumed to be proportional, with constant amplitude. The latter then take the form of sinus shapes as sketched in Figure 3.12(a), generating fluctuating stresses within the structure as illustrated in Figure 3.12(b).

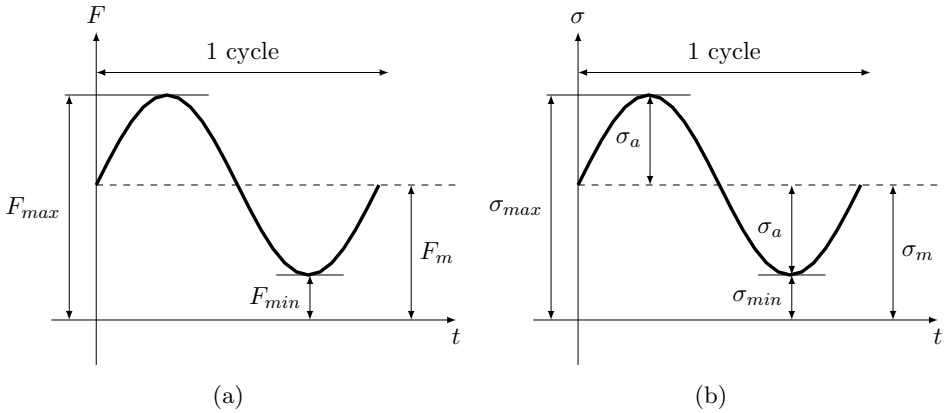

Figure 3.12: Illustration of the load under consideration.

The stress state within the structure is made up of an alternating and average component. The fatigue design procedure developed in this thesis takes advantage of the elastic linear model and the proportional nature of the load to model the force. The stress tensor component $\boldsymbol{\sigma}$ can be written as the sum of an alternating component $\boldsymbol{\sigma}_a$ and an average component $\boldsymbol{\sigma}_m$. Both of them can be calculated using a reference stress state ($\boldsymbol{\sigma}_{ref}$) deduced from the application of one reference static load case. Hence, under the application of a reference load, the alternating and average components can be expressed as a given fraction of the reference stress state, i.e.,

$\boldsymbol{\sigma}_a = c_a \cdot \boldsymbol{\sigma}_{ref}$ and $\boldsymbol{\sigma}_m = c_m \cdot \boldsymbol{\sigma}_{ref}$ with c_a and c_m the alternating and average component fractions respectively. It comes:

$$\boldsymbol{\sigma} = \boldsymbol{\sigma}_a + \boldsymbol{\sigma}_m = c_a \cdot \boldsymbol{\sigma}_{ref} + c_m \cdot \boldsymbol{\sigma}_{ref}, \tag{3.16}$$

with c_a and c_m input parameters provided by the user. Two choices are possible for setting the constants c_a and c_m. The first one, chosen in ARTICLE 3 and the PROCEEDING, consists in applying a static load case and considering that each of the components corresponds to a percentage of the total amplitude of the reference stress field. In this case we have $c_a + c_m = 1$. The second option is to apply a **unitary** reference load case and to multiply the obtained reference stress field by the parameters c_a and c_m to match the mean and alternating amplitudes of the real load. Recently, the work of [Oest and Lund(2017)] extended this procedure and proposed to compute the values of these coefficients using a Rainflow Counting Method ([Dowing and Socie(1982)]) along with the Palmgren-Miner's accumulation damage to calculate the loads with variable amplitudes.

The way of proceeding in this work allows considering cases of cyclic loading at constant amplitude typically encountered in turbomachinery under the hypothesis that mistuning is not considered in the design process. The advantage of calculating fatigue design by applying a reference load case is to enable an efficient and robust design approach. The main disadvantage is the limit of the load shape that can be considered. This point will be circumvented with the introduction of the Dang Van criterion.

Fatigue criteria in topology optimization

As described in the previous chapter, the different fatigue criteria are made of a combination of an equivalent alternating component ($\sigma^{eq}_{a,e}$) and an equivalent average component ($\sigma^{eq}_{m,e}$ or $\sigma^{eq}_{max,e}$) associated with material parameters. As described in Chapter 2, the alternating component is evaluated as the third of the equivalent Von Mises stress, see Eqn. (3.2), while the mean component is given by the hydrostatic pressure ($P_{H,e}$) which in matrix form at the element level e writes:

$$P_{H,e} = \frac{\mathbf{H}^0_e \mathbf{U}_e}{3}, \tag{3.17}$$

with $\mathbf{H}^0_e = \mathbf{W}\mathbf{T}^\mathbf{0}_\mathbf{e}$ with $\mathbf{W} = (1 \;\; 1 \;\; 0)^T$ and $\mathbf{T}^0_e$ the stress matrix defined in Section 2.3 of Chapter 2.

Following the notations introduced in [Duysinx and Sigmund(1998), Bruggi and Duysinx(2012), Collet et al.(2017)], and taking into account (3.16), we can pose the three following stress components at the element e:

$$\sigma^{eq}_{a,e} = c_a\sqrt{3J_2} = c_a\sqrt{\mathbf{U}^T_e \mathbf{M}^0_e \mathbf{U}_e}, \tag{3.18}$$

$$\sigma^{eq}_{m,e} = c_m \mathbf{H}^0_e \mathbf{U}_e, \tag{3.19}$$

$$\sigma^{eq}_{max,e} = c_a \mathbf{H}^0_e \mathbf{U}_e + c_m \mathbf{H}^0_e \mathbf{U}_e, \tag{3.20}$$

The various fatigue criteria written in the framework of density–based topology optimization using the aforementioned stress components are summarized in Table 3.5. More details concerning their mathematical developments are available in the dedicated articles placed in the Appendices.

	Goodman	Sines	Crossland
σ_f^*	$x_e^{(p-q)}\left(\dfrac{\overline{\sigma}_{a,e}^{eq}}{S_e}+\dfrac{\overline{\sigma}_{m,e}^{eq}}{S_{ut}}\right)$		
	$x_e^{(p-q)}\left(\dfrac{\overline{\sigma}_{a,e}^{eq}}{S_e}-\dfrac{\overline{\sigma}_{m,e}^{eq}}{\sigma_{yc}^0}\right)$	$\dfrac{x_e^{(p-q)}}{b}\left[\dfrac{\overline{\sigma}_{a,e}^{eq}}{\sqrt{3}}+\dfrac{a}{3}\overline{\sigma}_{m,e}^{eq}\right]$	$\dfrac{x_e^{(p-q)}}{b}\left[\dfrac{\overline{\sigma}_{a,e}^{eq}}{\sqrt{3}}+\dfrac{a}{3}\overline{\sigma}_{max,e}^{eq}\right]$
	$x_e^{(p-q)}\dfrac{\overline{\sigma}_{a,e}^{eq}}{S_e}$		

Table 3.5: Definition of fatigue strength criteria to be accounted in the structural optimization problem.

Sensitivity analysis

Once the expressions of the criteria have been established, their sensitivities can be evaluated to be used by a gradient–based optimization algorithm. For each of the fatigue stress criteria, one therefore has to evaluate $\frac{\partial \sigma_f^*}{\partial x_j}$ and in particular the three quantities $\frac{\partial \sigma_{a,e}^{eqp}}{\partial x_j}$, $\frac{\partial \sigma_{m,e}^{eqp}}{\partial x_j}$ and $\frac{\partial \sigma_{max,e}^{eqp}}{\partial x_j}$.

Without loss of generality, the derivatives of the different quantities of interest with respect to the design variables x_j are written as follows:

$$\begin{aligned}
\frac{\partial \sigma_{a,e}^{eq}}{\partial x_j} &= \delta_{ej}(p-q)x_e^{p-q-1}\ \overline{\sigma}_{a,e}^{eq} + x_e^{p-q}\frac{\partial \overline{\sigma}_{a,e}^{eq}}{\partial x_j},\\
\frac{\partial \sigma_{m,e}^{eq}}{\partial x_j} &= \delta_{ej}(p-q)x_e^{p-q-1}\ \overline{\sigma}_{m,e}^{eq} + x_e^{p-q}\frac{\partial \overline{\sigma}_{m,e}^{eq}}{\partial x_j},\\
\frac{\partial \sigma_{max,e}^{eq}}{\partial x_j} &= \delta_{ej}(p-q)x_e^{p-q-1}\ \overline{\sigma}_{max,e}^{eq} + x_e^{p-q}\frac{\partial \overline{\sigma}_{max,e}^{eq}}{\partial x_j},
\end{aligned} \tag{3.21}$$

In these expressions, the terms $\frac{\partial \overline{\sigma}_{a,e}^{eq}}{\partial x_j}$, $\frac{\partial \overline{\sigma}_{m,e}^{eq}}{\partial x_j}$ and $\frac{\partial \overline{\sigma}_{max,e}^{eq}}{\partial x_j}$ require the main computational burden and their evaluation can be obtained by implementing the classical techniques of adjoint or direct approaches. As specified in ARTICLE 3 and the PROCEEDING, an active-set selection strategy is used to reduce the number of constraints to be treated. Therefore, the adjoint approach, as particularized in Section 3.1.1 above, is used. At the end of the day, the final expressions are evaluated by:

$$\begin{aligned}
\frac{\partial \overline{\sigma}_{a,e}^{eq}}{\partial x_j} &= \boldsymbol{\lambda}^T\frac{\partial \mathbf{K}}{\partial x_j}\mathbf{U} \quad ; \quad \mathbf{K}\boldsymbol{\lambda} = -\left[c_a(\mathbf{U}_e^T\mathbf{M}_e^0\mathbf{U}_e)^{-\frac{1}{2}}\mathbf{M}_e^0\mathbf{U}_e\right]^T,\\
\frac{\partial \overline{\sigma}_{m,e}^{ep}}{\partial x_j} &= \boldsymbol{\mu}^T\frac{\partial \mathbf{K}}{\partial x_j}\mathbf{U} \quad ; \quad \mathbf{K}\boldsymbol{\mu} = -\left[c_m\mathbf{H}_e^0\right]^T,\\
\frac{\partial \overline{\sigma}_{max,e}^{eqp}}{\partial x_j} &= \boldsymbol{\gamma}^T\frac{\partial \mathbf{K}}{\partial x_j}\mathbf{U} \quad ; \quad \mathbf{K}\boldsymbol{\gamma} = -\left[c_m\mathbf{H}_e^0 + c_a\mathbf{H}_e^0\right]^T,
\end{aligned} \tag{3.22}$$

In (3.22), $\boldsymbol{\lambda}$, $\boldsymbol{\mu}$ and $\boldsymbol{\gamma}$ stand for the adjoint vectors to be determined solving each adjoint problem.

Numerical application

Numerical applications illustrate the topology optimization subjected to fatigue stress constraints. The considered test case is the L-shape benchmarks depicted in Figure 3.1. The optimized layouts are given in Figure 3.13. Please note that, the different numerical parameters of the optimization procedure to obtain the results in Figure 3.13 differ from those used in

ARTICLE 3 and PROCEEDING. The main reason is to match the numerical application of Section 3.1.3 and thus to maintain a consistency across the different examples. Furthermore, the results presented in ARTICLE 3 and the PROCEEDING are obtained for a test case where the load is different from Figure 3.1. In the results of this section, the MMA input parameters are kept at their default values, see [Svanberg(1987)] or ARTICLE 1. The value of the α_c parameter of the Eqn. (3.15c) is given by $\alpha_c = 2.8$ to correspond to the result of the Figure 3.6(c) reminded in Figure 3.13(a). The filter size r_{min} has also been changed to $r_{min} = 1.5l_e$ where l_e is the size of an element edge. The rest of the parameters are those reported in the published works.

As can be seen in Figure 3.13, different topologies are achieved with the considered fatigue criteria. The Goodman criterion is quite close to the reference solution if we consider its optimized weight, see Figure 3.14, but it remains heavier to reduce the stress concentrations to prevent the fatigue failure. The obtained topology is also different from the reference static stress solution. As far as the Sines and Crossland criteria are concerned, the latter have a fairly similar topology as well as a closer weight objective but heavier than the Goodman criterion which is consistent with their respective formulation. However, the Crossland criterion leads to a heavier structure. This can be explained by the fact that the mean component of the criterion is more restrictive to meet. It comes that, thicker structural members are obtained at the end of the optimization process.

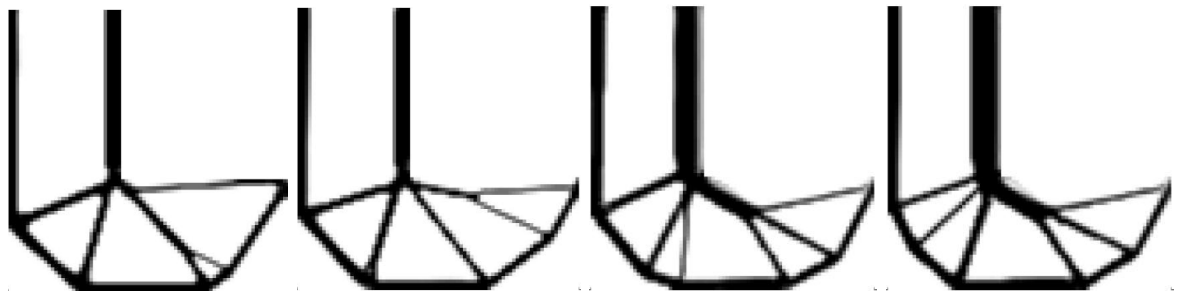

(a) (b) (c) (d)

Figure 3.13: Achieved designs using the fatigue design procedure: (a) Reference solution accounting for static stress constraints and compliance constraint (b) Goodman solution (c) Sines solution (d) Crossland solution.

3.2.2 Dang Van criterion

The approaches to introduce fatigue constraints, described in Section 3.2.1, are effective but are valid in the case of proportional and constant amplitude loading only. These particular conditions are encountered in very specific cases and under certain assumptions. In order to overcome this issue, we have introduced the Dang Van criterion in the topology optimization process. The theory of the Dang Van criterion has been presented in Section 2.4.3 of Chapter 2. The criterion, at the finite element level e, in its time discretized form, writes:

$$\max_l \left(\tau^l_{oct,e} + aP^l_{H,e} \right) \leq b, \tag{3.23}$$

with a and b the material parameters, $\tau^l_{oct,e}$ the octahedral shear stress and $P^l_{H,e}$ the hydrostatic pressure. In (3.23), l represents the $l-th$ time step after sampling of the continuous time

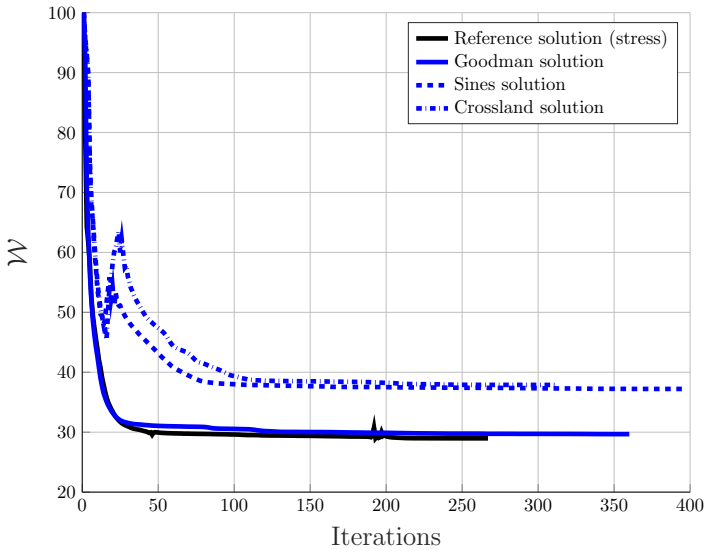

Figure 3.14: History of the objective function for the L-shape problem accounting for various fatigue criterion compared to the reference solution embedding static stress constraints only.

varying load. Hence, the criterion stipulates that the l damage values must be evaluated for each element and the highest value among these ones must remain below the fatigue limit b.

Load Modeling

As discussed in Section 2.4.3 of the previous chapter, the time varying load, $P(t)$, has to be discretized into several time steps. Let's consider the load in Figure 3.15 sampled into 25 time steps for instance represented by the dot points.

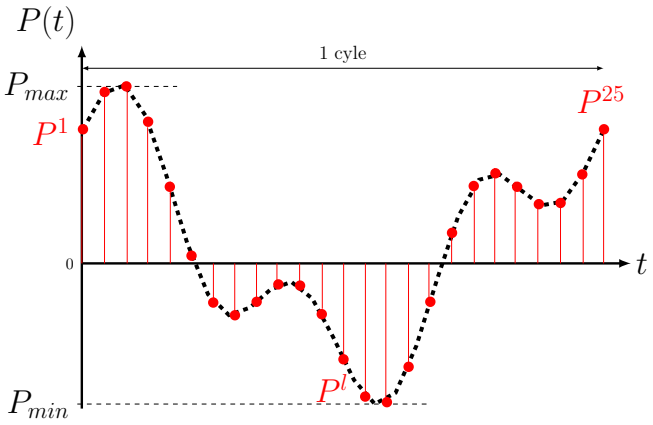

Figure 3.15: Loading illustration applied to the structure for fatigue sizing using the Dang Van criterion.

Following the time sampling, the discrete amplitudes of the load $P(t)$ related to each time step l are extracted and noted P^l with $l = 1, \cdots, n$ and here for instance $n = 25$. In [Dang Van et al.(1989)], the computation procedure implies that the n macroscopic stresses evaluated within an element e, noted $\boldsymbol{S}_e^l$, are determined following the solution of n equilibrium equations (3.32b) using finite element analysis. In this thesis, only one **unitary** reference static load case is considered to save CPU time. Indeed, for linear macrostructures, which is assumed here as discussed in the previous chapter, the reference stress field within an element e, noted $\boldsymbol{S}_e^{ref}$, resulting from the application of the reference load can be scaled up or down using the scalar value P^l. This allows computing the stress fields related to the magnitude of the load case associated to a time step l. Mathematically, it comes that the n stress states $\boldsymbol{S}_e^l$ are evaluated at the element level e as:

$$\boldsymbol{S}_e^l = P^l \cdot \boldsymbol{S}_e^{ref}, \tag{3.24}$$

By applying the procedure described above, any loading profile can be considered provided that the amplitudes corresponding to each time step l can be extracted. Let's note that the proposed computational procedure exhibits some advantages. First, as already mentioned, it is more computationally effective than solving n equilibrium equations. Second, the extension to account for multiple load case conditions, s with s being the number of independant load cases, is straightforward. For each of these separate load cases, a unitary reference load can be used to compute the associated reference stress fields $\boldsymbol{S}_e^{ref,s}$ and, following our procedure, the required macroscopic stress fields can be recovered as:

$$\boldsymbol{S}_e^{l,s} = P^{l,s} \cdot \boldsymbol{S}_e^{ref,s}, \tag{3.25}$$

Finally, let's note that any linear combinaison of the independant load cases can be considered as well. For instance, one might want to consider a load case that is a combinaision of torsion-bending which results in a complex stress state. With our procedure, the latter can be expressed as the linear combination of independant stress states corresponding to the torsion and bending sepraretely. This last comment emphasises the great flexibility of the proposed computational procedure. In ARTICLE 4, the case of several load cases is illustrated with the double L-shape example introduced in [Le et al.(2010)].

It should be noted that in the investigations of ARTICLE 4, only periodic loadings are treated, therefore, a single cycle is studied. In addition, only proportional loads are considered as the Dang Van criterion shows some limitation when the structure is subjected to non proportional loads, see [Dang Van and Papadopoulos(1999)]. To tackle such particular loading conditions, more advanced fatigue criteria, based on the same critical plane approach theory, have to be used such as the Papadopoulos criterion, see e.g., [Papadopoulos(1994), Papadopoulos(1995)].

For the numerical example illustrated in Section 3.2.2, the load submitted to the structure is the one represented in Figure 3.15. The values of P_{min} and P_{max} are given by $P_{min} = -0.9722[N]$ and $P_{max} = 1.3129[N]$ respectively.

Fatigue criterion in topology optimization

The criterion in (3.23) involves stress quantities that have already been encountered throughout this work, i.e., the equivalent Von Mises stress measure and the hydrostatic component, so their computation is similar. However, the use of the Dang Van criterion is based on a microscopic stress state with the evaluation of a stabilized residual stress field, $dev(\boldsymbol{\rho}^*)$. The later is determined when solving a "min-max" problem. At the element level e and for the time step l the microscopic stress $\boldsymbol{s}_e^l$ is expressed as the sum of the macroscopic stress $\boldsymbol{S}_e^l$ and the stabilized residual stress field $dev(\boldsymbol{\rho}_e^*)$:

$$\boldsymbol{s}_e^l = \boldsymbol{S}_e^l + dev(\boldsymbol{\rho}_e^*), \tag{3.26}$$

In (3.26), the analytical expression of the second term of the sum is unknown and therefore performing a derivative to use a gradient–based optimization algorithm is not obvious.

In this thesis, we have tailored a procedure to account for this component. Indeed, the evaluation of the stabilized residual stress field is carried out using only the knowledge of macroscopic stresses which are the input values of the "min-max" problem. Since $dev(\boldsymbol{\rho}_e^*)$ depends only on the macroscopic stress fields $\boldsymbol{S}_e^l$, it is reasonable to assume the proportionality dependency, that is:

$$dev(\boldsymbol{\rho}_e^*) = \boldsymbol{\alpha}_e^l : \boldsymbol{S}_e^l, \tag{3.27}$$

with $\boldsymbol{\alpha}_e^l$ a scaling matrix evaluated for each time step within an element e. Hence, there are as many matrices $\boldsymbol{\alpha}_e^l$ as there are time steps. Each one is used to evaluate the microscopic stress. At the end of the day, Eqn (3.26) can be written as:

$$\boldsymbol{s}_e^l = (\mathbf{I} + \boldsymbol{\alpha}_e^l) : \boldsymbol{S}_e^l, \tag{3.28}$$

Thus, in Eqn (3.28), all the elements are now known and the classic formalism of topology optimization with stress constraints, as defined in Section 3.1.1, can be applied to determine the equivalent Von Mises stress measure. The only difference is that now the $\mathbf{V}$ matrix is no longer constant and must be updated during the optimization process and it changes from one element to another. The computation of the $\mathbf{V}$ matrix is provided in Appendix B.

The fatigue criterion at the element level, noted d_e, considering that the fatigue limit is written as $b = x_e^q \overline{b}$, takes the form:

$$d_e = \frac{x_e^p}{x_e^q} \max_l \left(\frac{\overline{\tau_{oct,e}^l} + a\overline{P_{H,e}^l}}{\overline{b}} \right) \leq 1, \tag{3.29}$$

To manage the"$\max_l$" function, the maximum damage value is first computed for each element and then is frozen during an optimization iteration k. Although it is not differentiable, freezing the maximum has not lead to any numerical instabilities during our investigations. An alternative could be to replace the "max" function by a continuous function, such as a p-norm, for example. Finally the Dang Van fatigue criterion writes:

$$d_e^L = x_e^{p-q} \left(\frac{\overline{\tau_{oct,e}}^L + a\overline{P_{H,e}}^L}{\overline{b}} \right) \leq 1, \tag{3.30}$$

$$= x_e^{p-q} \overline{d_e}^L \leq 1, \tag{3.31}$$

where $L = \arg\max_l \left(\frac{\overline{\tau_{oct,e}^l} + a\overline{P_{H,e}^l}}{\overline{b}} \right)$ and denotes that the maximum computed damage for an element e is frozen.

The optimization problem that we solve in ARTICLE 4 is formulated in Eqn. (3.32) below and aims at the minimization of the structural weight ($\mathcal{W}$) under static (Eqn. (3.32c)) and fatigue constraints (Eqn. (3.32d)).

The static stress restrictions (3.32c) is here considered inspired by the optimization problems presented in [Holmberg et al.(2014)] and [Mrzygold(2012)].

$$\min_{\boldsymbol{x}} \quad \mathcal{W}(\boldsymbol{x}), \tag{3.32a}$$

$$\text{s.t.} \quad \mathbf{K}(\boldsymbol{x})\ \mathbf{U} \ = \ \mathbf{F}, \tag{3.32b}$$

$$x_e^{(p-q)} \frac{\overline{\sigma_e}}{\sigma_y^0} \leq 1, \ \ \forall e \tag{3.32c}$$

$$x_e^{(p-q)} \overline{d_e}^L \leq 1, \ \ \forall e \tag{3.32d}$$

$$0 \leq x_e \leq 1, \qquad e = 1, \ldots, n_e \tag{3.32e}$$

As mentioned above, a reference static load is applied to the structure and only one static problem is solved. Hence, the stress constraints (3.32c) aim at removing the stress concentrations of the reference stress field coming from the application of this reference load. Note that the various numerical experiments conducted on this problem have shown that, in contrast with the numerical examples of Section 3.2.1, integrating a global compliance constraint does not significantly reduce the CPU time. This global constraint is consequently not introduced in the optimization problem (3.32).

Sensitivity analysis

The definition of the damage in Eqn. (3.31) enables to compute the sensitivities of the constraints with respect to the design variables, i.e., $\frac{\partial d_e^L}{\partial x_j}$. In view of the formalism used, they are obtained in a straightforward manner using the equations of Section 3.1.1 and take the form defined in the Eqn. (3.35). Let's recall that the expression of the sensitivities of Eqn. (3.32c) have already been defined above.

$$\frac{\partial d_e^L}{\partial x_j} = \frac{\partial}{\partial x_j}\left(x_e^{p-q}\overline{d_e}^L\right), \tag{3.33}$$

$$= \frac{1}{\overline{b}}\left[(p-q)\delta_{ej}x_e^{p-q-1}(\overline{\tau_{oct,e}}^L + a\overline{P_{H,e}}^L) + x_e^{p-q}\boldsymbol{\Lambda}^T\frac{\partial \mathbf{K}}{\partial x_j}\mathbf{U}\right], \tag{3.34}$$

where $\boldsymbol{\Lambda}$ the adjoint vector is determined after solving the adjoint problem:

$$\mathbf{K}\boldsymbol{\Lambda} = -\left(\sqrt{\frac{2}{9}}\left[(\mathbf{U_e^T M_e^0 U_e})^{-\frac{1}{2}}\mathbf{M_e^0 U_e}\right] + \frac{a}{3}\mathbf{H}_e^0\right)^T, \tag{3.35}$$

Hence, the developments obtained in the previous section allow casting the Dang Van criterion into the same formalism as for the static stress constraints.

Numerical application

The numerical application is conducted on the L-shape benchmark illustrated in Figure 3.1. All the numerical parameters and materials data used for the simulations are given in ARTICLE 4.

The construction of the microscopic stress at the element level e for the time step l ($\boldsymbol{s}_e^l$) requires the solution of a "min-max" problem. When starting the optimization process, the stress state within each of the finite element is not stabilized. Thus, one "min-max" problem is required per element to compute the residual stress field $dev(\boldsymbol{\rho}_e^*)$. This means that at the beginning of the optimization process there are as many "min-max" problems to handle as they are elements. However, as the optimization process moves ahead, some solutions are no longer necessary because the stress state within the elements is stabilized and thus the required residual stress field becomes stable. Hence, a selection of only a subset of "min-max" problems is made to spare CPU time. The selection is made by evaluating the change between two successive iterations (k) of the equivalent static Von Mises stress value of each element e (σ_e^{VM}) as indicated in Eqn. (3.36).

$$|\sigma_{e,k+1}^{\text{VM}} - \sigma_{e,k}^{\text{VM}}| \leq 10^{-4}, \tag{3.36}$$

If (3.36) is fulfilled on an element e, then the "min-max" solution process is not performed for this element and the value of the stabilized residual stress tensor $dev(\boldsymbol{\rho}_e^*)$, computed at the previous iteration, is used to evaluate the damage (3.31). Otherwise, the "min-max" solution has to be performed to get the updated residual stress field.

In addition, in order to save computational time, an active-set selection strategy of both static (Eqn. (3.32c)) and fatigue (Eqn. (3.32d)) stress constraints is made. The selection procedures are referenced in ARTICLE 4.

In Figure 3.16, the design corresponds to the weight minimization under static stress constraints only. As discussed in Section 3.1.3, this type of solution respects structural integrity under static loading. When checking the fatigue resistance, submitted to the time varying load depicted in Figure 3.15, and using the Dang Van evaluation procedure, it comes that the optimized layout exhibits damage values higher than 1 (Figure 3.16(b)). This means that the structure will experience fatigue failure according to the definition given by (3.31). The most stressed limb, in red in Figure 3.16(b), calls for a bigger thickness when fatigue constraints are considered.

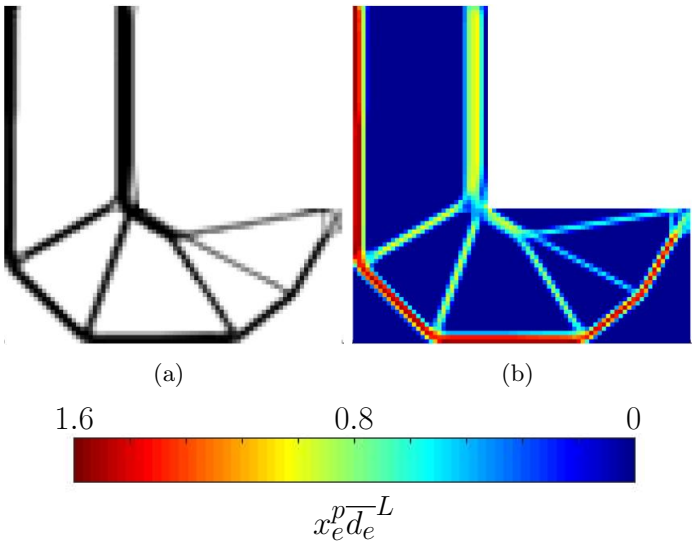

Figure 3.16: Optimized topology of the L-shape taking into account only the static stress constraints: (a) Design (b) Map of the damage evaluated in the sens of Dang Van.

Solving the problem (3.32), i.e., accounting for fatigue constraints from the beginning, into the optimization process, leads to the structure depicted in Figure 3.17(a). Normalized damage and static stress maps are provided in Figures 3.17(b) and 3.17(c) respectively. Let's note that for illustration purposes, the same color scale as in Figure 3.16 is used. The introduction of fatigue constraints enables to propose a layout which does not break under fatigue and which, at the same time, withstands a static load. To this end, the structure has thicker members in order to reduce stress concentrations and thus to withstand the time varying effort. In particular, the heavily loaded structural member in Figure 3.16(a) is, actually, much larger. It results that the optimized structure is heavier as illustrated in Figure 3.18(a). In this example, the topology of the design is globally preserved. However, other numerical investigations on different test cases have shown that this is generally not the case. The topology obtained following the solution in Eqn. (3.32) is different from the one obtained when static resistance only is considered. The reader can refer to ARTICLE 4 in the Appendices for illustrations and discussions of these results.

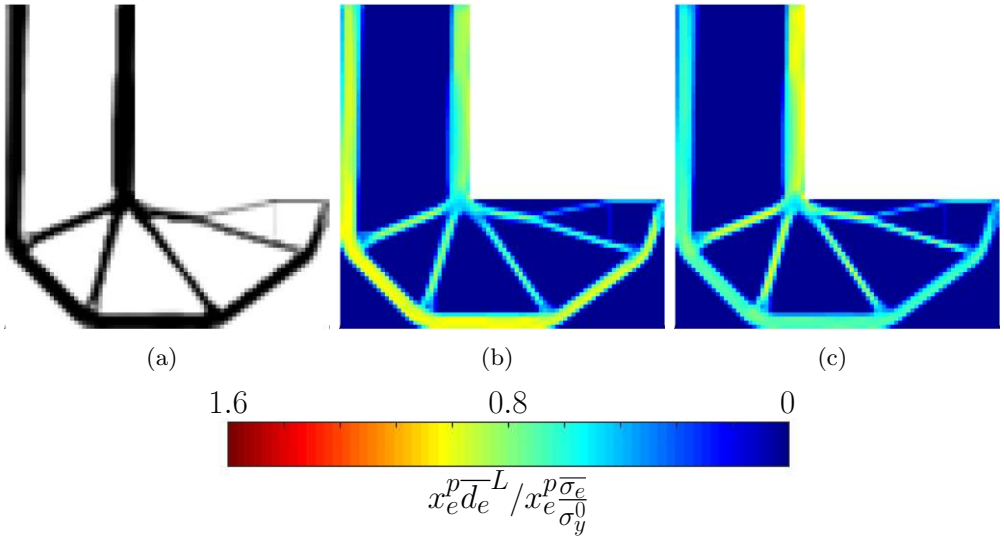

Figure 3.17: Optimized topology taking into account damage constraints in the sense of Dang Van: (a) Design (b) Maps of damage evaluated in the sense of Dang Van (c) Map of static stress.

Regarding the numerical performance of the approach proposed in this section, it is observed in Figure 3.18 that the number of iterations to achieve convergence when Dang Van fatigue constraints are introduced is comparable, even if superior, to the reference solution based on static stresses only. However, by observing Figure 3.19, the total time required to achieve convergence when fatigue is considered, noted as t_{tot}, is much greater than the reference time, t_{ref}, required when only static stresses are accounted for. This extra CPU time is due to the large percentage of effort spent in evaluating the Dang Van damage values (t_{dam}), see Figure 3.19. The selection strategy, see Eqn. (3.36), helps at reducing the number of "min-max" problems (Figure 3.20) but the total CPU time is still greater.

In order to further optimize the fatigue optimization procedure, several additional aspects can be considered. First of all, the numerical procedure of evaluation of the local damage values must be optimized within the optimization code by resorting to parallel computing. However, this is let as a perspective for future work. In addition, aggregation methods could be considered in order to further reduce the computational burden. Indeed, as illustrated in Figure 3.18(b),

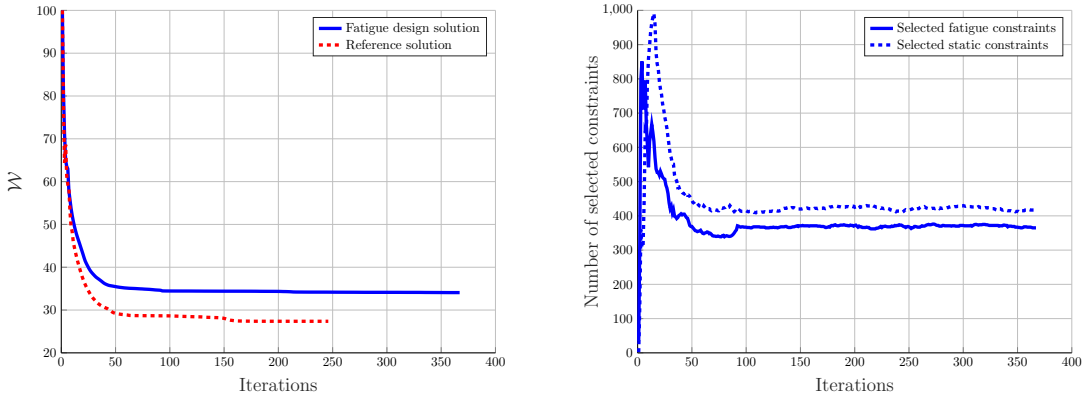

(a) (b)

Figure 3.18: Numerical performances of the L-shape benchmark: (a) Evolution of the objective function (W) along the optimization process for the pure stress constrained problem and the problem with damage control of Eqn. (18) (b) Evolution of the number of selected fatigue and stress constraints along the optimization process.

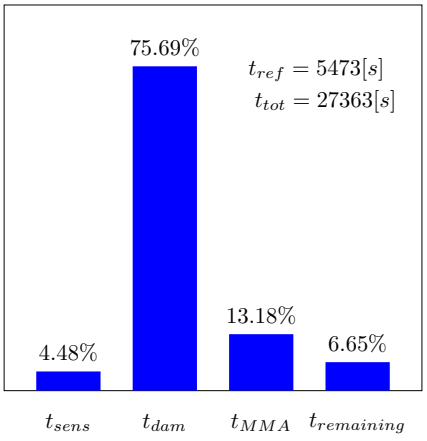

Figure 3.19: Percentage of time spent in the various part of the optimization algorithm for the L-shape benchmark.

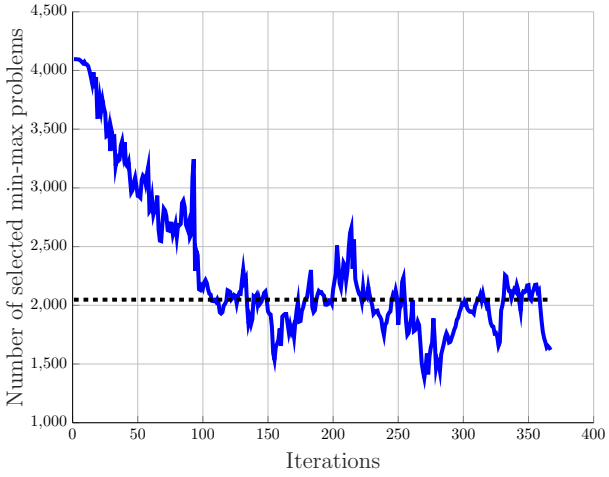

Figure 3.20: Evolution of the number of min-max problem solved along the optimization process for the L-shape benchmark.

the number of local constraints selected is not negligible and an aggregation, well controlled with proper numerical stabilization as discussed in Section 3.1.3, could improve the efficiency of the present developments.

The procedure that is developed has been validated on two other numerical applications exhibiting different characteristics, see ARTICLE 1. The results discussed in ARTICLE 4 confirmed the observations and also illustrated the great robustness of the proposed approach. Indeed, an example with different material limits and two time varying loads with different profiles is studied. A consistent fatigue strength solution is obtained illustrating that even in

complex problems, convergence is ensured. Let's recall that, as a perspective to this work, an improvement of the effectiveness of the method can be envisioned to treat larger scale problems.

3.3 Chapter conclusion

In this chapter, the developments made during this thesis have been synthesized and illustrated through various results from the articles placed in the Appendices.

A first part is dedicated to present the formalism adopted to compute the stresses in the context of density–based topology optimization. The equations of the previous chapter concerning the sensitivity analysis, necessary for considering gradient–based algorithms, are then particularized in the case of stress constraints.

Then, following the work carried out in ARTICLE 1, some features of stress–based topology optimization problems are briefly presented. A comparison of the usual encountered approaches in the literature are performed. The term "approach" is preferred to "method" because some changes to their initial formulation had to be made. However, their original essence is retained. It is shown that local approaches present the greatest robustness. Indeed, no numerical stabilization procedures are necessary to achieve convergence. However, this advantage comes at the cost of a significant computational time, not very viable from an industrial application perspective. It should be noted, however, that in the case of new developments, and in order to establish an new approach, these must not be discarded. To overcome the lack of efficiency of the local procedures, global and regional alternatives are studied and it is shown that they considerably reduce the required computational time to reach convergence. However, numerical stabilization procedures, that can be problem dependent, must be considered. This leads to solution processes whose convergence history is longer. It was also discussed that regional approaches do not bring significant efficiency gains when compared to purely global methods. Since their implementation is also more meticulous than the latter, the conclusion of our investigations is to consider methods with a single aggregation function when dealing with large problems.

Following these discussions, the architectured materials design problem embedding stress constraints is presented. The relevancy of our approach is discussed and the solution procedure, see ARTICLE 2, is illustrated on one test case. In this example, the introduction of stress constraints severely changes the topology of the final design while providing a better objective function value because of the presence of many local optima. Further analyses, conducted in ARTICLE 2, corroborate these observations. The resulting designs from the optimization process experience a reduction of their stress concentrations, thus enabling to propose mesostructures able to withstand external loading conditions contrary to those commonly encountered in the literature.

Finally, various fatigue strength criteria are introduced into the topology optimization problem subjected to stress constraints. Initially, following the investigations of ARTICLE 3 and the PROCEEDING, a simplified fatigue stress constrained procedure involving the application of proportional loads with constant amplitude is proposed. This is based on the use of Goodman, Sines and Crossland criteria for which the formalism of topology optimization with stress constraints is adapted in a straightforward manner. The developments are illustrated on a numerical example. In order to consider more complex time varying loads, the Dang Van criterion is introduced into the gradient–based optimization process in ARTICLE 4. The main difficulty of this approach concerns the impossibility of performing a stress derivative to evaluate the sensitivity analysis because the analytical expression of the residual stress field is unknown. We have therefore proposed an approximation procedure to circumvent this difficulty. A numerical example is then presented and discussed. It is shown that, though proving consistent fatigue resistant designs, the procedure requires some improvements of the numerical solution procedure

to reduce the computational time.

Chapter 4

Conclusions and perspectives

Contents

4.1 Contributions and conclusions

This research work contributes to the previous developments dealing with topology optimization problems subjected to stress constraints. Since the founding work of [Bendsoe and Kikuchi (1988)], topology optimization has reached a level of maturity compatible with the industrial design process. Although a decade has passed, after the important contribution of [Duysinx and Bendsoe (1998)], the work initiated here considers the resistance to failure of parts in the early stages of the optimization process. This subject has been left largely unexplored during many years. The industry's attraction for this tool has been a driving force of interest in this subject in the recent years. The thesis therefore aims at positioning itself along these developments by drawing inspiration from the stated industrial needs. In particular, the research work is devoted to account for stress–based constraints within the design problem. These are either static in nature or aim at offering an innovative solution capable to withstand time varying loads. In addition, the introduction of static stress constraints within the problem of architectured materials is also investigated.

The optimal material distribution is formulated using a density approach. Within the finite element discretization, the absence or presence of material is defined using an interpolation law linking the mechanical properties of the material to the design variables, i.e., the densities associated with each element. This representation is attractive because of its simplicity, its easy parametrization and its great generality. Numerical problems such as the checkerboard issue or the mesh dependency are tackled by using density filtering techniques.

The optimization problem is solved using the mathematical programming approach requiring the sensitivities of the objective and constraints functions with respect to the design variables. The effectiveness of the sensitivity analysis plays a key role in the implementation of the optimization process. Various methods are available to evaluate numerically the derivatives. In this thesis, the adjoint approach is generally privileged and each of the quantities of interest have been carried out using this approach.

Since the introduction of static stress constraints into density-based topology optimization ([Duysinx and Bendsøe(1998)]), and in particular since the attractiveness formulated by the industry on the design method considered here, numerous research works have been dedicated on the subject. Since the first investigations on truss structures, many difficulties have been identified and investigated: the singularity phenomenon, the huge CPU requirement and the non-linearity of the constraints. Over the past years, the problem of singularity and non-linearity have seen effective methods proposed to circumvent them and are now relatively well mastered. The open question of the problem in stress constraints remains the effectiveness of the numerical solution due to the large computational burden inherent to this type of large scale problems. Many methods are available in the literature and claim to be effective without any real fair point of comparison. Although computation times or a number of iterations are most often provided in the contributions, it is difficult to have a rigorous idea of the performance of one approach with respect to one another. Hence, Article[1] aims at paving the way to a fair evaluation of their performance and their real ability to reduce the computational burden. It includes a description of proposed standardized benchmarks for comparison in this work and for future works on the topic. A study on some particular aspects of the problem of stress constrained topology optimization is also held with the aim of revisiting the theoretical foundations but also to define the expectations concerning such a problem. This discussion is as general as possible and similar results are expected to be observed with the use of Level-set methods for instance. Then, some theoretical aspects related to density–based methods are presented as a premise to a comparison of usual approaches of the literature, i.e., p-norm/p-mean functions ([Duysinx and Sigmund(1998)]), KS function ([Paris et al.(2009)]) or some aggregation techniques ([Le et al.(2010), Paris et al.(2010), Holmberg et al.(2013)]). We insist on the term approach because in order to make a fair comparison, some adaptations of the methods in the literature have been necessary, e.g., resorting to the same relaxation technique, here the qp-relaxation, or using a different optimization algorithms, e.g., MMA. The study is intended to be as close as possible to the initial methods, but, in its own spirit, it makes the comparison in order to illustrate their real numerical efficiency to be able to draw up a list of recommendations for further works. The thesis shows that the performance of each of compared approaches is changing and that the choice of one over the others depends on the user expectations. When execution time efficiency is the main target, aggregation-based approaches are recommended. Although computationally efficient, these ones require numerical stabilization procedures due to the highly non-linear nature introduced by aggregation functions. Conversely, if the objective is to obtain a more robust solution scheme or if the main focus is on developing new concepts, applied on academic examples, local approaches might still be considered as a valid alternative. It is nevertheless important to keep in mind that the huge computational time is a common characteristic. Through the comparisons conducted in this research, it is shown the importance of specifying the set of numerical parameters that are used to obtain the simulation results. The former have a significant impact on the performance as well as on the obtained final solution, illustrating the presence of many local optima.

Since the emergence and awareness of the new possibilities offered by additive manufacturing techniques in the fabricating of mechanical components, the advanced designs can today exhibit regions made of lattice structures or graded materials. It is known in nature that porous structures, such as in bones ([Lan Levengood and Zhang(2014)]) or wood ([Greil et al.(1998)]), take benefit of cellular structures to optimize their capability of withstanding the various loads in service. Since the founding work of [Sigmund(1994)], the use of topology optimization to design materials with high mechanical properties has been the subject of numerous contributions in various fields. However, the problem of resistance of the materials has not been largely

covered. In most contributions, it is desired to minimize the value of the maximum stress under prescribed material resources e.g., a volume constraint. However, although stress concentrations are actually reduced, the structural integrity of the design cannot be guaranteed. Indeed, there is no control on the stress state and it is possible that it is over the yield strength of the material for example. It is the essence of Article[2] to provide an alternative formulation to the design of architectural materials. In this piece of work, local stress constraints are placed as restrictions in the optimization problem. The study is limited to so-called periodic materials and therefore a Representative Unit Cell (RUC) subjected to periodic boundary conditions is considered. The strain field that undergoes the RUC is generally not known since no macroscopic structural analysis is performed yet. As a result, the fields applied are arbitrarily defined and so is the level of stresses reached. Consistently, the maximum permissible stress limit is also arbitrary. The advantage of doing this and due to linear elastic modelling, the method advocated here can be extended to prevent yielding of the material by replacing the arbitrary stress limit by the actual yield stress of the material. Indeed, if the the far field is known, i.e., comes from a macroscopic analysis, then the actual material properties can be used without modifying the formulation of the optimization problem proposed in Article[2]. The proposed formulation is validated and shows its robustness on known case studies from the literature but also on an original example with several load cases. In this thesis, the problem that is considered seeks to obtain equivalent optimal elastic properties while limiting the stress level below a certain threshold. It is shown that our solution procedure is able to reduce stress concentrations and to propose configurations which are able to exhibit extremal stiffness properties with lower maximum microstructural stresses. It is also shown that sometimes one find solutions with major changes in the final layout while having a better value of the objective function. This illustrates the presence of many local minima within the design space and that the introduction of stress constraints is generally favorable to drive the optimized solution to more favorable parts of the design space.

Design against fatigue failure of mechanical components is an essential element of certification and design of mechanical components. It is essential to take this aspect into account as soon as the early design stages of a component. Topology optimization coupled with fatigue failure criteria is an efficient tool to meet the assigned targets. In the aerospace and automotive industries, mechanical components are most often, though not always, subjected to high cycle loads. The corresponding fatigue models therefore involve the nominal stress state within the parts in their formulation. Extending the introduction of stress constraints as described in Article[1] is therefore considered in our contributions to account for fatigue failure as soon as the preliminary design stage carried out using topology optimization. This has already been considered by some authors but generally with models that are difficult to use in practice. In this research work, fatigue failure is introduced by adapting tools which are usually encountered in aeronautics and in the automotive sector. Article[3] introduces the augmented Goodman criterion, i.e., taking into account the negative values of the mean stress component, widely used in the industry. The particularity of the approach is to consider a linear elastic state of the structure. Thus, the total stress state can always be written as a linear combination of an alternating and a mean component. Therefore, in order to make the method effective, only one reference static load case has to be considered and the two components characterizing the stress state are obtained using weighting parameters. Moving along, the multiaxial aspect of the stress field can be accounted for by using the Sines method, see [Norton(2000)], allowing to calculate equivalent quantities representing the alternating and mean components which are later introduced into the fatigue criterion. The approach described in this contribution is successfully tested on different examples. A similar procedure is followed to consider the Sines

([Sines(1959)]) and Crossland ([Crossland(1956)]) criteria (see Proceeding[1]). The numerical applications illustrate that fatigue constraints can modify substantially the optimized layout. Although the proposed method is effective, it is limited to the case where a proportional loading of constant amplitude is applied to the structures. To consider more complex load cases, we decide to follow the approach that is used in the automotive industry. Article[4] introduces the Dang Van criterion into the topology optimization process. This criterion is based on a multi-scale approach using microscopic stresses. These ones are obtained as the sum of the macroscopic stresses, i.e., the stresses evaluated from a finite element analysis, and a stabilized residual stress field due to localized plasticity. The latter fatigue procedure has already been studied in the past, see e.g., [Mrzygold(2012)], but in this work the criterion is introduced into a gradient–based optimisation framework which is common in industry. The major difficulty encountered lies in evaluating the sensitivity of the residual stress tensor for which no analytical expression is available. Thus this research work illustrates and develops a computational procedure and shows how this sensitivity can nevertheless be computed to restore to gradient–based algorithms. The robustness and the generality of the approach is tested on different examples including several load cases and material properties. The numerical results illustrate the fundamental modifications characterizing the optimized designs able to withstand the fatigue locally.

All the developments illustrated in this research work have been conducted using academic tools written in the programming language Matlab®. At the end of the reasearch, the optimizer used is the Matlab®version of the Method of Moving Assymptotes ([Svanberg(1987)]).

4.2 Perspectives

The developments realized in this research aim at answering to the aerospace and mechanical engineers facing designs ruled by static or fatigue resistance. However, several questions are still unsolved.

Solving the optimization problem including stress constraints using mathematical programming raises the question about the numerical efficiency of the optimization procedure. The MMA algorithm ([Svanberg(1987)]) is massively used in the literature. The latter only requires information from the first derivatives. Conversely, due to the computational efficiency of aggregation approaches, these are prone to be used in large scale problems. However, their non-linear nature can lead to oscillatory behavior which is an obstacle. Providing second order derivatives to the optimizer might mitigate this harmful effect. We believe that it could be considered as an interesting perspective to account for the second derivative as in the case of an SQP algorithm ([Schittkowski(1981)]) for instance. In addition, the dual solver, which is the convex strongest solution procedure, may prove to be not adapted in the case of stress constraints. A second perspective which sounds to be interesting is to propose a new and more appropriate way to treat more efficiently the non-convex behavior of stress constraints.

As discussed in this work, the design problem of architectured materials developed in this thesis makes use of an arbitrary stress limit to reduce stress concentrations. The reason of this approach is that the value of the macroscopic strain field or far field applied on the base cell is unknown. Therefore, a natural extension of the work is to include the formulation of the proposed design problem into a two-scale procedure, see e.g.,([Feyel(2003)]). The solution of the macroscopic problem provides the far strain field and it defines naturally a physical boundary condition and it allows applying as a stress limit the true yield strength of the material to

guarantee the structural integrity at both the mesoscopic and macroscopic level. The computational time associated with the two-level procedure as well as the connectivity of the different optimizations performed on the basic cells constitute additional challenges.

The Dang Van criterion enables to consider complex loading conditions thus enabling to propose innovative optimized structures able to withstand them. However, some improvements of the procedure proposed here are still expected. First, the solution of elementary "min-max" problems which are used to determine the stabilized residual stress field should be optimized. Indeed, it is shown in our investigations that the percentage of time required for the residual stress field evaluation represents a large part of the total CPU time. The improvements can be looked for in the algorithm itself but also on the use of parallel computing. Second, although Dang Van's criterion is general and can be applied to a large set of applications, studies have shown that it is not suitable in the case of highly non-proportional loading. The elaboration of the Papadopulos criterion [Papadopoulos(1994), Papadopoulos(1995)] allows to overcome these limitations and can be considered as an extension of the developments carried out in this thesis. Indeed, the basic theory of Papadopoulos remains identical to Dang Van's with the exception that the Papadopoulos criterion considers a limitation on the accumulated plastic strain on crystals that undergo plastic slip. The determination of this quantity is relatively complex as discussed in [Dang Van and Papadopoulos(1999)].

Finally a natural extension of all the developments held in this thesis is to consider 3D applications with the aim of solving large-scale industrial problems. To do this, advanced high performance computing techniques must be employed. The latter have not been considered in the present research work as they call for specific coding skills. Conversely to the many examples illustrating this work, these are essential in order to be able to solve large scale problems including stress and fatigue restrictions. Some adaptations of the existing tools should therefore be necessary in order to take benefit of the developments of this thesis and transfer them to the world of industrial design.

Chapter 5

List of publications

Articles

1. Collet, M., Zhang, S., Fernandez Sanchez, E., Norato, J. & Duysinx, P. (2018). On solution aspects and techniques of density–based methods for the stress constrained topology optimization of selected benchmark problems, *to be submitted to Structural and Multidisciplinary Optimization- Springer*

2. Collet, M., Noël, L., Bruggi, M., & Duysinx, P. (2018). Topology optimization for microstructural design under stress constraints. *Structural and Multidisciplinary optimization, 1-19, https://doi.org/10.1007/s00158-018-2045-9*

3. Collet, M., Bruggi, M., & Duysinx, P. (2017). Topology optimization for minimum weight with compliance and simplified nominal stress constraints for fatigue resistance. *Struct Multidisc Opti 55:839-855. DOI 10.1007/s00158-016-1510-6*

4. Collet, M., Bauduin, S., Fernandez Sanchez, E., Alarcon Soto, P., & Duysinx, P. (2018). On the Dang Van criterion for fatigue design using topology optimization, *to be submitted to Structural and Multidisciplinary Optimization- Springer*

Proceeding of conference

1. Collet, M., Bruggi, M., Bauduin S., & Duysinx, P. (2015). Stress-based topology optimization with fatigue failure constraints. In Proceedings of the Fifteenth International Conference on Civil, Structural and Environmental Engineering Computing.

Bibliography

[Aboudi et al.(2012)] Aboudi, J, Arnold, S.M, Bednarcyk, B.A.(2012) Micromechanics of composite materials: A generalized multiscale analysis approach. Butterworth-Heinemann

[Achtziger and Bendsøe(1995)] Achtziger, W, Bendsøe, M.P.(1995) Design for maximal flexibility as a simple computational model of damage. Structural Optimization 10:258-268.

[Achtziger and Bendsøe(1999)] Achtziger, W, Bendsøe, M.P.(1999) Optimal topology design of discrete structures resisting degradation effects. Structural Optimization 17:74-78

[Achtziger and Kanzow(2008)] Achtziger, W, Kanzow C. (2008) Mathematical programs with vanishing constraints: optimality conditions and constraint qualifications, Mathematical Programming 114, 69.

[Adelman and Haftka(1993)] Adelman, H. M, Haftka, R. T.(1993) Sensitivity analysis of discrete systems. In Progress in Astronautics and Aeronautics, volume 150, pages 291–315. American Institute of Aeronautics and Astronautics, Washington.

[Allair et al.(2002)] Allaire, G, Jouve, F, ToaderA.-M.(2002) A level-set method for shape optimization. Comptes Rendus Mathématique, 334(12):1125–1130.

[Amir(2017)] Amir, O.(2017) Stress-constrained continuum topology optimization: a new approach based on elasto-plasticity. Struct Multidisc Optim 55:1797–1818

[Amir and Lazarov(2018)] Amir, O, Lazarov, BS.(2018) Achieving stress-constrained topological design via length scale control. Struct Multidiscip Optim. https://doi.org/10.1007/s00158-018-2019-y

[Andreassen et al.(2011)] Andreassen, E, Clausen, A, Schevenels, M, Lazarov, BS, Sigmund, O. (2011) Efficient topology optimization in MATLAB using 88 lines of code. Struct Multidiscip Optim 43:1–16

[Andreassen and Andreasen(2014)] Andreassen, E, Andreasen, C. S. (2014) How to determine composite material properties using numerical homogenization. Computational Materials Science 83:488-495

[Andreassen et al.(2015)] Andreassen, E, Jensen, J. S, Sigmund, O,Thomsen, J. J. (2015). Optimal Design of Porous Materials. DTU Mechanical Engineering. (DCAMM Special Report; No. S172).

[Ballard et al.(1995)] Ballard, P, Dang Van, K, Deperrois, A, Papadopoulos, I.V.(1995)High Cycle Fatigue and a Finite Element Analysis. Fatigue Fract. Engng Mater. Struct. Vol. 18, No. 3, pp. 397-41 1

[Bannantine et al.(1990)] Bannantine, J.A, Comer, J.J, Handrock, J.L. (1990) Fundamentals of metal fatigue analysis. Prentice Hall.

[Barnier and Brisset (1999)] Barnier, N, Brisset, P.(1999) Optimisation par algorithme génétique sous contraintes. Technique et Science Informatiques, Hermès-Lavoisier, 1999, 18 (1), pp 1-29.

[Beckers(1999)] Beckers, M.(1999) Topology optimizaton using a dual method with discrete variables. Structural Optimization, 17:14-24.

[Bendsøe and Kikuchi(1988)] Bendsøe, M, Kikuchi, N. (1988) Generating optimal topologies in structural design using a homogeneization method. Comp Meth Appl Mech Eng 71:197–224

[Bendsøe(1989)] Bendsøe, M.P. (1989) Optimal Shape as a material distribution problem. Structural Optimization, 1, 193-202

[Bendsøe and Diaz(1998)] Bendsøe, M.P, Dìaz, A.R N. (1998) A method for treating damage related criteria in optimal topology design of continuum structures. Structural Optimization 16:108-115.

[Bendsøe and Sigmund(1999)] Bendsøe, M, Sigmund O. (1999) Material interpolation schemes in topology optimization. Archive of Applied Mechanics 69 (1999) 635-654

[Bendsøe and Sigmund(2003)] Bendsøe, M, Sigmund, O. (2003) Topology optimization - Theory, methods and applications, Springer, EUA, New York

[Besoussan et al.(1978)] Bensoussan, A, Lions, J.L, Papanicolaou, G.(1978) Asymptotic analysis for periodic structures. North-Holland

[Berke and Khot(1974)] Berke, L, Khot, N. (1974) Use of optimality criteria methods for large scale systems. AGARD-LS-70

[Bernasconi(2002)] Bernasconi, A. (2002)Efficient algorithms for calculation of shear stress amplitude and amplitude of the second invariant of the stress deviator in fatigue criteria applications. International Journal of Fatigue 24:649-657

[Bernasconi and Papadopoulos(2000)] Bernasconi, A, Papadopoulos, I.V. (2000)Efficiency of algorithms for shear stress amplitude calculation in critical plane class fatigue criteria. Computational Materials Sciences 34:355-368

[Bruggi and Venini(2008)] Bruggi, M, Venini, P. (2008) A mixed FEM approach to stress-constrained topology optimization. Int J Numer Methods Eng 73(11):1693–714

[Bruggi(2008)] Bruggi, M. (2008) On an alternative approach to stress constraints relaxation in topology optimization. Struct Multidiscip Optim 36:125–141

[Bruggi and Cinquini(2009)] Bruggi, M, Cinquini, C. (2009) An alternative truly–mixed formulation to solve pressure load problems in topology optimization. Comput Methods Appl Mech Engrg 198(17–20):1500–1512

[Bruggi(2016)] Bruggi, M. (2016) Topology optimization with mixed finite elements on regular grids. Comp Meth Appl Mech Eng, 305:133–153

[Bruggi and Duysinx(2012)] Bruggi, M, Dusyinx, P. (2012) Topology optimization for minimum weight with compliance and stress constraints. Struct Multidisc Optim 46(3):369-384

[Bruggi and Duysinx(2013)] Bruggi, M, Dusyinx P. (2013) A stress–based approach to the optimal design of structures with unilateral behavior of material or supports. Struct Multidisc Optim 46(3):369-384

[Bruns(2005)] Bruns, TE. (2005) A reevaluation of the SIMP method with filtering and an alternative formulation for solid-void topology optimization. Struct Multidisc Optim 30(5):428–436

[Bruyneel et al.(2002)] Bruyneel, M, Duysinx P, Fleury C. (2002) A family of MMA approximations for structural optimization. Structural and Multidisciplinary Optimization, 24:263–276.

[Bruyneel et al.(2005)] Bruyneel, M, Duysinx, P. (2005)Note on topology optimization of continuum structures including self-weight. Struct Multidisc Optim 29: 245–256

[Byrd et al.(1999)] Byrd, R. H, Hribar, M.E, Nocedal, J. (1999)An Interior Point Algorithm for Large-Scale Nonlinear Programming. SIAM Journal on Optimization, Vol 9, No. 4, 1999, pp. 877–900

[Budynas and Nisbett(2011)] Budynas, R.G, Nisbett, J.K. (2011) Shigley's Mechanical Engineering Design, 9th edition New York: McGraw-Hill

[Cadman et al.(2013)] Cadman, J.E, Zhou, S, Chen, Y, Li, Q. (2013) On design of multifunctional microstructural materials. J Mater Sci 48:51-66

[Cheng and Jiang(1992)] Cheng, GD, Jiang, Z. (1992) Study on topology optimization with stress constraints. Eng Optim 20:129–148

[Cheng and Guo(1997)] Cheng, GD, Guo, X. (1997) ε–relaxed approach in topology optimization. Struct Optim 13: 258–266

[Collet et al.(2015)] Collet, M, Bruggi, M, Bauduin S, Duysinx, P. (2015). Stress-based topology optimization with fatigue failure constraints. In Proceedings of the Fifteenth International Conference on Civil, Structural and Environmental Engineering Computing.

[Collet et al.(2017)] Collet, M, Bruggi, M, & Duysinx, P. (2017) Topology optimization for minimum weight with compliance and simplified nominal stress constraints for fatigue resistance. Structural and Multidisciplinary Optimization, 55:839–855

[Crossland(1956)] Crossland, B. (1956) Effect of large hydrostatic pressures on the torsional fatigue strength of an alloy steel. Int. Conference on Fatigue of Metals. Institution of mechanical engineers, London : pp.138-149.

[Dang Van et al.(1973)] Dang Van K. (1973) Sur la résistance à la fatigue des Métaux, Sciences et techniques de l'armement. 47, 3ème Fasc, Mémorial de l'artillerie française, Paris, Imprimerie Nationale

[Dang Van et al.(1989)] Dang Van K, Griveau B, Message O. (1989) On a new multiaxial fatigue criterion: Theory and Applications. Biaxial and Multiaxial Fatigue, EGF3 (Edited by M.W. Brown and K.J.Miller) Mechanical Engineering Publications, London,pp 479-496

[Dang Van(2001)] Dang Van K. (2001) Multiaxial Fatigue criteria based on a multiscale approach. Handbook of Materials Behavior Models. ISBN 0-12-443341-3

[Dang Van(2010)] Dang Van K.(2010) On a unified fatigue modeling for structural analysis based on the shakedown concept. Ciêcia & Tecnologia dos Materiais, Vol.22, No 3/4.

[Dang Van and Papadopoulos(1999)] Dang Van K.Y, Papadopoulos Y.V.(1999) High-cycle metal fatigue: From theory to applications. Springer-Verlag Wien GmbH. ISBN 9783211831441

[Deaton and Grandhi(2013)] Deaton J.D, Grandhi R.V. (2013) Topology Optimization of Thermal Structures with Stress Constraints. 54th AIAA/ASME/ASCE/AHS/ASC Structures, Structural Dynamics, and Materials Conference

[Deaton and Grandhi(2014)] Deaton J.D, Grandhi R.V. (2014) A survey of structural and multidisciplinary continuum topology optimization: post 2000. Structural and Multidisciplinary Optimization 49:1–38

[De Leon et al.(2015)] De Leon D.M, Alexandersen J, Fonseca J.S.O, Sigmund O. (2015)Stress-constrained topology optimization for compliant mechanism design. Struct Multidisc Optim 52:929–943

[van Dijk et al.(2013)] van Dijk N. P, Maute K, Langelaar M, van Keulen F. (2013). Level-set methods for structural topology optimization: a review. Structural and Multidisciplinary Optimization, 48:437–472.

[Dorn et al.(1964)] Dorn WS, Gomory RE, Greenberg HJ. (1964) Automatic design of optimal structures. J Méc 3:25-52

[Dowing and Socie(1982)] Downing S. D, Socie D. F.(1982) Simple rainflow counting algorithms. INT. J. FATIGUE, 31-40.

[Duysinx et al.(1995)] Duysinx, P., Zhang,W.H, Fleury, C, Nguyen,V.H, Haubruge S. (1995) A New Separable Approximation Scheme for Topological Problems and Optimization Problems Characterized by a Large Number of Design Variables. Proceedings of the First World Congress of Structural and Multidisciplinary Optimization, Goslar, Germany, May 28 - June 2, 1995, pp 108-109.

[Duysinx(1996)] Duysinx P. (1996) Optimisation topologique: Du milieu continu à la structure élastique. Thèse de Doctorat, Université de Liège, Belgique

[Duysinx(1997)] Duysinx P. (1997) Layout optimization : A mathematical programming approach. Paper partially presented at the XIXth IUTAM International Congress of Theoretical and Applied Mechanics, Kyoto, Japan, August 25-31, 1996 and at the IXth Nordic Seminar of Computational Mechanics, Lyngby, Denmark, October 25-26.

[Duysinx and Bendsøe(1998)] Duysinx P, Bendsøe, MP. (1998) Topology optimization of continuum structures with local stress constraints. Int J Numer Methods Eng 43: 1453–1478

[Duysinx and Sigmund(1998)] Duysinx P, Sigmund O. (1998) New developments in handling stress constraints in optimal material distribution. 7th Symposium on Multidisciplinary Analysis and Optimization AIAA–98–4906: 1501–1509

[Duysinx et al.(2008)] Duysinx P, Van Miegroet L, Lemaire E, Brüls O, Bruyneel M. (2008) Topology and generalized shape optimization: why stress constraints are so importants ? Int J.Simul.Multidisc.Des.Optim. 2:253–258

[Duysinx(2016)] Duysinx P.(2016) Performances et comportement des véhicules. Université de Liège

[Eiben and Smith(2003)] Eiben A.E, Smith J.E. (2003) Introduction to Evolutionary Computing. Springer-Verlag, Berlin Heidelberg, 2003.

[Eschenauer and Olhoff(2001)] Eschenauer HA, Olhoff N. (2001) Topology optimization of continuum structures: A review. Appl Mech Rev 54:331–389.

[Fernandez et al.(2018)] Fernandez E, Collet M, Alarcon P, Bauduin S, Duysinx P.(2018) On the aggregation of maximum size constraints in density-based topology optimization. Struct Multidiscip Optim. *In preparation*

[Feyel(2003)] Feyel, F. (2003) A multilevel finite element method (FE^2) to describe the response of highly non-linear structures using generalized continua. Comput. Methods Appl. Mech. Engrg. 192: 3233–3244

[Fleury(1973)] Fleury, C.(1973) Méthodes numériques d'optimisation des structures. Rapport interne LTAS, SF-19.

[Fleury(1979a)] Fleury, C.(1979a) Structural weight optimization by dual methods of convex programming. International Journal for Numerical Methods in Engineering, 14(12):1761–1783.

[Fleury(1979b)] Fleury, C.(1979b) A unified approach to structural weight minimization. Computer Methods in Applied Mechanics and Engineering, 20(1):17–38.

[Fleury(1982)] Fleury, C.(1982) Reconciliation of Mathematical Programming and Optimality Criteria Methods. In: Foundations of Structural Optimization: A Unified Approach, (Morris,A.J., ed.), chap. 10, pp 363-404, John Wiley& Sons, 1982.

[Fleury and Braibant(1986)] Fleury, C, Braibant, V.(1986) Structural optimization: A new dual method using mixed variables. International Journal for Numerical Methods in Engineering, 23:409–428.

[Fleury(1989a)] Fleury, C. (1989a) Conlin: an efficient dual optimizer based on convex approximation concepts. Structural optimization, 1:81–89.

[Fleury(1989b)] Fleury, C. (1989b) First and second order convex approximation strategies in structural optimization. Structural optimization, 1(1):3–10.

[Fleury(1993)] Fleury, C.(1993) Sequential convex programming for structural optimization problems. In G. I. N. Rozvany, editor, Optimization of Large Structural Systems, volume 231 of NATO ASI Series, pages 531–553. Springer Netherlands.

[Fleury(2007)] Fleury, C. (2007) Structural optimization methods for large scale problems: status and limitations. Proceedings of the ASME 2007 International Design Engineering Technical Conferences & Computers and Information in Engineering Conference, IDETC/CIE, September 4-7, Las Vegas, Nevada, USA.

[Fox(1965)] Fox, R.L. (1965). "Constraint Surface Normals for Structural Synthesis Techniques, AIAA Journal, vol. 3, n°8, pp 1517-1518.

[Gibiansky and Sigmund(2000)] Gibiansky, L.V, Sigmund, O. (2000) Multiphase composites with extremal bulk modulus. Journal of the Mechanics and Physics of Solids 48, 461–498.

[Gillis(1966)] Gillis, P.P.(1966) Manson-Coffin fatigue.Volume 14, Issue 12, December 1966, Pages 1673-1676

[Golub et Van Loan(1996)] Golub, G.H, Van Loan C.F. (1996)Matrix computations- Third edition. John's Hopkins University press

[Grabovsky and Kohn(1995)] Grabovsky, Y, Kohn, R.V. (1995) Microstructures minimizing the energy of a two phase elastic composite in two space dimensions. ii: The Vigdergauz microstructure. Journal of Mechanics and Physics of Solids 43(6), 949-972

[Green and Haftka(1991)] Greene, W.H, Haftka, R.T. (1991) Computational aspects of sensitivity calculations in linear transient structural analysis. Structural Optimization, 3(3):176–201.

[Greil et al.(1998)] Greil, P, Lifka, T, Kaindl, A. (1998) Biomorphic Cellular Silicon Carbide Ceramics from Wood: I. Processing and Microstructure. Journal of the European Ceramic Society, Volume 18, Issue 14, December 1998, Pages 1961-1973

[Grunwald and Schnack(1997)] Grunwald, J, Schnack E.(1997) A fatigue model for shape optimization. Structural Optimization 14:36-44

[Guedes and Kikuchi(1990)] Guedes, J.M., Kikuchi, N.: Preprocessing and postprocessing for materials based on the homogenization method with adaptive

nite element methods. Computer Methods in Applied Mechanics and Engineering 83, 143-198 (1990)

[Guest et Prévost(2006)] Guest, J.K, Prévost, J.H.(2006) Optimizing multifunctional materials: design of microstructures for maximized stiffness and fluid permeability. International Journal of Solids and Structures 43, 7028–7047

[Guilherme et Fontseca(2007)] Guilherme, CEM, Fonseca, JSO. (2007) Topology optimization of continuum structures with epsilon-relaxed stress constraints. In:Alves M, da Costa Mattos HS (eds) Solid mechanics in Brazil, vol 1. ABCM, Rio de Janeiro, pp 239–250

[Gurson(1977)] Gurson, A.L. (1977) Continuum theory of ductile rupture by void nucleation and growth: Part I - Yield criterion and flow rules for porous ductile media.J. Eng. Mater. Technol 99(1), 2-15

[Han(1976)] Han, S.P. (1976) Superlinearly Convergent Variable Metric Methods for General Nonlinear Programming. Mathematical Programming, vol. 11, pp 263-282.

[Haftka and Adelman(1989)] Haftka, R. T, Adelman, H. M. (1989) Recent developments in structural sensitivity analysis. Structural Optimization, 1:137–151.

[Haftka and Gürdal(1992)] Haftka, R.T, Gürdal, Z. (1992) Elements of structural optimization. Dordrecht: Kluwer

[Hassani and Hinton(1997)] Hassani, B, Hinton, E (1997) A review of homogenization and topology optimization i:homogenization theory for media with periodic structure. Computers and Structures 69, 707:717

[Hassani and Hinton(1998a)] Hassani, B, Hinton, E.(1998) A review of homogenization and topology optimization ii:homogenization theory for media with periodic structure. Computers and Structures 69, 719:738

[Hassani and Hinton(1998b)] Hassani, B, Hinton, E.(1998) A review of homogenization and topology optimization iii:homogenization theory for media with periodic structure. Computers and Structures 69, 739:756

[Hashin and Strickman (1963)] Hashin, Z, Shtrikman, S. (1963) A variational approach to the theory of the elastic behaviour of multiphase materials. Journal of the Mechanics and Physics of Solids 11, 127: 140.

[Holmberg et al.(2013)] Holmberg E, Torstenfelt B, Klarbring A. (2013) Stress constrained topology optimization. Struc Multidisc Optim 48:33– 47

[Holmberg et al.(2014)] Holmberg E, Torstenfelt B, Klarbring A. (2014) Fatigue constrained topology optimization. Struc Multidisc Optim 50:207– 219

[IPCC(2014)] IPCC, 2014: Climate Change 2014: Mitigation of Climate Change. Contribution of Working Group III to the Fifth Assessment Report of the Intergovernmental Panel on Climate Change [Edenhofer, O., R. Pichs-Madruga, Y. Sokona, E. Farahani, S. Kadner, K. Seyboth, A. Adler, I. Baum, S. Brunner, P. Eickemeier, B. Kriemann, J. Savolainen, S. Schlömer, C. von Stechow, T. Zwickel and J.C. Minx (eds.)]. Cambridge University Press, Cambridge, United Kingdom and New York, NY, USA.

[Jeong et al.(2014)] Jeong, SH, Choi, D–H, Yoon, GH. (2014) Fatigue and static failure considerations using a topology optimization method. Applied Mathematical Modelling 39:1137–1162

[Jensen and Sigmund(2011)] Jensen, J, Sigmund, O. (2011) Topology optimization for nano-photonics. Laser & Photonics Reviews 5, 308–321.

[Jia et al.(2017)] Jia, H, Misra, A, Poorsolhjouy, P, Liu, C (2017) Optimal structural topology of materials with micro-scale tension-compression asymmetry simulated using granular micromechanics. Materials & Design 115:422-432

[Kaya et al.(2010)] Kaya, N, Karen, I, Öztürk, F (2010) Re-design of a failed clutch fork using topology and shape optimization by the response surface method. Materials and Design 31:3008–3014

[Kennedy and Eberhart(1995)] Kennedy, J, Eberhart, R(1995). Particle swarm optimization. In Proceedings of IEEE International Conference on Neural Networks, volume 4, pages 1942–1948 vol.4, 1995.

[Kim and Park(2010)] Kim, Y.I, Park, G.J. (2010) Nonlinear dynamic response structural optimization using equivalent static loads. Comput. Methods Appl. Mech. Engrg. 199:660–676

[Kiyono et al.(2016)] Kiyono, C.Y, Vatanabe, S.L, Silva, E.C.N, Reddy, J.N. (2016)A new multi-p-norm formulation approach for stress-based topology optimization design; Composite Structures 156: 10–19

[Kirsch(1989)] Kirsch, U. (1989) Optimal topologies of truss structures, ComputerMethods in AppliedMechanics and Engineering 72, 15 .

[Kirsch(1990)] Kirsch, U. (1990) On singular topologies in optimal structural design. Struct Optim 2:133–142

[Kirsch(1993)] Kirsch, U. (1993) Structural optimization. Berlin, Heidelberg, New York: Springer

[Koutiri(2011)] Koutiri, I. (2011). Effet des fortes contraintes hydrostatiques sur la tenue en fatigue des matériaux métalliques. Mécanique des matériaux. Arts et Métiers ParisTech, Français.

[Kouznetsova et al.(2001)] Kouznetsova, V, Brekelmans W.A.M, Baaijens F.P.T. (2001) An approach to micro-macro modeling of heterogeneous materials, Comput. Mech. 27 (1): 37–48

[Koziel and Leifsson(2013)] Koziel, S, Leifsson, L. (2013) Surrogate-Based Modeling and Optimization. Springer-Verlag, New York, 2013.

[Kuci(2018)] Kuci, E. (2018) Shape and topology optimization for electro-mechanical energy converters, Phd Thesis, University of Liège, February 2018.

[Lalanne(1999)] Lalanne, C. (1999) Mechanical vibration & shock. Volume IV, Fatigue damage. Hermes Penton Science, 1999.19

[Lan Levengood and Zhang(2014)] Lan Levengood, S.K, Zhang, M. (2014) Chitosan-based scaffolds for bone tissue engineering. J. Mater. Chem. B, 2014,2, 3161-3184

[Le et al.(2010)] Le C, Norato J, Bruns TE, Ha, C and Tortorelli, D.A. (2010) Stress–based Topology Optimization for Continua. Struct Multidiscip Optim 41:605–620

[Lee et al.(2012)] Lee, E, James, K, Martins, J. (2012) Stress-constrained topology optimization with design-dependent loading, Structural and Multidisciplinary Optimization 46, 647–661

[Lewiński and Rozvany(2008)] Lewiński, T, Rozvany, G.I.N. (2008)Exact analytical solutions for some popular benchmark problems in topology optimization III: L-shaped domains. Struct Multidisc Optim (2008) 35:165–174

[Lipton and Stuebner(2006)] Lipton, R, Stuebner, M. (2006) Inverse homogenization and design of microstructure for pointwise stress control.The Quarterly Journal of Mechanics and Applied Mathematics, Vol. 59, pp. 131–169

[Lipton and Stuebner(2007)] Lipton, R, Stuebner, M. (2007) Optimal design of composite structures for strength and stiffness: an inverse homogenization approach.Struct Multidisc Optim (2007) 33:351–362

[Lian et al.(2017)] Lian, H, Chistiansen, A.N, Tortorelli, D.A, Sigmund, O, Aage, N.(2017) Combined shape and topology optimization for minimization of maximal von Mises stress.Struct Multidisc Optim

[Liu et al.(2016)] Liu, Q, Chan, R, Huang, X (2016) Concurrent topology optimization of macrostructures and material microstructures for natural frequency. Materials & Design 106:380-390

[Luo et al.(2013)] Luo, Y, Yu, Wang, Yu, M, Kang, Z. (2013) An enhanced aggregation method for topology optimization with local stress constraints. Comput. Method Appl. Mech. Engrg. 254:31– 41

[Ma et al.(1993)] Ma, Z.D, Kikuchi, N, Hagiwara, I. (1993) Structural topology and shape optimization for a frequency response problem. Computational Mechanics, 13(3):157–174, 1993.

[Mandel et al.(1977)] Mandel, J, Halphen, B, Zarka, J (1977) Adaptation d'un structure elasto-plastique à écrouissage cinématique. Mech. Res. Comm. 4:309-314

[Mattheck(1998)] Mattheck, C. (1998) Design in Nature: Learning from trees. Springer-Verlag, Berlin, Heidelberg.

[Michel et Suquet(1993)] Michel, J.C, Suquet, P.M.(1993) On the strength of composite materials: variational bounds and computational aspects. In M.P. Bendsoe and C. Mota Soares. Topology design of structures. Pp 355-374. Kluwer Academic Publishers.

[Michel et al.(1998)] Michel, J.C, Moulinec, H, Suquet, P.(1998) Effective properties of composite materials with periodic microstructure: a computational approach.Comput. Methods Appl. Mech. Engrg. 172 (1999) 109-143

[Miehe et Koch(2002)] Miehe, C, Koch, A. (2002) Computational micro-to-macro transitions of discretized microstructures undergoing small strains.Archive of Applied Mechanics 72 (2002) 300–317

[Mitchell(1996)] Mitchell, M. (1996) An Introduction to Genetic Algorithms. MIT University Press

[Mlejnek and Schirrmacher (1993)] Mlejnek, H.P, Schirrmacher, R. (1993) An engineer's approach to optimal material distribution and shape finding. Computer Methods in Applied Mechanics and Engineering, 106(1):1-26

[Moin(2010)] Moin, P. (2010) Fundamentals of engineering numerical analysis. Cambridge university press, New-York, second edition, 2010.

[Mok et al.(2016)] Mok, S.-W, Nizak, R, Fu, S-C, Ho, K-W k, Qin, L, B.F. Saris, D, Chan, K-M, Malda, J. (2016)From the printer: Potential of three-dimensional printing for orthopaedic applications. Journal of Orthopaedic Translation, Volume 6, July 2016, Pages 42-49

[Morel et al.(2010)] Morel, A, Bignonnet, A, Germain, G, Morel, F. (2010) Teaching durability in automotive applications using a reliability approach. Int J Interact Des Manuf 4:281–287

[Mrzygold and Zielinski(2006)] Mrzygold, M, Zielinski, A.P. (2006) Numerical implementation of multiaxial high-cycle fatigue criterion to structural optimization. Journal of Theoretical and Applied Mechanics, 44(3),pp 691–712

[Mrzygold and Zielinski(2007)] Mrzygold, M, Zielinski, A.P. (2007) Parametric structural optimization with respect to the multiaxial high-cycle fatigue criterion. Struct Multidisc Optim 33: 161–171

[Mrzygold(2012)] Mrzygold, M. (2012) Multi-constrained topology optimization using constant criterion surface algorithm. Bulletin of the Polish Academy of Sciences, Technical Sciences, 60(2):229-236

[Myers et al.(2009)] Myers, R.H, Montgomery, D.C, Anderson-Cook, C.M. (2009) Response Surface Methodology:Process and Product Optimization Using Designed Experiments. John Wiley & Sons, New York, third edition.

[Neto et al.(2015)] Neto, M.A, Amaro, A, Roseiro, L, Cirne, J, Leal, R. (2015) Engineering Computation of Structures: The Finite Element Method. Springer International Publishing Switzerland.

[Nguyen et al.(2012)] Nguyen, V.-D, Béchet, E, Gueuzaine, C, Noels, L. (2012) Imposing periodic boundary conditions on arbitrary meshes by polynomial interpolation. Computational Materials Science, 55:390-406.

[Noël and Duysinx(2017)] Noël, L, Duysinx, P. (2017) Shape optimization of microstructural designs subject to local stress constraints within an XFEM-level set framework. Struct Multidisc Optim 55:2323–2338

[Noël(2016)] Noël, L. (2016) Level set optimization of bimaterial structures and microstructures considering stress and damage resistance. Doctoral thesis, University of Liège, Belgium

[Norton(2000)] Norton, R. L. (2000). Machine design: An integrated approach. Upper Saddle River, N.J: Prentice Hall

[Oest and Lund(2017)] Oest, J, Lund, E. (2017) Topology optimization with finite-life fatigue constraints. Struct Multidisc Optim, *available online*

[Olhoff et al.(1993)] Olhoff, N, Thomsen, J, Rasmussen, J. (1993) Topology optimization of bimaterial structures. In: Pedersen P (ed) Optimal design with advanced materials. Elsevier, Amsterdam, pp 191–206

[Osher and Sethian(1988)] Osher, S, Sethian, J.A. (1988) Fronts propagating with curvature-dependent speed: Algorithms based on Hamilton-Jacobi formulations. Journal of Computational Physics, 79(1):12–49.

[Papuga(2011)] Papuga, J. (2011) A survey on evaluating the fatigue limit under multiaxial loading. Int. J. of fatigue 33, 153-165.

[Papadopoulos(1994)] Papadopoulos, I.V. (1994), A new criterion of fatigue strength for out-of-phase bending and torsion of hard metals, Int. J Fatigue, Vol. 16, 377-384.

[Papadopoulos(1995)] Papadopoulos, I.V. (1995), A high-cycle fatigue criterion applied in biaxial and triaxial out-of-phase stress conditions, Fatigue Fract. Engng Mater. Struct .. Vol. 18, 79-91.

[Papadopoulos et al.(1997)] Papadopoulos, I.V, Davoli, P, Gorla, C, Filippini, M, Bernasconi, A. (1997) A comparative study of multiaxial high-cycle fatigue criteria for metals Int. J. Fatigue Vol.19 No.3 pp 219-235.

[Paris et al.(2009)] Paris, J, Navarrina, F, Colominas, I, Casteleiro, M. (2009) Topology optimization of continuum structures with local and global stress constraints. Struct Multidiscip Optim 39:419–437

[Paris et al.(2010)] Paris, J, Navarrina, F, Colominas, I, Casteleiro, M. (2010) Block aggregation of stress constraints in topology optimization of structures. Adv Eng Soft, 41: 433–441

[Park and Kang(2003)] Park, G.J, Kang, B.S. (2003)Validation of a structural optimisation algorithm transforming dynamic loads into equivalent static loads. Journal of optimization theory and applications: Vol 118, No.1., pp.191–200

[Perdersen(1998)] Perdersen, P. (1998)Some general optimal design results using anisotropic, power law nonlinear elasticity, Structural Optimization 15:73-80

[Perdersen(2000)] Pedersen, P. (2000) On optimal shapes in materials and structures. Struct Multidisc Optim 19:169-182.

[Peirera et al.(2004)] Pereira, JT, Fancello, EA, Barcellos, CS. (2004) Topology optimization of continuum structures with material failure constraints. Struct Multidisc Optim 26(1–2):50–66

[Ponte-Castenada and De Botton(1992)] Ponte-Castenada, P, De Botton, G.(1992) On the homogenized yield strength two-phase composites. Proc. R. Soc. London. A. (438) 439-444.

[Roux et al.(1998)] Roux, W.J, Stander, N ,Haftka, R.T. (1998) Response surface approximations for structural optimization. International Journal for Numerical Methods in Engineering, 42 (3):517–534.

[Rozvany and Sobieszczanski(1992)] Rozvany, GIN, Sobieszczanski-Sobieski, J. (1992) New optimality criteria methods: forcing uniqueness of the adjoints strains by corner-rounding at constraints intersections. Struct Optim 4:244–246

[Rozvany et al.(1994)] Rozvany, GIN, Zhou, M, Sigmund, O. (1994) Topology Optimization in Structural Design. In Adeli H (ed.): Advances in Design Optimization, pp. 340:399. London: Chapman and Hall, 1994

[Rozvany and Biker(1994)] Rozvany, GIN, Birker, T. (1994) On singular topologies in exact layout optimization. Struct Optim 8:228–235

[Rozvany(1996)] Rozvany, GIN. (1996) Difficulties in truss topology optimization with stress, local buckling and system stability constraints. Struct Optim 11:213–217

[Rozvany(1996b)] Rozvany, GIN. (1996). Some shortcomings in Michell's truss theory. In: Struct. Opt., 1996. 12, 244-250.

[Rozvany(2001)] Rozvany, GIN. (2001) On design-dependent constraints and singular topologies. Struc Multidisc Optim 21,164-172.

[Rozvany(2001b)] Rozvany, GIN (2001)Stress ratio and compliance based methods in topology optimization – a critical review.Struct Multidisc Optim 21, 109–119

[Rozvany(2009)] Rozvany, GIN (2009) A critical review of established methods of structural topology optimization. Struct Multidiscip Optim 37:217–237

[Saad(2003)] Saad, Y. (2003)Iterative Methods for Sparse Linear Systems - Second edition. SIAM

[Safran(2010)] Safran magazinz(2010) Quatres mains pour un moteur, Safran Magazine, no 10, juin 2010, p.17-18

[Sanchez-Hubert and Sanchez-Palencia(1992)] Sanchez-Hubert, J, Sanchez-Palencia, E (1992) Introduction aux méthodes asymptotiques et à l'homogénéisation. Collection mathématiques appliquées pour la Maîtrise. Masson. Partis. 1992.

[Sanchez-Palencia (1983)] Sanchez-Palencia, E.(1983) Homogenization method for the study of composite media. In: F. Verhulst (ed.) Asymptotic Analysis II, Lecture Notes in Mathematics, vol. 985, pp. 192:214. Springer Berlin Heidelberg

[Schijve(2003)] Schijve, J. (2003) Fatigue of structures and materials in the 20th century and the state of the art. International Journal of Fatigue 25:679-702

[Schittkowski(1981)] Schittkowski, K. (1981) The Non-Linear Programming Method of Wilson, Han and Powell with an Augmented Lagrangian Type Line Search Function, Part 1: Convergence Analysis; Part 2: An Efficient Implementation with Least Square Problems, Numerical Mathematics, vol. 38, pp 38-114, pp115-127.

[Schittkowski(1985)] Schittkowski, K. (1985) NLPQL: A Fortran Subroutine solving Constrained Nonlinear Programming Problems. Annals of Operation Research, pp 485-500.

[Schmit(1960)] Schmit, L.A. (1960) Structural design by systematic synthesis. In Proceedings of the 2nd ASCE Conference on Electronic Computation, pages 105–132, Pittsburg.

[Schmit(1976)] Schmit, L.A, Miura, H. (1976) Approximation concepts for efficient structural synthesis. NASA Contractor Report, NASA-CR 2552.

[Schütz(1996)] Schütz, W. (1996) A history of fatigue Engineering Fracture Mechanics Vol. 54, No. 2, pp. 263–300

[Sherif and Irschif(2010)] Sherif, K, Irschik, H. (2010) Efficient Topology Optimization of Large Dynamic Finite Elements Systems Using Fatigue. AIAA Journal Vol.48, No.7.

[Sigmund(1994)] Sigmund, O. (1994) Materials with prescribed constitutive parameters: an inverse homogenization problem. Int. J. Solids Structures. Vol.31. No 17. pp 2313-2329.

[Sigmund(1995)] Sigmund, O. (1995) Tailoring materials with prescribed elastic properties. Mechanics of Materials 20:351-368

[Sigmund(1999)] Sigmund, O. (1999) A new class of extremal composites. Journal of the Mechanics and Physics of Solids 48(2000) 397-428

[Sigmund and Torquato(1999)] Sigmund, O, Torquato, S. (1999). Design of smart composite materials using topology optimization. Smart Materials and Structures 8, 365– 379.

[Sigmund(2001)] Sigmund, O. (2001) A 99 line topology optimization code written in Matlab. Struct Multidisc Optim 21, 120–127

[Sigmund and Maute(2013)] Sigmund, O, Maut, K. (2013) Topology optimization approaches: A comparative review. Struc Multidisc Optim 48:1031-1055

[Sigmund(2007)] Sigmund, O. (2007) Morphology-based black and white filters for topology optimization. Structural and Multidisciplinary Optimization 33(4-5):401–424

[Simon(2013)] Simon, D. (2013). Evolutionary Optimization Algorithms: Biologically-Inspired and Population-Based Approaches to Computer Intelligence. John Wiley & Sons, 2013.

[Sines(1959)] Sines, G.(1959) Metal Fatigue. Behavior of metals under complex static and alternating stresses., Mac Graw Hill, New York:pp.145-169.

[Smaoui et al.(1988)] Smaoui, H, Fleury, C, Schmit, L.A. (1988)Advances in Dual Algorithms and Convex Approximation Methods. Proceedings of AIAA/ASME/ASCE 29th Structures, Structural Dynamics and Material Conference, pp 1339-1347, 1988.

[Stephens et al.(2010)] Stephens, R.I, Fatemi, A, Stephens, R.R, Fuchs, H.O. (2010) Metal Fatigue in Engineering. A Wiley-Interscience publication. John Wiley & Sons, 2 edition. ISBN 9780471510598

[Starnes Jr and Haftka(1979)] Starnes, Jr J.H, Haftka, R.T. (1979) Preliminary design of composite wings for buckling, strength, and displacement constraints. Journal of Aircraft, 16(8):564–570.

[Stolpe and Svanberg(2001a)] Stolpe, M, Svanberg, K. (2001) On the trajectories of the epsilon-relaxation approach for stress-constrained truss topology optimization, Structural and Multidisciplinary Optimization 21, 140.

[Stolpe and Svanberg(2001b)] Stolpe, M, Svanberg K. (2001) An alternative interpolation scheme for minimum compliance topology optimization, Struct Multidisc Optim 22, 116–124

[Stolpe and Svanberg(2003)] Stolpe, M, Svanberg, K. (2003) Modelling topology optimization problems as linear mixed 0-1 programs. Int J Numer Methods Eng 57:723–739

[Suquet(1982)] Suquet, P.(1982) Une méthode duale en homogénéisation : application aux milieux élastiques. Journal de Mécanique Théorique et Appliquée pp. 79:98

[Svärd(2015a)] Svärd, H. (2015) Topology Optimization of Fatigue-Constrained Structures, Doctoral Thesis, KTH Engineering Sciences, Stockholm, Sweden

[Svärd(2015b)] Svärd, H.(2015) Interior value extrapolation: a new method for stress, evaluation during topology optimization, Struct Multidisc Optim 51:613–629

[Svanberg(1987)] Svanberg, K. (1987) Method of moving asymptotes - A new method for structural optimization. Int J Numer Methods Eng 24:359–373

[Svanberg(1995)] Svanberg, K.(1995) A globally convergent version of MMA without lineserach. In Proceedings of the 1st World Congress of Structural and Multidisciplinary Optimization, Goslar, Germany, 1995.

[Svanberg(2002)] Svanberg, K. (2002) A class of globally convergent optimization methods based on conservative convex separable approximations. SIAM Journal on Optimization, 12(2):555–573.

[Svanberg(2007)] Svanberg, K.(2007)MMA and GCMMA - version September 2007. Stockholm, Sweden

[Svanberg et Werme(2007)] Svanberg, K, Werme, M. (2007) Sequential integer programming methods for stress constrained topology optimization. Struct Multidisc Optim 34(4):277–299

[Sved and Ginos(1968)] Sved G, Ginos, Z. (1968) Structural optimization under multiple loading. Int J Mech Sci 10:803–805

[Takezawa et al.(2014)] Takezawa, A, Yoon, G.H, Jeong, S.H, Kobashi, M, Kitamura, M. (2014) Structural topology optimization with strength and heat conduction constraints. Comput. Methods Appl. Mech. Engrg. 276:341–361

[Tortorelli et Michaleris(1994)] Tortorelli, D, Michaleris, P. (1994) Design sensitivity analysis: Overview and review. Inverse Problems in Engineering, 1:1, 71-105

[Torquato(2002)] Torquato S.(2002) Random Heterogeneous Materials–Microstructure and Macroscopic Properties. Springer, New York, 2002

[Tyrus et al.(2007)] Tyrus, J.M, Gosz, M, DeStantiago, E. (2007) A local finite element implementation for imposing periodic boundary conditions on composite micromechanical models. International Journal of Solids and Structures, 44(9):2972-2989

[Van Keulen et al.(2005)] van Keulen, F, Haftka, R.T, Kim, N.H. (2005) Review of options for structural design sensitivity analysis. Part 1: Linear systems. Computer Methods in Applied Mechanics and Engineering, 194:3213–3243.

[Vassilevski(2008)] Vassilevski, P.S. (2008) Multilevel Block Factorization Preconditionners - Maxtrix–based analysis and algorithms for solving finite element equations. Springer

[Verbart(2015)] Verbart, A.(2015) Topology optimization with stress constraints. Phd Thesis, TU DELFT

[Verbart et al.(2017)] Verbart, A, Langelaar, M, Van Keulen, F. (2017) A unified aggregation and relaxation approach for stress-constrained topology optimization.Struct Multidisc Optim 55:663–679

[Vigdergauz(2001)] Vigdergauz, S.(2001) The effective properties of a perforated elastic plate numerical optimization by genetic algorithm. International Journal of Solids and Structures 38, 8593- 8616

[Wang and Yao(2004)] Wang, Y.Y, Yao, W.X. (2004) Evaluation and comparison of several multiaxial fatigue criteria. International Journal of Fatigue 26:17–25

[Weber(1999)] Weber, B. (1999) Fatigue multiaxiale des structures industrielles sous chargement quelconque. Thèse de doctorat. INSA Lyon.

[Weibull (1939)] Weibull, W. (1939) A statistical theory of the strength of materials. Ingeniörsvetenskapsakademiens handlingar. Generalstabens litografiska anstalts förlag, 1939.

[Weiβgraebe et al.(2016)] Weiβgraebe, P., Leguillon, D., Becker, W.(2016)A review of Finite Fracture Mechanics: crack initiation at singular and non-singular stress raiser.Arch Appl Mech 86:375–401

[Witteveen et al.(2009)] Witteveen, W, Puchner, K, Sherif, K, Irschik, H. (2009) Efficient topology optimization for large and dynamically loaded FE models. *In proceedings of the IMAC-XXVII*

[Xia(2015)] Xia, L. (2015) Towards Optimal Design of Multiscale Nonlinear Structures. Dissertation submitted for the degree of Doctor of Philosophy of Advanced Mechanics, Sorbonne Universités, Université de Technologie de Compiègne.

[Xia and Breitkopf(2015)] Xia, L, Breitkopf, P. (2015) Design of materials using topology optimization and energy-based homogenization approach in Matlab. Struct Multidisc Optim 52:1229–1241

[Yang and Chen(1996)] Yang, RJ, Chen, CJ. (1996) Stress-based topology optimization. Struct Multidisc Optim 12(2):98-105

[Yan et al.(2018)] Yan, S, Wang, F, Sigmund, O. (2018) On the non-optimality of tree structures for heat conduction. International Journal of Heat and Mass Transfer 122:660-680

[You and Lee(1995)] You, B-R, Lee, S-B. (1995) A critical review on multiaxial fatigue assessments of metals Int. J. Fatigue Vol.18 No4 pp.235-244.

[Zhang et al.(2017)] Zhang, S, Gain, A.L, Norato, J.A. (2017)Stress-based topology optimization with discrete geometric components. Comput. Methods Appl. Mech. Engrg. 325:1–21

[Zhou and Sigmund(2017)] Zhou, M, Sigmund, O.(2017) On fully stressed design and p-norm measures in structural optimization.Struct Multidisc Optim 56:731–736

[Zienkiewicz and Campbell(1973)] Zienkiewicz, O.C, Campbell, J.S. (1973) Shape optimization and sequential linear programming. In R. H. Gallagher and O. C. Zienkiewicz, editors, Optimum Structural Design, pages 109–126. Wiley, New York.

Chapter 6

Appendices

Appendix A: Sensitivity of global stress constraints

p-norm and p-mean along with the qp-relaxation

The definition of the two aggregation functions along with the qp-relaxation are given below. The subscripts PN and PM stand for p-norm and p-mean respectively:

$$\begin{aligned}\sigma_{PN} &= \left[\sum_{e=1}^{NE}\left(x_e^{p-q}\frac{\overline{\sigma_e}}{\sigma_y^0}\right)^r\right]^{\frac{1}{r}}\\ \sigma_{PM} &= \left[\frac{1}{NE}\sum_{e=1}^{NE}\left(x_e^{p-q}\frac{\overline{\sigma_e}}{\sigma_y^0}\right)^r\right]^{\frac{1}{r}}\end{aligned}$$

with σ_y^0 being the stress limit, NE the number of elements that are aggregated, p and q the penalization exponent of the SIMP law and the relaxation exponent of the qp-relaxation respectively. $\overline{\sigma_e} = \sqrt{\mathbf{U}_e^T\mathbf{M}_e^0\mathbf{U}_e}$ is the Von Mises stress measure of element e. Note that the p-exponent is replaced by an r-exponent in order to avoid any confusion between the power p of the SIMP law and the aggregation parameter.

We want to compute $\dfrac{\partial\sigma_{PN/PM}}{\partial x_j}$, it comes:

$$\begin{aligned}\frac{\partial\sigma_{PN/PM}}{\partial x_j} &= \frac{\partial}{\partial x_j}\left[\left[\frac{1}{NE}\sum_{i=e}^{NE}\left(x_e^{p-q}\frac{\overline{\sigma_e}}{\sigma_y^0}\right)^r\right]^{\frac{1}{r}}\right]\\ &= \frac{1}{r}\left[\frac{1}{NE}\sum_{e=1}^{NE}\left(x_e^{p-q}\frac{\overline{\sigma_e}}{\sigma_y^0}\right)^r\right]^{\frac{1}{r}-1}\cdot\frac{\partial}{\partial x_j}\left[\frac{1}{NE}\sum_{e=1}^{NE}\left(x_e^{p-q}\frac{\overline{\sigma_e}}{\sigma_y^0}\right)^r\right]\\ &= \frac{1}{r}\left[\frac{1}{NE}\sum_{e=1}^{NE}\left(x_e^{p-q}\frac{\overline{\sigma_e}}{\sigma_y^0}\right)^r\right]^{\frac{1}{r}-1}\cdot\frac{1}{NE}\sum_{e=1}^{NE}\left[\frac{\partial}{\partial x_j}\left(x_e^{p-q}\frac{\overline{\sigma_e}}{\sigma_y^0}\right)^r\right]\\ &= \frac{1}{r}\left[\frac{1}{NE}\sum_{e=1}^{NE}\left(x_e^{p-q}\frac{\overline{\sigma_e}}{\sigma_y^0}\right)^r\right]^{\frac{1}{r}-1}\cdot\frac{1}{NE}\sum_{e=1}^{NE}r\left(x_e^{p-q}\frac{\overline{\sigma_e}}{\sigma_y^0}\right)^{(r-1)}\left[\frac{\partial}{\partial x_j}\left(x_e^{p-q}\frac{\overline{\sigma_e}}{\sigma_y^0}\right)\right]\end{aligned}$$

by developing the sensitivity of local stress constraints, one has:

$$\begin{aligned}\frac{\partial\sigma_{PN/PM}}{\partial x_j} &= \frac{1}{r}\left[\frac{1}{NE}\sum_{e=1}^{NE}\left(x_e^{p-q}\frac{\overline{\sigma_e}}{\sigma_y^0}\right)^r\right]^{\frac{1}{r}-1}\cdot\frac{1}{NE}\cdot r\sum_{e=1}^{NE}\left(x_e^{p-q}\frac{\overline{\sigma_e}}{\sigma_y^0}\right)^{(r-1)}\left[\boldsymbol{(p-q)\delta_{ej}x_e^{p-q-1}\frac{\overline{\sigma_e}}{\sigma_y^0}}+\right.\\ &\qquad\left.\boldsymbol{x_e^{p-q}\frac{1}{\sigma_y^0}\frac{\partial\overline{\sigma_e}}{\partial x_j}}\right]\\ &= \left[\frac{1}{NE}\sum_{e=1}^{NE}\left(x_e^{p-q}\frac{\overline{\sigma_e}}{\sigma_y^0}\right)^r\right]^{\frac{1}{r}-1}\cdot\frac{1}{NE}\sum_{e=1}^{NE}\left(x_e^{p-q}\frac{\overline{\sigma_e}}{\sigma_y^0}\right)^{(r-1)}\left[\boldsymbol{(p-q)\delta_{ej}x_e^{p-q-1}\frac{\overline{\sigma_e}}{\sigma_y^0}}+\right.\\ &\qquad\left.\boldsymbol{x_e^{p-q}\frac{1}{\sigma_y^0}\frac{\partial\overline{\sigma_e}}{\partial x_j}}\right]\end{aligned}$$

What is written in bold is the classical sensitivity analysis for local stress constraints. We can go a step further:

$$\frac{\partial \sigma_{PN/PM}}{\partial x_j} = \left[\frac{1}{NE}\sum_{e=1}^{NE}\left(x_e^{p-q}\frac{\overline{\sigma_e}}{\sigma_y^0}\right)^r\right]^{\frac{1}{r}-1} \cdot \frac{1}{NE}\left[\sum_{e=1}^{NE}\left(x_e^{p-q}\frac{\overline{\sigma_e}}{\sigma_y^0}\right)^{(r-1)}(p-q)\delta_{ej}x_e^{p-q-1}\frac{\overline{\sigma_e}}{\sigma_y^0} + \sum_{e=1}^{NE}\left(x_e^{p-q}\frac{\overline{\sigma_e}}{\sigma_y^0}\right)^{(r-1)} x_e^{p-q}\frac{1}{\sigma_y^0}\frac{\partial \overline{\sigma_e}}{\partial x_j}\right]$$

By analogy with the work carried out in [Duysinx and Sigmund(1998)] and by recalling from the local stress constraints sensitivity computation that :$\frac{\partial \overline{\sigma_e}}{\partial x_j} = \boldsymbol{\lambda}^T \frac{\partial \mathbf{K}}{\partial x_j}\mathbf{U}$ with $\boldsymbol{\lambda}$ being the solution of $\mathbf{K}\boldsymbol{\lambda} = -\frac{\mathbf{M}_e^0\mathbf{U}_e}{\sqrt{\mathbf{U}_e^T\mathbf{M}_e^0\mathbf{U}_e}}$,we can finally write:

$$\frac{\partial \sigma_{PN/PM}}{\partial x_j} = \left[\frac{1}{NE}\sum_{e=1}^{NE}\left(x_e^{p-q}\frac{\overline{\sigma_e}}{\sigma_y^0}\right)^r\right]^{\frac{1}{r}-1} \cdot \frac{1}{NE}\left[\sum_{e=1}^{NE}\left(x_e^{p-q}\frac{\overline{\sigma_e}}{\sigma_y^0}\right)^{(r-1)}(p-q)\delta_{ej}x_e^{p-q-1}\frac{\overline{\sigma_e}}{\sigma_y^0} + \boldsymbol{\Lambda}^T\frac{\partial \mathbf{K}}{\partial x_j}\mathbf{U}\right]$$

with $\boldsymbol{\Lambda}$ being the global adjoint vector solution of the adjoint problem:

$$\mathbf{K}\boldsymbol{\Lambda} = -\sum_{i=e}^{NE}\left(x_e^{p-q}\frac{\overline{\sigma_e}}{\sigma_y^0}\right)^{r-1}\frac{x_e^{p-q}}{\sigma_y^0}\left(\frac{\mathbf{M}_e^0\mathbf{U_e}}{\sqrt{\mathbf{U}_e^T\mathbf{M}_e\mathbf{U}_e}}\right)$$

Kresselmeier–Steinhauser function (KS) along with the *qp*-relaxation

The Kresselmeier–Steinhauser function (KS) along with the *qp*-relaxation may take the form:

$$\sigma_{KS} = \frac{1}{\mu}ln\left(\sum_{e=1}^{NE}exp\left\{\mu\left(x_e^{p-q}\frac{\overline{\sigma_e}}{\sigma_y^0} - 1\right)\right\}\right)$$

where μ is the aggregation parameter. We want to evaluate $\dfrac{\partial \sigma_{KS}}{\partial x_j}$, that is:

$$\begin{aligned}
\frac{\partial \sigma_{KS}}{\partial x_j} &= \frac{1}{\mu}\frac{\partial}{\partial x_j}\left[ln\left(\sum_{e=1}^{NE} exp\left\{\mu\left(x_e^{p-q}\frac{\overline{\sigma_e}}{\sigma_y^0}-1\right)\right\}\right)\right] \\
&= \frac{1}{\mu}\left[\frac{\frac{\partial}{\partial x_j}\left(\sum_{e=1}^{NE} exp\left\{\mu\left(x_e^{p-q}\frac{\overline{\sigma_e}}{\sigma_y^0}-1\right)\right\}\right)}{\sum_{e=1}^{NE} exp\left\{\mu\left(x_e^{p-q}\frac{\overline{\sigma_e}}{\sigma_y^0}-1\right)\right\}}\right] \\
&= \frac{1}{\mu\sum_{e=1}^{NE} exp\left\{\mu\left(x_e^{p-q}\frac{\overline{\sigma_e}}{\sigma_y^0}-1\right)\right\}}\left[\frac{\partial}{\partial x_j}\left(\sum_{e=1}^{NE} exp\left\{\mu\left(x_e^{p-q}\frac{\overline{\sigma_e}}{\sigma_y^0}-1\right)\right\}\right)\right] \\
&= \frac{1}{\mu\sum_{e=1}^{NE} exp\left\{\mu\left(x_e^{p-q}\frac{\overline{\sigma_e}}{\sigma_y^0}-1\right)\right\}}\left[\sum_{e=1}^{NE}\left(\frac{\partial}{\partial x_j} exp\left\{\mu\left(x_e^{p-q}\frac{\overline{\sigma_e}}{\sigma_y^0}-1\right)\right\}\right)\right] \\
&= \frac{1}{\mu\sum_{e=1}^{NE} exp\left\{\mu\left(x_e^{p-q}\frac{\overline{\sigma_e}}{\sigma_y^0}-1\right)\right\}}\left[\sum_{e=1}^{NE}\left(\frac{\partial}{\partial x_j}\mu\left(x_e^{p-q}\frac{\overline{\sigma_e}}{\sigma_y^0}-1\right)\right)\cdot\left(exp\left\{\mu\left(x_e^{p-q}\frac{\overline{\sigma_e}}{\sigma_y^0}-1\right)\right\}\right)\right] \\
&= \frac{1}{\sum_{e=1}^{NE} exp\left\{\mu\left(x_e^{p-q}\frac{\overline{\sigma_e}}{\sigma_y^0}-1\right)\right\}}\left[\sum_{e=1}^{NE}\left(\frac{\partial}{\partial x_j}\left(x_e^{p-q}\frac{\overline{\sigma_e}}{\sigma_y^0}-1\right)\right)\cdot\left(exp\left\{\mu\left(x_e^{p-q}\frac{\overline{\sigma_e}}{\sigma_y^0}-1\right)\right\}\right)\right]
\end{aligned}$$

by developing the sensitivity of local stress constraints, one has:

$$\frac{\partial \sigma_{KS}}{\partial x_j} = \frac{1}{\sum_{e=1}^{NE} exp\left\{\mu\left(x_e^{p-q}\frac{\overline{\sigma_e}}{\sigma_y^0}-1\right)\right\}}\left[\sum_{e=1}^{NE}\left(\boldsymbol{(p-q)\delta_{ej}x_e^{p-q-1}\frac{\overline{\sigma_e}}{\sigma_y^0}+x_e^{p-q}\frac{\partial\overline{\sigma_e}}{\sigma_y^0}}\right)\cdot\left(exp\left\{\mu\left(x_e^{p-q}\frac{\overline{\sigma_e}}{\sigma_y^0}-1\right)\right\}\right)\right]$$

what is in bold is the classical evaluation of the local stress constraints. We can go a step further following the same procedure as for p-norm and p-mean:

$$\frac{\partial \sigma_{KS}}{\partial x_j} = \frac{1}{\sum_{e=1}^{NE} exp\left\{\mu\left(x_e^{p-q}\frac{\overline{\sigma_e}}{\sigma_y^0}-1\right)\right\}}\left[\sum_{e=1}^{NE}\left((p-q)\delta_{ej}x_e^{p-q-1}\frac{\overline{\sigma_e}}{\sigma_y^0}\left(exp\left\{\mu\left(x_e^{p-q}\frac{\overline{\sigma_e}}{\sigma_y^0}-1\right)\right\}\right)\right)+\boldsymbol{\Lambda}^T\frac{\partial\mathbf{K}}{\partial x_j}\mathbf{U}\right]$$

with $\boldsymbol{\Lambda}$ being the adjoint vector, solution of the adjoint problem:

$$\mathbf{K}\boldsymbol{\Lambda} = -\sum_{e=1}^{NE}\frac{x_e^{p-q}}{\sigma_y^0}\left(exp\left\{\mu\left(x_e^{p-q}\frac{\overline{\sigma_e}}{\sigma_y^0}-1\right)\right\}\right)\left(\frac{\mathbf{M}_e^0\mathbf{U}_e}{\sqrt{\mathbf{U}_e^T\mathbf{M}_e\mathbf{U}_e}}\right)$$

Appendix B: J_2 formalism for the computation of the microscopic stress used in the Dang Van criterion

---

Equivalent Von Mises stress for topology optimization

Let's consider a finite element mesh with NE elements. We know by definition that the equivalent Von Mises stress at the element level e is given by:

$$\sigma_e^{\mathrm{VM}} = \sqrt{3J_2}$$

where $J_2 = \frac{1}{2}trace(\boldsymbol{S_e^2})$ with $\boldsymbol{S}_e$ the deviatoric stress tensor at the element level. We can compute the element stress tensor $\boldsymbol{\Sigma}_e$, for instance at the center of one element, by solving the finite element analysis. The deviatoric stress tensor in term of the stress components coming from the finite element analysis is therefore given by:

$$\boldsymbol{S}_e = \boldsymbol{\Sigma}_e - \frac{1}{3}trace(\boldsymbol{\Sigma}_e)$$

We recall that $trace(\boldsymbol{\Sigma}_e) = \Sigma_{kk}$. For instance in 2D plane stress, the trace is equal to : $\Sigma_{XX} + \Sigma_{YY}$. The deviatoric stress tensor is therefore given by:

$$\boldsymbol{S}_e = \begin{pmatrix} \Sigma_{XX} - \frac{1}{3}(\Sigma_{XX} + \Sigma_{YY}) & \Sigma_{XY} & 0 \\ \Sigma_{XY} & \Sigma_{YY} - \frac{1}{3}(\Sigma_{XX} + \Sigma_{YY}) & 0 \\ 0 & 0 & -\frac{1}{3}(\Sigma_{XX} + \Sigma_{YY}) \end{pmatrix}$$

$\boldsymbol{S_e^2}$ is easy to get and is defined as:

$$\boldsymbol{S_e^2} = \begin{pmatrix} \left[\Sigma_{XX} - \frac{1}{3}(\Sigma_{XX} + \Sigma_{YY})\right]^2 + \Sigma_{XY}^2 & & \\ & \left[\Sigma_{YY} - \frac{1}{3}(\Sigma_{XX} + \Sigma_{YY})\right]^2 + \Sigma_{XY}^2 & \\ & & \frac{1}{9}\left[(\Sigma_{XX} + \Sigma_{YY})\right]^2 \end{pmatrix}$$

The trace is therefore given by:

$$\begin{aligned} trace(\boldsymbol{S_e^2}) &= \left[\Sigma_{XX} - \frac{1}{3}(\Sigma_{XX} + \Sigma_{YY})\right]^2 + \Sigma_{XY}^2 + \left[\Sigma_{YY} - \frac{1}{3}(\Sigma_{XX} + \Sigma_{YY})\right]^2 + \Sigma_{XY}^2 + \frac{1}{9}\left[(\Sigma_{XX} + \Sigma_{YY})\right]^2 \\ &= \underbrace{\left[\frac{2}{3}\Sigma_{XX} - \frac{1}{3}\Sigma_{YY}\right]^2}_{(*)} + \Sigma_{XY}^2 + \underbrace{\left[\frac{2}{3}\Sigma_{YY} - \frac{1}{3}\Sigma_{XX}\right]^2}_{(**)} + \Sigma_{XY}^2 + \frac{1}{9}\underbrace{\left[(\Sigma_{XX} + \Sigma_{YY})\right]^2}_{(***)} \end{aligned}$$

By developing the three terms $(*)$,$(**)$ and $(***)$ we have:

$$\begin{aligned} (*) &= \frac{4}{9}\Sigma_{XX}^2 - \frac{4}{9}\Sigma_{XX}\Sigma_{YY} + \frac{1}{9}\Sigma_{YY}^2 \\ (**) &= \frac{4}{9}\Sigma_{YY}^2 - \frac{4}{9}\Sigma_{XX}\Sigma_{YY} + \frac{1}{9}\Sigma_{XX}^2 \\ (***) &= \frac{1}{9}\left(\Sigma_{XX}^2 + 2\Sigma_{XX}\Sigma_{YY} + \Sigma_{YY}^2\right) \end{aligned}$$

Now gathering each term as:

$$\begin{aligned}
\text{terms in } \Sigma_{XX}^2 \quad &: \quad \underbrace{\left(\frac{4}{9}+\frac{1}{9}+\frac{1}{9}\right)}_{A}\Sigma_{XX}^2 \\
\text{terms in } \Sigma_{YY}^2 \quad &: \quad \underbrace{\left(\frac{1}{9}+\frac{4}{9}+\frac{1}{9}\right)}_{B}\Sigma_{YY}^2 \\
\text{terms in } \Sigma_{XY}^2 \quad &: \quad \underbrace{2}_{C}\Sigma_{XY}^2 \\
\text{terms in } \Sigma_{XX}^2 \quad &: \quad \underbrace{\left(-\frac{4}{9}-\frac{4}{9}+\frac{2}{9}\right)}_{D}\Sigma_{XX}\Sigma_{YY}
\end{aligned}$$

we can finally write:

$$\sqrt{3J_2} = \sqrt{\frac{3}{2}trace(\boldsymbol{S_e^2})} = \sqrt{\frac{3}{2}\left(A\Sigma_{XX}^2 + B\Sigma_{YY}^2 + D\Sigma_{XX}\Sigma_{YY} + C\Sigma_{XY}^2\right)}$$

Now recalling that the stress $\mathbf{\Sigma_e}$ is obtained in a finite element framework as : $\mathbf{\Sigma_e} = \mathbf{T_e U_e}$ it is easy to demonstrate that we can write the equivalent Von Mises stress as:

$$\sqrt{3J_2} = \sqrt{\mathbf{U_e^T M_e^0 U_e}}$$

with $\mathbf{M_e^0} = \mathbf{T_e^T V^1 T_e}$ and $\mathbf{V^1}$:

$$\mathbf{V^1} = \begin{pmatrix} \frac{3}{2}A & \frac{3}{4}D & 0 \\ \frac{3}{4}D & \frac{3}{2}B & 0 \\ 0 & 0 & \frac{3}{2}C \end{pmatrix}$$

here in particular we have:

$$\mathbf{V^1} = \begin{pmatrix} 1 & -\frac{1}{2} & 0 \\ -\frac{1}{2} & 1 & 0 \\ 0 & 0 & 3 \end{pmatrix}$$

and therefore:

$$\sqrt{3J_2} = \sqrt{\Sigma_{XX}^2 + \Sigma_{YY}^2 - \Sigma_{XX}\Sigma_{YY} + 3\Sigma_{XY}}$$

which is the well known Von Mises stress criterion in term of the stress tensor components. In the next paragraph the same procedure is derive to compute the $\mathbf{V}$ matrix in the framework of the Dang Van fatigue criterion.

Equivalent Von Mises stress for topology optimization including local plasticity for the Dang Van fatigue criterion

In the Dang Van theory, the stress tensor that has to be accounted for in the fatigue criterion is the deviatoric part of the microscopic stress at time step l:

$$\boldsymbol{s}_e^l = \boldsymbol{S}_e^l + dev(\boldsymbol{\rho}_e^*) \tag{6.1}$$

where $\boldsymbol{S}_e^l$ is similar to what is exposed in the previous section and $dev(\boldsymbol{\rho}_e^*)$ is the deviatoric part of the stabilized residual stress tensor. The analytical expression of the former being unknown, a computational procedure must be tailored to perform a gradient–based topology optimization.

Physically, the term $dev(\boldsymbol{\rho}_e^*)$ is used to correct the local value of the stresses, e.g., taking into account some local stress concentrations at the microscopic level. Since we know that the latter is the solution of a min-max problem using as inputs $\boldsymbol{S}_e^l$ with $l = 1, \cdots, NS$ with NS being the number of sampling steps, we can rewrite the solution of the min-max problem at the element level:

$$\boldsymbol{s}_{\boldsymbol{e}}^l = \boldsymbol{S}_e^l + \boldsymbol{\alpha}_e^l : \boldsymbol{S}_e^l; \quad \text{where } dev(\boldsymbol{\rho}_e^*) = \boldsymbol{\alpha}_e^l : \boldsymbol{S}_e^l$$

or:

$$\boldsymbol{s}_e^l = (\mathbf{I} + \boldsymbol{\alpha}_e^l) : \boldsymbol{S}_e^l \tag{6.2}$$

This hypothesis relies on the fact that the only purpose of $dev(\boldsymbol{\rho}_e^*)$ is to bring correction to the stresses locally. Since, its value is known when solving the min-max problem, a scaling matrix $\boldsymbol{\alpha}_e^l$ is constructed and inserted in the problem following Eqn. (6.2).

Practically, the term $dev(\boldsymbol{\rho}_e^*)$ needs to be determined as required by the Dang Van procedure. Since its expression is unknown, we make the hypothesis that the latter is proportional to the macroscopic deviatoric stress tensor. Dropping the scrip $(\cdot)^l$; for clarity, the procedure being identical for each time step l, and considering Eqn. (6.2) with the framework of the previous section, one has:

$$\boldsymbol{s}_e = \begin{pmatrix} (1+\alpha_{XX})\left(\Sigma_{XX} - \frac{1}{3}(\Sigma_{XX}+\Sigma_{YY})\right) & (1+\alpha_{XY})\Sigma_{XY} & 0 \\ (1+\alpha_{XY})\Sigma_{XY} & (1+\alpha_{YY})\left(\Sigma_{YY} - \frac{1}{3}(\Sigma_{XX}+\Sigma_{YY})\right) & 0 \\ 0 & 0 & -(1+\alpha_{ZZ})\frac{1}{3}(\Sigma_{XX}+\Sigma_{YY}) \end{pmatrix}$$

So $\boldsymbol{s}_e^2$ where only the diagonal terms are of interest:

$$\boldsymbol{s}_e^2 = \begin{pmatrix} (1+\alpha_{XX})^2\left[\Sigma_{XX} - \frac{1}{3}(\Sigma_{XX}+\Sigma_{YY})\right]^2 + & & \\ (1+\alpha_{XY})^2\Sigma_{XY}^2 & & \\ & (1+\alpha_{YY})^2\left[\Sigma_{YY} - \frac{1}{3}(\Sigma_{XX}+\Sigma_{YY})\right]^2 + & \\ & (1+\alpha_{XY})^2\Sigma_{XY}^2 & \\ & & \frac{(1+\alpha_{ZZ})^2}{9}\left[(\Sigma_{XX}+\Sigma_{YY})\right]^2 \end{pmatrix}$$

The trace of $\boldsymbol{s}_e^2$ is given by:

$$trace(\boldsymbol{s}_e^2) = \underbrace{(1+\alpha_{XX})^2}_{a}\left[\Sigma_{XX} - \frac{1}{3}(\Sigma_{XX}+\Sigma_{YY})\right]^2 + \underbrace{2(1+\alpha_{XY})^2}_{b}\Sigma_{XY}^2 + \underbrace{(1+\alpha_{YY})^2}_{c}\left[\Sigma_{YY} - \frac{1}{3}(\Sigma_{XX}+\Sigma_{YY})\right]^2 + \underbrace{\frac{(1+\alpha_{ZZ})^2}{9}}_{d}\left[(\Sigma_{XX}+\Sigma_{YY})\right]^2$$

or

$$trace(\boldsymbol{s}_e^2) = a(\frac{4}{9}\Sigma_{XX}^2 - \frac{4}{9}\Sigma_{XX}\Sigma_{YY} + \frac{1}{9}\Sigma_{YY}^2) + b\Sigma_{XY}^2 + c(\frac{4}{9}\Sigma_{YY}^2 - \frac{4}{9}\Sigma_{XX}\Sigma_{YY} + \frac{1}{9}\Sigma_{XX}^2) + d(\left(\Sigma_{XX}^2 + 2\Sigma_{XX}\Sigma_{YY} + \Sigma_{YY}^2\right))$$

Now gathering each term as, one gets:

$$\begin{aligned}
\text{terms in } \Sigma^2_{XX} &: \underbrace{\left(\frac{4a}{9}+\frac{c}{9}+d\right)}_{A}\Sigma^2_{XX} \\
\text{terms in } \Sigma^2_{YY} &: \underbrace{\left(\frac{a}{9}+\frac{4c}{9}+d\right)}_{B}\Sigma^2_{YY} \\
\text{terms in } \Sigma^2_{XY} &: \underbrace{b}_{C}\Sigma^2_{XY} \\
\text{terms in } \Sigma^2_{XX} &: \underbrace{\left(-\frac{4a}{9}-\frac{4c}{9}+2d\right)}_{D}\Sigma_{XX}\Sigma_{YY}
\end{aligned}$$

we can finally write:

$$\sqrt{3J_2} = \sqrt{\frac{3}{2}trace(\mathbf{s_e^2})} = \sqrt{\frac{3}{2}\left(A\Sigma^2_{XX}+B\Sigma^2_{YY}+D\Sigma_{XX}\Sigma_{YY}+C\Sigma^2_{XY}\right)}$$

which has a similar expression to we have determined in the previous section. We can therefore write this expression in matrix form as:

$$\sqrt{3J_2} = \sqrt{\mathbf{U_e^T M_e^{02} U_e}}$$

with $\mathbf{M_e^{02}} = \mathbf{T_e^T V_e^2 T_e}$ and $\mathbf{V_e^2}$:

$$\mathbf{V_e^2} = \begin{pmatrix} \frac{3}{2}A & \frac{3}{4}D & 0 \\ \frac{3}{4}D & \frac{3}{2}B & 0 \\ 0 & 0 & \frac{3}{2}C \end{pmatrix}$$

The formalism that is developed here remains identical to classical stress–based topology optimization in spite of some differences. First, the V-matrix is no longer identical for every elements. Second, for a particular element e, there are as many V-matrices as they are time steps,i.e., $\mathbf{V}_e^2 = \mathbf{V}_e^{2,l}(\boldsymbol{\alpha}_e^l)$. All computations done, the full expression of this matrix is given by:

$$\mathbf{V}_e^{2,l} = \begin{pmatrix} \frac{3}{2}\left(\frac{4(1+\alpha^l_{XX})^2}{9}+\frac{(1+\alpha^l_{YY})^2}{9}+\frac{(1+\alpha^l_{ZZ})^2}{9}\right) & \frac{3}{4}\left(-\frac{4(1+\alpha^l_{XX})^2}{9}-\frac{4(1+\alpha^l_{YY})^2}{9}+\frac{2(1+\alpha^l_{ZZ})^2}{9}\right) & 0 \\ \frac{3}{4}\left(-\frac{4(1+\alpha^l_{XX})^2}{9}-\frac{4(1+\alpha^l_{YY})^2}{9}+\frac{2(1+\alpha^l_{ZZ})^2}{9}\right) & \frac{3}{2}\left(\frac{(1+\alpha^l_{XX})^2}{9}+\frac{4(1+\alpha^l_{YY})^2}{9}+\frac{(1+\alpha^l_{ZZ})^2}{9}\right) & 0 \\ 0 & 0 & \frac{3}{2}2(1+\alpha^l_{XY})^2 \end{pmatrix}$$

we can see that if α is zero, i.e., if no residual stresses are present, we recover $\mathbf{V}^1$.

In conclusion, if we come back to our main hypothesis, we are able to derive a procedure identical to a classical Von Mises evaluation with a modified V-matrix that needs to be updated for each element and for each time step along the optimization process.

Appendix C: Computation of the relaxed stresses for the three–bar truss example

Geometry and numerical parameters

The goal pursed here aims at deriving the stress constraints formulation for the three bar truss example of Figure 6.1.

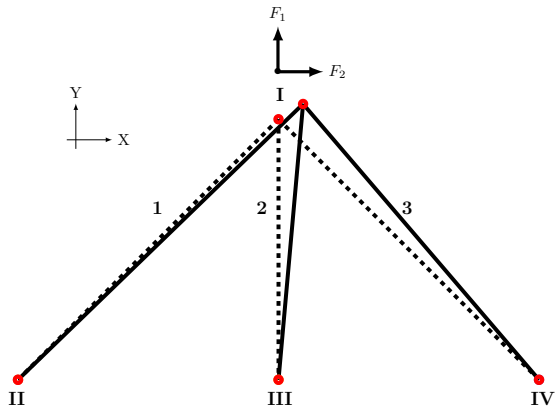

Figure 6.1: Three bar truss example

The material properties and numerical parameters are summarized in Table 6.1

$L_1 = L_3$	$\sqrt{2}$
L_2	1
$A_i (i = 1, \cdots, 3)$	1
$E_{0,i} (i = 1, \cdots, 3)$	1
σ^U	3
σ^L	-3
α	45°

Table 6.1: Material parameters

In order to use the material interpolation law, we need to introduce the densities x_i $(i = 1, \cdots, 3)$ as design variables. We assume that $x_1 = x_3$. It is more convenient to have a problem with two degrees of freedom for graphical representation.

Stress computation without interpolation law

In this section we derive the stress computation of the problem without interpolation, i.e., $E(x_i) = 1 (i = 1, \cdots, 3)$. In the following, the Finite Element Method (FEM) is used to

compute first the displacements of node 1 in Figure 6.1. Practically we want to solve the static equilibrium equation:

$$\mathbf{K}^s\mathbf{U}^s = \mathbf{F}$$

where $\mathbf{K}^s$ is the structural stiffness matrix made of the assembly of the element stiffness matrices, $\mathbf{U}^s$ is the structural displacement, i.e., evaluated in the global axes, and $\mathbf{F}$ is the applied load.

The element stiffness matrices of bar element in 2D can be written without loss of generality as:

$$\mathbf{K}_{e,i} = \frac{E_i(x)A_i}{L}\begin{pmatrix} c^2 & sc & -c^2 & -sc \\ sc & s^2 & -sc & -s^2 \\ -c^2 & -sc & c^2 & sc \\ -sc & -s^2 & sc & s^2 \end{pmatrix}$$

where c and s are the cosine and sine of the angle between the bar element and the reference horizontal axis. All computations done, the general element stiffness matrices for the three bar elements can be written as:

$$\mathbf{K}_{e,1} = \frac{E_1(x)A_1}{L_1^3}\begin{pmatrix} 1 & 1 & -1 & -1 \\ 1 & 1 & -1 & -1 \\ -1 & -1 & 1 & 1 \\ -1 & -1 & 1 & 1 \end{pmatrix}$$

$$\mathbf{K}_{e,2} = \frac{E_2(x)A_2}{L_2^3}\begin{pmatrix} 0 & 0 & 0 & 0 \\ 0 & 1 & 0 & -1 \\ 0 & 0 & 0 & 0 \\ 0 & -1 & 0 & 1 \end{pmatrix}$$

$$\mathbf{K}_{e,3} = \frac{E_3(x)A_3}{L_3^3}\begin{pmatrix} 1 & -1 & -1 & 1 \\ -1 & 1 & 1 & -1 \\ 1 & 1 & 1 & -1 \\ 1 & -1 & -1 & 1 \end{pmatrix}$$

To solve the equilibrium equation, the degrees of freedom related to nodes 2,3 and 4 should be removed from the global structural stiffness matrix because of the boundary conditions. Therefore, only the red components of our element structural matrices are considered in the assembly process. The reduced structural matrix, $\mathbf{K}_{red}$ can be constructed as:

$$\mathbf{K}_{red} = \frac{E_1(x)A_1}{L_1^3}\begin{pmatrix} 1 & 1 \\ 1 & 1 \end{pmatrix} + \frac{E_2(x)A_2}{L_2^3}\begin{pmatrix} 0 & 0 \\ 0 & 1 \end{pmatrix} + \frac{E_3(x)A_3}{L_3^3}\begin{pmatrix} 1 & -1 \\ -1 & 1 \end{pmatrix}$$

Recalling that: $L_1 = L_3 = \sqrt{2}$, $L_2 = 1$ and $A_1 = A_2 = A_3 = 1$ and after some algebra, $\mathbf{K}_{red}$ takes the final form:

$$\mathbf{K}_{red} = \begin{pmatrix} \frac{E_1(x)+E_3(x)}{2\sqrt{2}} & \frac{E_1(x)-E_3(x)}{2\sqrt{2}} \\ \frac{E_1(x)-E_3(x)}{2\sqrt{2}} & E_2(x) + \frac{E_1(x)+E_3(x)}{2\sqrt{2}} \end{pmatrix}$$

The problem to be solved now becomes:

$$\mathbf{K}_{red}\mathbf{U}^s_{red} = \mathbf{F}_k$$

with $k = 1, 2$ and refers to the number of load cases. Once the global displacements are found, the stresses in each bar i can be evaluated reminding that only the displacements of node 1 are different from zero:

$$\boldsymbol{\sigma}_i = \frac{E_i}{L_i}\mathbf{U}^{local}_{1,long}$$

where $\mathbf{U}^{local}_{1,long}$ stands for the displacements of node 1 in the local axes of the bar along its longitudinal direction (the bar element works only in traction/compression). We have now in hands all formulas to compute the stresses in the bars.

In the present section we recall that we are interested in computing the stresses for full material density, i.e., $E(x_i) = 1 (i = 1, \cdots, 3)$ so:

$$\mathbf{K}_{red} = \begin{pmatrix} \frac{1}{\sqrt{2}} & 0 \\ 0 & 1 + \frac{1}{\sqrt{2}} \end{pmatrix}$$

The inverse of this matrix is given by:

$$\mathbf{K}^{-1}_{red} = \begin{pmatrix} \sqrt{2} & 0 \\ 0 & \frac{1}{1+\frac{1}{\sqrt{2}}} \end{pmatrix}$$

The displacements in the global axes for both load cases one (LC1) and two (LC2) are given by:

$$\mathbf{U}_{LC1} = \begin{pmatrix} \sqrt{2} & 0 \\ 0 & \frac{1}{1+\frac{1}{\sqrt{2}}} \end{pmatrix} \begin{pmatrix} 0 \\ 1.5 \end{pmatrix} = \begin{pmatrix} 0 \\ \frac{1.5}{1+\frac{1}{\sqrt{2}}} \end{pmatrix}$$

$$\mathbf{U}_{LC2} = \begin{pmatrix} \sqrt{2} & 0 \\ 0 & \frac{1}{1+\frac{1}{\sqrt{2}}} \end{pmatrix} \begin{pmatrix} \alpha \\ 0 \end{pmatrix} = \begin{pmatrix} \alpha\sqrt{2} \\ 0 \end{pmatrix}$$

Stresses in Bar 1

The local (green) and global axes (red) for Bar 1 can be seen in Figure 6.2

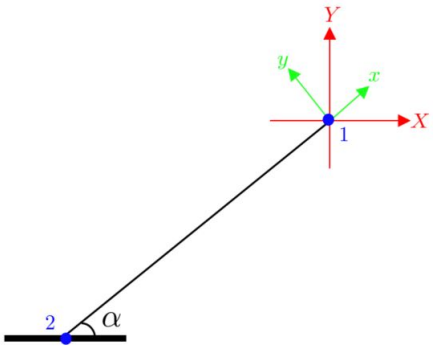

Figure 6.2: Local and global axes for Bar 1

For the first load case, the solution of our finite element analysis shows that only the global component of the displacement along "Y" axis, noted $U_{LC1,Y}$, is non zero. Since the bar element only responds in traction and compression, only the displacement in the local "x" axis is non zero:

$$\begin{aligned} U_{LC1,x} &= U_{LC1,Y} \cdot sin(\alpha) \\ &= \frac{1}{\sqrt{2}} \frac{1.5}{1 + \frac{1}{\sqrt{2}}} \end{aligned}$$

The stress in bar 1 for load case 1, noted $\sigma^{1,1}$, reads (recalling that $E_{0,1} = 1$):

$$\sigma^{1,1} = \frac{E_{0,1}}{L_1}\left(\frac{1}{\sqrt{2}}\frac{1.5}{1+\frac{1}{\sqrt{2}}}\right) = \frac{1}{2}\frac{1.5}{1+\frac{1}{\sqrt{2}}}$$

Following the same development, the local displacement of node 1 for the second load case is written:

$$U_{LC2,x} = U_{LC2,X} \cdot sin(\alpha) = \alpha$$

The stress in bar 1 for load case number 2, noted $\sigma^{1,2}$, reads:

$$\sigma^{1,2} = \frac{E_{0,1}}{L_1}\alpha = \frac{\alpha}{\sqrt{2}}$$

Stresses in Bar 2

The local (green) and global axes (red) for Bar 2 are reminded in Figure 6.3. This time, the local and global axes confounded. Therefore it is straightforward to write that the stress in bar 2 for load case number 1, noted $\sigma^{2,1}$, with $E_{0,2} = 1$ reads:

$$\sigma^{2,1} = \frac{E_{0,2}}{L_2}\left(\frac{1.5}{1+\frac{1}{\sqrt{2}}}\right) = \frac{1.5}{1+\frac{1}{\sqrt{2}}}$$

and as for the stress in bar 2 for the second load case, noted σ_{22}:

$$\sigma^{2,2} = 0$$

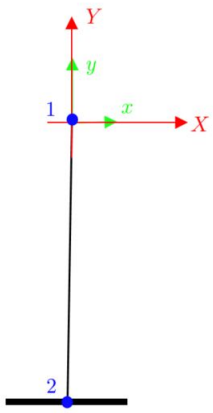

Figure 6.3: Local and global axes for Bar 2

Stresses in Bar 3

Because of the symmetry and the equivalent behavior of bar 3 with respect to bar 1 it is straightforward to write that the stress in bar 3 for load case 1, noted $\sigma^{3,1}$, takes the form:

$$\sigma^{3,1} = \sigma^{1,1}$$

and finally, the stress in bar 3 for the load case number 2, noted $\sigma^{3,2}$:

$$\sigma^{3,2} = -\sigma^{1,2}$$

Summary of the results

The summary of the previous investigations is given below:

$$\begin{pmatrix}\sigma^{1,1}\\ \sigma^{2,1}\end{pmatrix} = \frac{1.5}{1+\frac{1}{\sqrt{2}}}\begin{pmatrix}0.5\\ 1\end{pmatrix}$$

$$\begin{pmatrix}\sigma^{1,2}\\ \sigma^{2,2}\end{pmatrix} = \frac{1}{\sqrt{2}}\begin{pmatrix}\alpha\\ 0\end{pmatrix}$$

$$\begin{pmatrix}\sigma^{3,1}\\ \sigma^{3,2}\end{pmatrix} = \begin{pmatrix}\sigma^{1,1}\\ -\sigma^{1,2}\end{pmatrix}$$

It is clear that the stresses are in tension for bar 1 and bar 2 for both load cases. Due the symmetry and the loading conditions, the stress in bar 3 is in traction for the first load case and in compression for the second load case. However, since in our particular case, stress limits are the same in tension and compression, see Table 6.1, the stress constraint in compression is the same as the stress constraint in tension. Therefore, to avoid redundancy we will only consider three stress constraints in traction. These fully describe the control of the stress within the whole structure. So,

$$\begin{array}{rcl}\sigma^{1,1} & \leq & \sigma^U\\ \sigma^{2,1} & \leq & \sigma^U\\ \sigma^{1,2} & \leq & \sigma^U\end{array}$$

with σ^U being the stress limit in traction given in Table 6.1.

Interpolation law

The interpolation law is recalled below taking into account that $E_{0,i} = 1$ with $i = 1, \cdots, 3$. In its general form, an interpolation law can write: $E(x) = f(x)E_0$

	$f(x)$	Conventional form ($E(x) = f(x)E_0$)	final form ($E_0 = 1$)
SIMP	x^p	x^pE_0	x^p

Table 6.2: Conventional interpolation laws

The parameter p is the interpolation parameter. In the following, we derive the stresses computed in conjunction with the interpolation law.

Stress computation with the SIMP law

Let us recall the expression of the elementary stiffness matrix:

$$K_{red} = \begin{pmatrix}\frac{E_1(x)+E_3(x)}{2\sqrt{2}} & \frac{E_1(x)-E_3(x)}{2\sqrt{2}}\\ \frac{E_1(x)-E_3(x)}{2\sqrt{2}} & E_2(x)+\frac{E_1(x)+E_3(x)}{2\sqrt{2}}\end{pmatrix}$$

Introducing the material interpolation law (SIMP) into the generic expression of the element stiffness matrices and, considering:

$$E_1(x) = E_3(x) = x_1^p; \quad E_2(x) = x_2^p$$

The stiffness matrix takes the form:

$$\mathbf{K}_{red} = \begin{pmatrix} \frac{x_1^p}{\sqrt{2}} & 0 \\ 0 & x_2^p + \frac{x_1^p}{\sqrt{2}} \end{pmatrix}$$

and its inverse:

$$\mathbf{K}_{red}^{-1} = \begin{pmatrix} \frac{\sqrt{2}}{x_1^p} & 0 \\ 0 & \frac{1}{x_2^p + \frac{x_1^p}{\sqrt{2}}} \end{pmatrix}$$

The displacement for both load cases are therefore computed as follows:

$$\mathbf{U}_{LC1} = \begin{pmatrix} \frac{\sqrt{2}}{x_1^p} & 0 \\ 0 & \frac{1}{x_2^p + \frac{x_1^p}{\sqrt{2}}} \end{pmatrix} \begin{pmatrix} 0 \\ 1.5 \end{pmatrix} = \begin{pmatrix} 0 \\ \frac{1.5}{x_2^p + \frac{x_1^p}{\sqrt{2}}} \end{pmatrix}$$

$$\mathbf{U}_{LC2} = \begin{pmatrix} \frac{\sqrt{2}}{x_1^p} & 0 \\ 0 & \frac{1}{x_2^p + \frac{x_1^p}{\sqrt{2}}} \end{pmatrix} \begin{pmatrix} \alpha \\ 0 \end{pmatrix} = \begin{pmatrix} \frac{\alpha\sqrt{2}}{x_1^p} \\ 0 \end{pmatrix}$$

Following the same procedure as in the previous section, the stress values read:

$$\boldsymbol{\sigma}_i = \frac{E_i(x)}{L_i} \mathbf{U}_{1,long}^{local}$$

we can deduce that $\boldsymbol{\sigma}_i(x_i) = f(x_i)\boldsymbol{\sigma}_i$, where $f(x_i)$ is the interpolation function, so:

$$\begin{pmatrix} \sigma^{1,1} \\ \sigma^{2,1} \end{pmatrix} = \frac{1.5}{x_2^p + \frac{x_1^p}{\sqrt{2}}} \begin{pmatrix} x_1^p \\ x_2^p \end{pmatrix} \begin{pmatrix} 0.5 \\ 1 \end{pmatrix}$$

$$\begin{pmatrix} \sigma^{1,2} \\ \sigma^{2,2} \end{pmatrix} = \frac{1}{\sqrt{2}x_1^p} \begin{pmatrix} x_1^p \\ x_2^p \end{pmatrix} \begin{pmatrix} \alpha \\ 0 \end{pmatrix}$$

$$\begin{pmatrix} \sigma^{3,1} \\ \sigma^{3,2} \end{pmatrix} = \begin{pmatrix} \sigma^{1,1} \\ -\sigma^{1,2} \end{pmatrix}$$

Topology optimization problem

The topology optimization problem is stated below. In particular, the stress constraints are written in their relaxed form using either the ε-relaxation or the qp-relaxation.

Formulation of the optimization problem

The general formulation of the weight minimization problem subjected to stress constraints takes the form:

$$\begin{cases} \min & \mathcal{W} \\ \text{s.t} & \mathbf{K}_{red}\mathbf{U}_{red}^{s} = \mathbf{F}_k \\ & x_i^p \sigma_i^L \leq \sigma_i \leq x_i^p \sigma_i^U \end{cases}$$

The weight can be expressed as:

$$\mathcal{W} = \sum_{i=1}^{3} x_i A_i L_i = 2\sqrt{2}x_1 + x_2 \tag{6.3}$$

Furthermore, it was shown in the previous sections that only three stresses, i.e., $\sigma^{1,1}, \sigma^{1,2}, \sigma^{2,1}$, should only be taken into account. Those are related to a traction behaviour of the bar and consequently only the upper bound is used, i.e., $\sigma_i^U = 3$. The problem can finally writes:

$$\begin{cases} \min & 2\sqrt{2}x_1 + x_2 \\ \\ \text{s.t} & \mathbf{K}_{red}\mathbf{U}_{red}^s = \mathbf{F}_k \\ \\ & \sigma^{1,1} \leq 3f(x_1) \\ & \sigma^{2,1} \leq 3f(x_2) \\ & \sigma^{1,2} \leq 3f(x_1) \end{cases}$$

In the following, the stresses are relaxed making use of both the ε-relaxation and the *qp*-relaxation.

Relaxation for SIMP law

First, let's consider the following optimization problem:

$$\begin{array}{ll} \min & \mathcal{W} \\ \text{s.t.} & \sigma \leq \sigma^* \end{array}$$

where $\mathcal{W}$ is the structural weight, σ is the local stress measure and σ^* is the equivalent stress limit. The constraint in the previous equation can be rewritten:

$$\sigma - \sigma^* \leq 0$$

Solving the optimization problem with the reformulated constraint cannot be performed resorting to classical non-linear programming algorithm. To overcome this issue, under the condition that $x > 0$, the constraint is reformulated as:

$$x(\sigma - \sigma^*) \leq 0$$

where $x > 0$ represents the density. We note that this modification does not change the initial design space.

Even if the the new problem can be attacked by non linear programming technique, the optimizer cannot reached the global optimum because the latter is embedded in a degenerative subspace of the design space. Therefore, a relaxation of the constraints are needed. Several ways are possible along which one has the ε-relaxation and the *qp*-relaxation. In the system below we provide the relaxed topology optimization problem where the constraints were modified assuming that $0 \leq x_1, x_2, \leq 1$:

$$\begin{cases} \min & 2\sqrt{2}x_1 + x_2 \\ \\ \text{s.t} & K_{red}U_{red}^s = F_k \\ \\ & (\sigma^{1,1} - 3f(x_1, p))x_1 \leq \varepsilon \\ & (\sigma^{2,1} - 3f(x_2, p))x_2 \leq \varepsilon \\ & (\sigma^{1,2} - 3f(x_1, p))x_1 \leq \varepsilon \end{cases} \qquad \begin{cases} \min & 2\sqrt{2}x_1 + x_2 \\ \\ \text{s.t} & K_{red}U_{red}^s = F_k \\ \\ & \sigma^{1,1} - 3f(x_1, q) \leq 0 \\ & \sigma^{2,1} - 3f(x_2, q) \leq 0 \\ & \sigma^{1,2} - 3f(x_1, q) \leq 0 \end{cases}$$

In order to preserve conciseness of the analytical expressions we don't recall in the following the analytical values of $\sigma^{1,1}, \sigma^{2,1}, \sigma^{1,2}$.

$$\begin{cases} \min & 2\sqrt{2}x_1 + x_2 \\ \\ \text{s.t} & K_{red}U^s_{red} = F_k \\ \\ & (\sigma^{1,1} - 3x_1^p)x_1 \leq \varepsilon \\ & (\sigma^{2,1} - 3x_2^p)x_2 \leq \varepsilon \\ & (\sigma^{1,2} - 3x_1^p)x_1 \leq \varepsilon \end{cases} \qquad \begin{cases} \min & 2\sqrt{2}x_1 + x_2 \\ \\ \text{s.t} & K_{red}U^s_{red} = F_k \\ \\ & \sigma^{1,1} - 3x_1^q \leq 0 \\ & \sigma^{2,1} - 3x_2^q \leq 0 \\ & \sigma^{1,2} - 3x_1^q \leq 0 \end{cases}$$

Appendix D: Article 1

Collet, M., Zhang, S., Fernandez Sanchez, E., Norato, J. & Duysinx, P. (2018). On solution aspects and techniques of density–based methods for the stress constrained topology optimization of selected benchmark problems, *to be submitted to Structural and Multidisciplinary Optimization- Springer*

Summary: Article [1] provides a fair comparison of usual approaches from the existing literature about stress-based topology optimization problems. In particular, it proposes a series of standardized benchmarks that can be used for future works. The paper also discusses in more details some pertinent characteristics when stress constraints are considered, and in particular, it informs about what to expect when using the above-mentioned benchmarks. The latter are then used to compare the most common approaches aiming at minimizing the weight of the design under several stress constraints formulations. Some of these formulations have been slightly modified from their original published version to get the fairest comparisons possible between the different approaches. However, the key ideas of each of these approaches have been retained. Finally, Article [1] also illustrates and comments the numerical performances as well as the shape of the achieved topologies.

Appendix E: Article 2

Collet, M., Noel, L., Bruggi, M., & Duysinx, P. (2018). Topology optimization for microstructural design under stress constraints. *Structural and Multidisciplinary optimization, 1-19, https://doi.org/10.1007/s00158-018-2045-9*

Summary: Article [2] focuses on how static stress constraints are introduced into the topology optimization tool to design tailored materials. The work carried out deals with periodic materials which can be studied by means of an idealized Representative Unit Cell (RUC) with periodic boundary conditions. The aim is to obtain specific elastic properties while maintaining the stress concentration level below some prescribed threshold everywhere within the microstructural layouts. For instance, one would seek to maximize the bulk modulus or try to get a structure with a negative Poisson's ratio and at the same time to prevent failure by controlling the stresses. In the literature, an optimization problem is usually formulated as finding a structure with prescribed elastic properties requirements and in which stress concentrations are minimized. The problem here is reversed by assigning a prescribed stress limit for some test strain fields. This ensures the local stress level to remain below a prescribed value. In this work, the macroscopic far strain field is unknown. To circumvent this issue, arbitrary test strain fields are therefore applied to generate stress peaks within the optimized structure. The stress limit is consequently arbitrary as well. The homogenization tool used in this article allows to calculate the equivalent elastic properties. The proposed procedure to achieve this is tested on several examples, namely the Vigdergauz single inclusion microstructure, the design of material with a negative Poisson's ratio and an original application involving several load cases.

Appendix F: Article 3

Collet, M., Bruggi, M., & Duysinx, P. (2017). Topology optimization for minimum weight with compliance and simplified nominal stress constraints for fatigue resistance. *Struct Multidisc Opti 55:839-855. DOI 10.1007/s00158-016-1510-6*

Summary: In Article [3] fatigue strength is also considered throughout the topology optimization process. Stresses are used as inputs to build the fatigue model for mechanical components withstanding a large number of loading cycles. In the case of proportional loads with constant amplitude, the Goodman criterion is a judicious choice for the fatigue sizing of mechanical parts. In this perspective, this criterion is introduced into the topology optimization process. The Sines method and Goodman's criterion, see e.g., [Norton(2000)], are then used to compute alternating and mean equivalent stresses to account for the multiaxial nature of the stress field. Due to the linear elasticity of the problem, a reference load case is applied to the structures which in turn allows to determine the alternating and mean components through the use of weighting factors. The optimization is performed using gradient based algorithms. The method proposed here is illustrated for several test cases.

Appendix G: Article 4

Collet, M., Bauduin, S., Fernandez Sanchez, E., Alarcon Soto, P., & Duysinx, P. (2018). On the Dang Van criterion for fatigue design using topology optimization, *submitted to Structural and Multidisciplinary Optimization- Springer*

Summary: Article [4] investigates the introduction of the Dang Van fatigue criterion [Dang Van et al.(1989)] into the topology optimization process. This criterion is more general and potentially more widely applicable as it allows to consider complex loading cases. It is therefore incorporated in a gradient-based optimization process to study its impact. The Dang Van criterion has already been introduced in previous contributions, see e.g., [Mrzygold and Zielinski (2006)], but with non gradient-based methods. It is known to be in good adequacy with experimental tests. Its approach is based on the use of the critical plane which is a crystallographic plane in the vicinity of which local plasticity is more likely to arise in the first place. This way gives a far more accurate representation of the stress state. The paper shows how to take this criterion into account throughout the topology optimization process to design fatigue resistant parts in the best possible way. Several examples are illustrated and demonstrate how robust and versatile the approach used in this work is.

Appendix H: Proceeding

Collet, M., Bruggi, M., Bauduin S., & Duysinx, P. (2015). Stress-based topology optimization with fatigue failure constraints. In Proceedings of the Fifteenth International Conference on Civil, Structural and Environmental Engineering Computing.

Summary: Proceeding [1] extends the developments of Article [3] to enable the use of two other fatigue strength criteria, namely the Sines [Sines(1959)] and Crossland [Crossland(1956)] criteria. The study evaluates and compares the effects of these criteria on the final topology of the structure as well as the objective function to be minimized, i.e., the weight.